Geomechanical modelling of stress magnitude and orientation across fault and its relation to hydraulic fracturing

Ehtesham Karatela, B.S. (University of Karachi)

This thesis is submitted in partial fulfilment of the requirements for the

Master of Science (Petroleum Geoscience)

Australian School of Petroleum,
The University of Adelaide
October, 2012

Contents

ABSTRACT

With intense exploration around the world, easily extractable hydrocarbons are getting more and more difficult to find. Major conventional hydrocarbon accumulations have been targeted and are being produced; but increased world's consumption has led petroleum exploration and production industry to consider exploiting targets that were not believed to be economical. Tight reservoirs include shale gas, shale oil, coal seam gas (CSG) and tight sands. This concept has changed the conventional view of shales from being source and seal rock to unconventional perception –as reservoir. These reservoirs have minimal porosity and permeability which is not sufficient to produce at economic rates. Developing these reserves may require hydraulic fracturing to create a predictable network of fractures with height of several hundred feet through which hydrocarbons can easily flow towards borehole. Even if these reservoirs are fracture stimulated at best of the knowledge and skills; production from two wells in the same field is never the same.

For a successful fracturing treatment, it is necessary to understand impact of existing fractures, faults and stress regimes in the subsurface. Geologic structures influence the stress field locally and show deviation from the regional trend of stress pattern. This study utilizes geomechanical modeling with static elastic moduli to depict stress magnitude and orientation around faults. For the purpose, stress magnitudes estimated by Reynolds *et al.,* (2006) are used. Strike-slip stress regime prevails in at the depth interval selected. A thorough study using different lithologies, σ_H azimuth and fault size is carried out. Stress concentrate at the fault tips on opposite quadrants of the fault tips. Fluctuation in stress magnitude increases with increase in fault size. However, the variation diminishes after fault size of 1500 meters. These models help in understanding the orientation of fractures during hydraulic fracturing and help to recognize stress barriers that may affect production from an unconventional reservoir.

ACKNOWLEDGEMENTS

First and foremost, I would like to thank God for helping me throughout the year specially in the time period when I struggled. My sincere thanks to my principal supervisor Dr. Dennis Cooke and co-supervisor Dr. Hani Abul Khair. Their excellent supervision and regular discussion sessions has helped me in finishing this project in the required time. I was lucky to have such friendly and technically strong supervisors.

This project provided me with an opportunity to understand the role of stress in subsurface and helped to understand the factors affecting the process of hydraulic fracturing. It was a pleasant experience working with Geofrac research consortium at Australian School of Petroleum (ASP).

My deepest thanks to all the staff at ASP for all of the knowledge they shared to me. I would like to thank all the teachers who provided with a new insight in petroleum geosciences. In particular Kathryn Amos, Bruce Ainsworth, Andy Mitchell, Guillaume Backe and John Kaldi whose attention provided significant knowledge and influenced me to get involve with structure and geomechanics.

A special thanks to Ian West who has always been there to help regarding technical issues particularly with the software. I would like to thanks my classmates and my friends in Masters Petroleum engineering for the fun moments we shared.

I would like to thank my parents, brothers and cousin in Adelaide; whose moral support soothed me throughout the year. I hope this thesis brings something positive to the industry and helps others doing research relating geomechanics.

Chapter 1

Introduction

1.1 Hydraulic fracturing

Production of oil and gas has a history of more than a century. In the early days oil from seepages was utilized where the seal integrity has been compromised. The increasing demand of oil resulted in drilling the first well of exploration history in Pennsylvania in the year 1859. The need of energy is more intensified and the major reservoirs of the world are at the verge of depletion. To cope up with the energy need, oil and gas industry is considering various ways to exploit tight reservoirs such as shale gas, shale oil, tight sands and coal seam gas (CSG). These reservoirs do not flow at economic rates until they are hydraulically fractured.

A hydraulic fracturing treatment is carried out by pumping specially engineered fluids at high pressure into the reservoir interval to be treated, causing a fracture to prop open. Usually a single fracture is created in two directions at 180° and theoretically assumed to be similar in shape and dimension. The fracture created needs to be remained open after the pressure is reduced, a propant such as sand is used to prop open the fracture after the pumping operation is stopped (Holditch, 2007).

To hydraulically fracture a reservoir, particularly shale gas, various criterions need to be considered before selecting an appropriate candidate. To produce commercial quantities of gas, shale should have appropriate amount of absorbed and adsorbed gas content, thermally mature, thick enough to contain the fracture treatment within itself and accurate information of stress conditions around borehole, high young's modulus and low Poisson's ratio (King, 2010). All fracture simulation treatments are not always successful (Reynolds *et al.,* 2006), potentially due to number of reasons explained by King (2010). Across North America a number of shale gas plays show production variability (Baihly *et al.,* 2010). One of the possible reasons in the variation of production from wells is the stress along well bore which can control the initiation and development of fracture (King, 2010).

1.2 Influence of stress

A total of 3400 dependable measurements of tectonic stress are available defining global stress patterns (Zoback *et al.,* 1990). The world stress map project has provided important stress data using a number of conventional methods such as borehole breakouts and minifrac test (Tingay *et al.,* 2005). The notable development in determining global stress magnitude and orientation has led to use this

vital information in exploration and production process. However, variation in stress magnitude due to local geologic structures in sedimentary basins is poorly understood (Tingay *et al.,* 2005).

Cooper basin is one the most prolific onshore basin of Australia with most prominent shale gas prospects in Australia (World gas resources, 2011). Since 1963, 129×10^9 m^3 (4.6 tcf) of gas and 4.6×10^6 kL (29.1 mmstb) of oil have been produced (GSA, 2011). Due to intense exploration ample amount of stress data sets in the form of borehole breakouts, drilling induced tensile fractures (DITF), overcoring measurements and earthquake focal mechanism is available. Most of the stress data is from borehole breakouts and drilling induced tensile fractures, east-west orientation of maximum horizontal stress (σ_{Hmax}) is mostly constant throughout the basin (Reynolds *et al.,* 2005). Assessment of surrounding areas determines clockwise rotation of σ_{Hmax}, from north-south in Amadeus basin to east-west in cooper basin (Reynolds *et al.,* 2005). In the Cooper basin, stress regimes vary with depth. Reynolds *et al.* (2004) and Reynolds *et al.* (2006) produced stress-depth plots determining change in stress regime with depth. Fractures initiated in strike-slip stress regime will open in direction of minimum horizontal stress but will change its orientation as soon as it enters in thrust fault stress regime. Such fractures are called T- fractures and cause a significant problem in acquiring desirable results from hydraulic fracturing. The in situ stress field plays an important part in not only determining the orientation of new fracture but also define the fractures that may be more vulnerable to flow in a naturally fractured reservoir (Reynols *et al.,* 2004). Apart from tectonic stresses, less consideration has been given to the local change of stress.

1.3 Methodology

This thesis includes a number of stress simulations with variable fault sizes and stress magnitude of strike slip stress regime to understand the variation in stress magnitude with change in size of the fault and rapid change in stress magnitude at the fault tips. The simulations are made using Schlumberger's stress simulation package *Poly 3D* which is based on Boundary element method (BEM). The software use average values of Young's modulus (YM) and Poisson's ratio (PR). Simulation results imply that stress perturbation is a function of size of the fault, lithology and σ_{Hmax} azimuth. This approach allows evaluation of a very large number of models and quantitative assessment of stress disturbance around the fault tips. Stress magnitudes utilized for geomechanical modelling were used from Reynolds *et al.,* (2006). Selected data points represent strike-slip stress regime in Cooper basin (Fig 1.1).

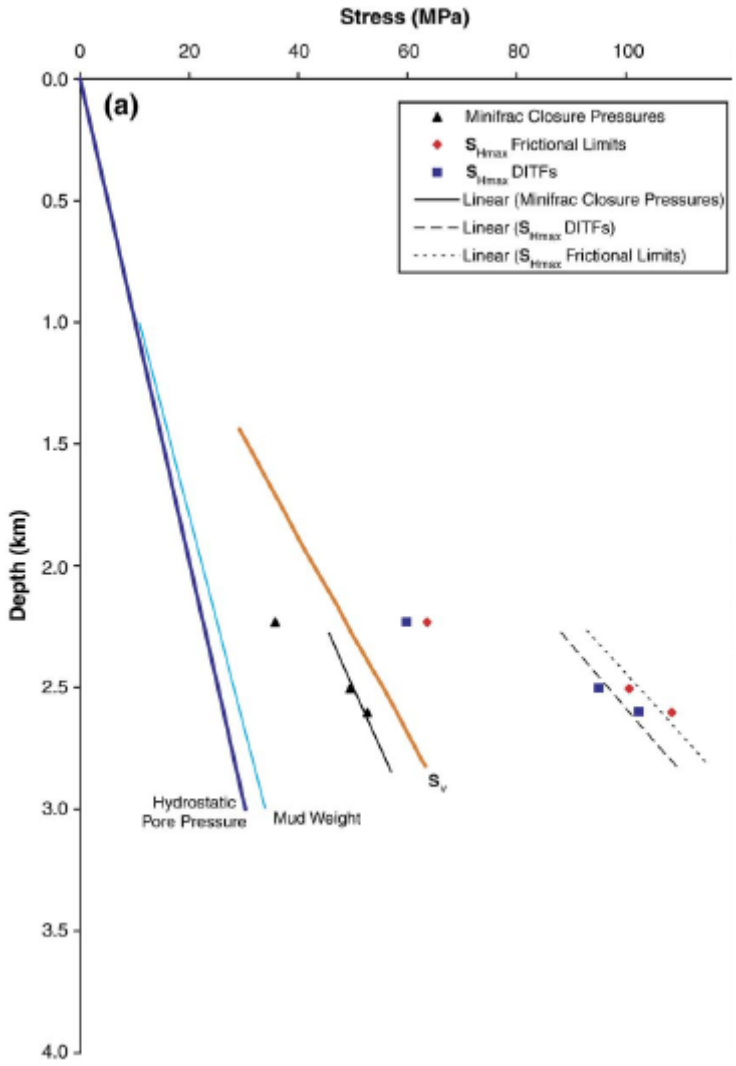

Figure 1.1, Stres vs depth plot; showing magnitude for stresses. Modified from Reynolds (2006)

1.4 Aims and Objective

The prime aim of this project is to determine the change of stress magnitude particularly at the fault tips with change in size of the fault and impact of lithology on this variation. Plane view of simulations can be used to predict magnitude of minimum horizontal stress and direction of fractures that may be created during hydraulic fracturing. Using geomechanical modelling can be fruitful to recognize stress trends in sub surface especially at the locations where stress amplitude fluctuates rapidly

Chapter 2

The *in situ* Stress tensors

2.1 Introduction

This chapter concisely defines the *in situ* stress tensors and stress regimes which form the basics of this thesis. In simplest terms, stress can be defined as the force (F) acting on a specified area (A).

$$\sigma = \frac{F}{A}$$

The S.I. unit for stress is Pascal (Pa). Due to large amount of stress involved in geological processes, stress is defined as Mega pascals (10^6). In rock mechanics, stress acting on a homogenous and isotropic body can be resolved into nine components oriented in three dimensions. This description of three normal (S_{11}, S_{22}, s_{33}) and six shear stress (S_{12}, S_{13}, S_{21}, S_{23}, S_{31}, S_{32}) is expressed as stress tensor.

$$\sigma = \begin{matrix} \sigma_{11} & \sigma_{12} & \sigma_{13} \\ \sigma_{21} & \sigma_{22} & \sigma_{23} \\ \sigma_{31} & \sigma_{32} & \sigma_{33} \end{matrix}$$

The normal stresses on the principal planes are termed as principal stresses, typically defined with conventional methodology as $S_1 > S_2 > S_3$. The stress within the earth at depths is conventionally compressive, therefore positive. Tensile stress does not occur at greater depths (Zoback, 2007).

2.2 Anderson's Classification

E.M. Anederson (1951) proposed a classification applying the concept of stress tensor to the earth crust. He assumed that stress magnitudes of principal stresses (S_1, S_2 and S_3) correspond to the S_V, S_{Hmax} and S_{hmin} depending on the geological setting of the area and fault style (Fig 2.1). Each fault type is associated with a particular stress regime that determines the relative stress magnitude

(Zoback, 2007). The stress regimes are normal fault stress regime ($S_V > S_{H\,max} > S_{h\,min}$), strike-slip stress regime ($S_{Hmax} > S_V > S_{h\,min}$) and reverse fault regime ($S_{H\,max} > S_{h\,min} > S_V$).

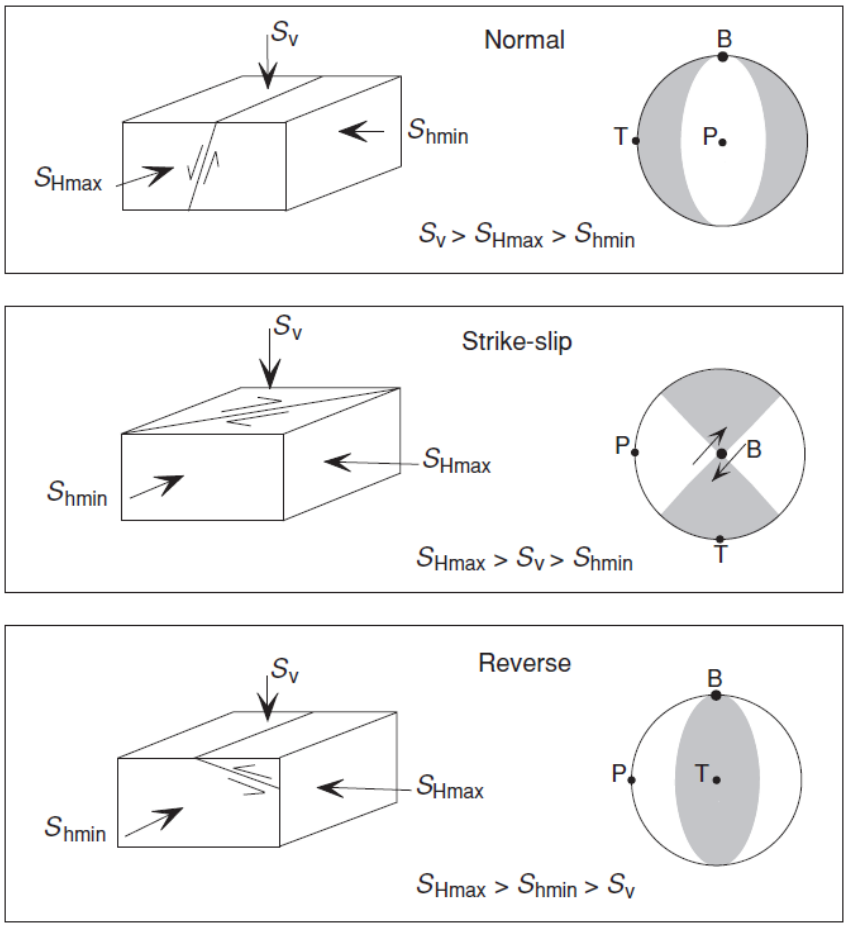

Figure 2.1 Pictorial representation of Anderson's Classification from Zoback (2007)

2.3 Stress around a borehole

When a well is drilled, the stress from the rocks is removed and shifted to well bore. Mud density, weight on the surface of rocks being drilled and pressure of the fluids circulating in the borehole are the primary factors that keep the well stable (Watterson, 1999); otherwise fluid from the formation will enter the borehole resulting in borehole instability. Kirsch (1989) proposed various equations determining stress components around borehole as a function of far field stress (Reynolds, 2001). Following equation is a simpler form defining stress at the wellbore.

$$\sigma\theta = 2\sigma Hmax\ Cos2\theta$$

Where,

σ_θ = circumferential stress

θ = Angle around well bore

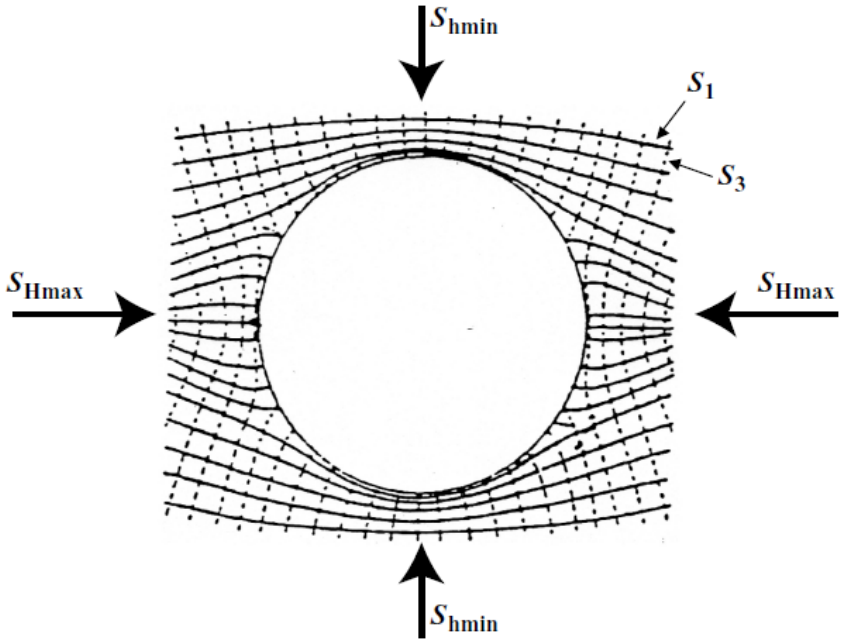

Figure 2.2, Schematic diagram representing stress around vertical borehole from Zoback (2007).

The removal of rock due to drilling cause the concentration of stress around the well bore. In a vertical well stress path is compressive in the direction of S_{hmin} as compare to the stress pattern in S_{Hmax} orientation (Zoback, 2007). Stress concentration is a function of position and distance from the well which would affect the fracture development away from the bore hole.

2.4 Stress at the fault tips

The magnitude and orientation of the stress field can change locally due to any discontinuity such as faults and fractures (Homberg *et al.*, 1997; Gudmudsson, 2000; Bourne and Willemse, 2001; Kattenhorn and Marshall, 2006; Cooke, 2011). High magnitude stress concentrates at the tips causing deviation of stress pattern from the regional stress field. Fractures propagate on a plane parallel to S_{Hmax} locally (Bourne and Willemse, 2001); therefore the knowledge of stress confined at fault tips is necessary to understand the mode of fracture deviation during fracture treatment. The studies of previous authors determine that stress concentrates in two quadrants, with size of stress accumulation depending on far field azimuth. Fig 2.3 shows the concentration of stress on a strike slip fault.

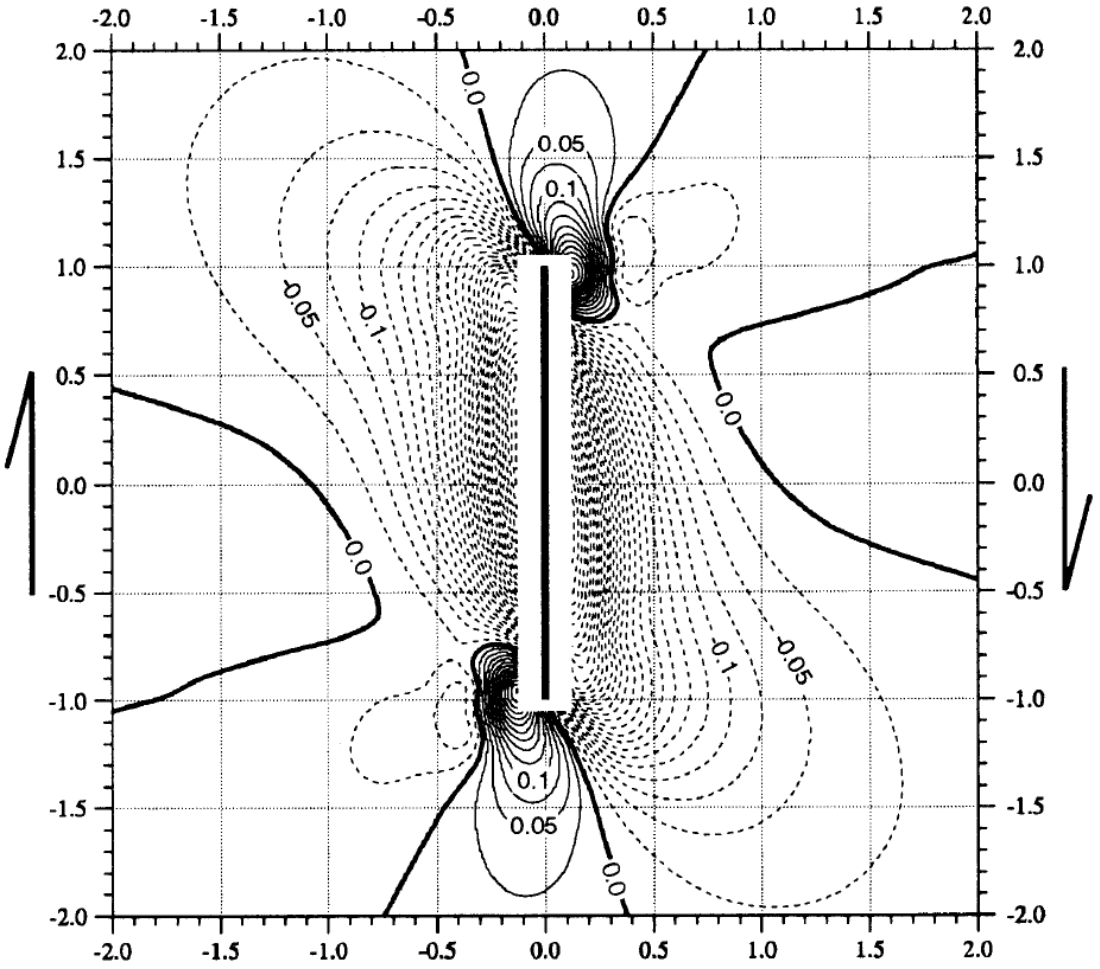

Figure 2.3 Concentration of stress (both compression and tension)on opposite quardants of fault tips. From Bourne and Willemse (2001)

Chapter 3

Measurement of stress magnitude and orientation

3.1 Introduction

This chapter summarize conventional methods used to determine stress magnitude and direction described by Zoback and Haimson (2001) and world stress map project (public domain project since 1989). These methods include borehole breakouts, drill induced tensile fractures (DITF), earthquake focal mechanism, hydraulic fracturing, overcorring and seismic. However, an eccentric method, prediction of stress, strain and displacement using computer simulations is being used as well (Thomas, 1993; Swyer and Davatzes, 2012). A brief introduction of the usual methods is presented in this chapter to help the reader understand and compare between conventional methods and computer based geomechanical modelling of stress analysis used in this thesis. In section 3.4, a review of hydraulic fracture treatment procedure is presented that shall explain the importance of stress during the process.

3.2 Borehole breakouts

3.2.1 Theory

Borehole breakouts are dark continuous elongated features which can be observed on image logs. Bell and Gough (1979) explained these features as stress related that are formed due to concentration of stress around borehole. They form when circumferential stress surpasses the compressive strength of the rock (Reynolds *et al.,* 2005). Maximum and minimum horizontal stress act perpendicular to each other in a vertical well, borehole breakouts enlarge in minimum horizontal stress direction (Tingay *et al.,* 2005).

Borehole breakouts are reliable indicators of orientation of maximum horizontal stress (S_1) (Zoback *et al.,* 1985; Brudy *et al.,* 1997). However conflict exists to the extent at which breakouts can be used to determine stress magnitude (Engelder, 1993). Stress orientations defined from borehole breakouts are consistent with other stress indicators such as hydraulic fracturing, overcoring and earthquake focal mechanism and contributes up to 22% of the stress data in world stress map project (Reynolds, 2001). Fig 3.1 represent borehole breakout in a vertical well.

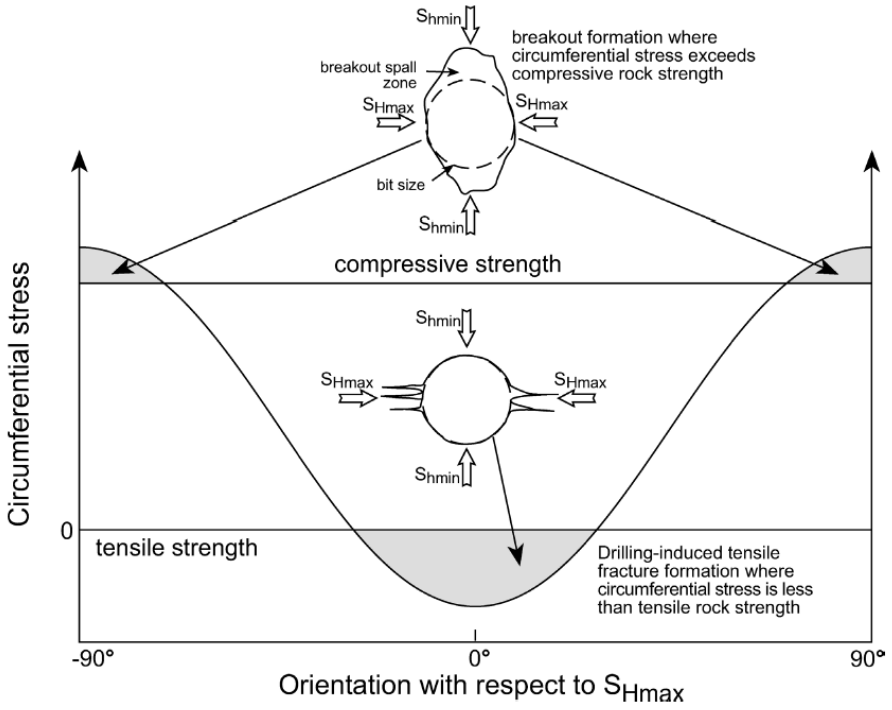

Figure 3.1 From Reynolds (2005), Orientation of minimum and horizontal stress resulting in borehole breakout.

Borehole breakouts are distinct, beginning and ending suddenly (Bell and Gough, 1979; Tingay *et al.*, 2005). The length of a borehole breakout is independent of the depth in a well, lithology and dip of the bed (Bell and Cough, 1979).

3.2.2 Interpretation

Dipmeter and image logs are the most appropriate tools to measure borehole breakouts. In older wells dipmeter is a commonly used tool and has now been replaced by imaging tools. The four arm dipmeter tool has four pad electrodes arranged in a coplanar orthogonal pattern (Plumb and Hickman, 1985). The pads are pressed against the wellbore wall and measure formation resistivity from opposite sides of the wall. The reference pad (pad 1) is magnetically oriented while two independent callipers measure well bore diameter between pads 1-3 and 2-4 (Plumb and Hickman, 1985). The limitation on calliper measurements is that it may only measures those breakouts which are larger than the length and width of pad and diameter of well bore (Plumb and Hickman, 1985).

There are a number of borehole enlargements that are not related to stress around well bore (Fig 3.2). These enlargements in a well are possibly influenced by lithology, natural fracture, consolidation and drilling history (Rider, 2002). Plumb and Hickman (1985) has set criteria to foil misidentification of breakouts, according to which breakouts are symmetric with the axis and are in the direction of minimum horizontal stress; while other elongations in the well may have been formed by drill pipe wear. Therefore, identification of breakouts calls for measure of symmetrical electrical conductivity anomalies by dipmeter.

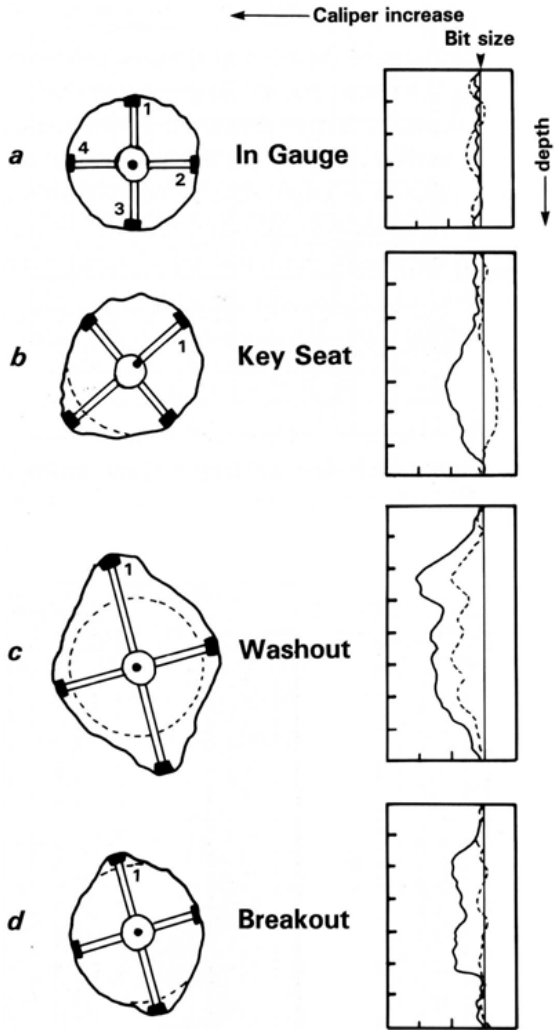

Figure 3.2 Modified from Rider (2002), Schematic representation of borehole shapes and caliper log profile. Fig 3.2a, in gauge. Fig 3.2b, Key seat. Fig 3.2c, washout caused by drilling wear. Fig 3.2d, Breakout showing symmetrical elongation.

Image logs provide a more confident interpretation of breakouts than the dipmeter tool. They are being used more frequently in new wells. The tool consists of 4 or 6 pads with different number of "buttons" depending on the tool. These buttons measure the electrical conductivity of the formation. Breakouts are poorly imaged (reduced pad-wall contact) in the zones of low resistivity where drilling mud has invaded the formation (Reynolds, 2001). Breakout intervals which are not associated to the spalling of wellbore wall are identified using image logs. Fig 3.3 shows borehole breakouts recognised by image logs.

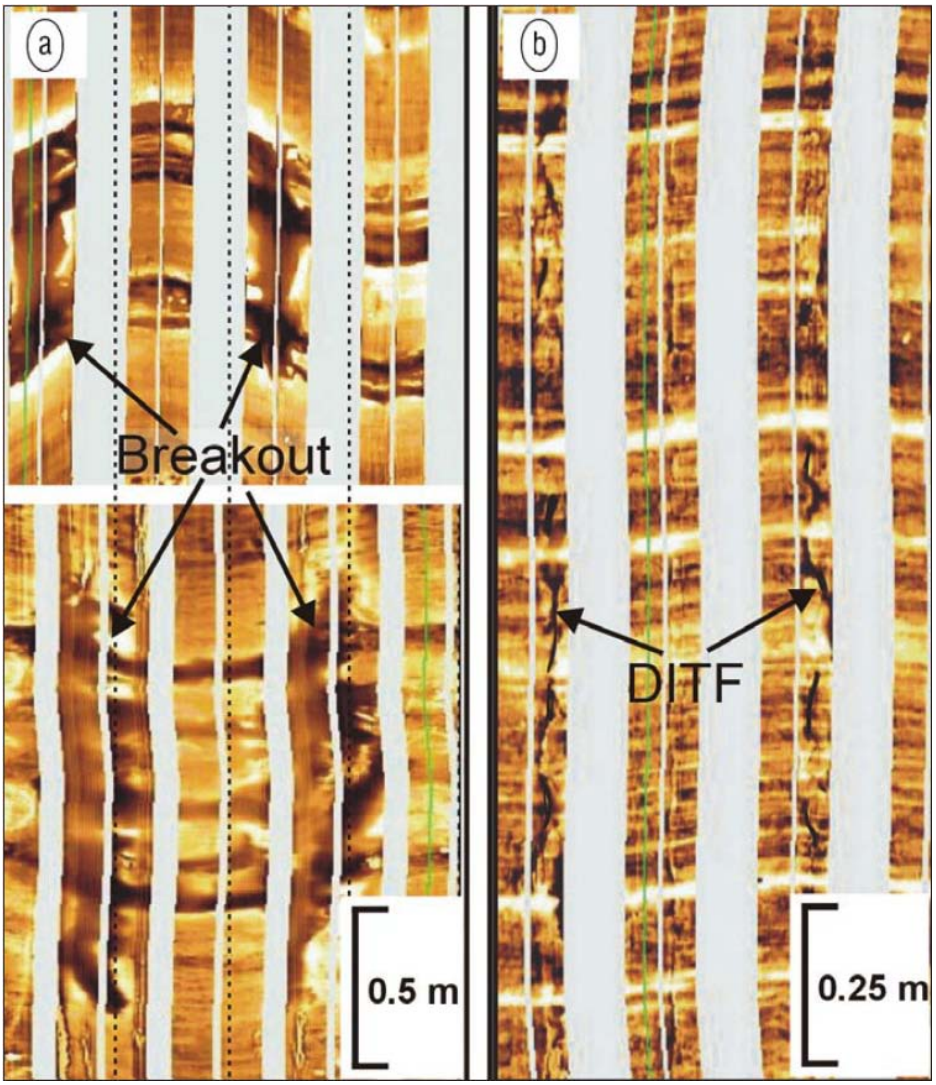

Figure 3.3, Interpretation of borehole breakouts and drilling induced tensile fractures. From Tingay *et al*., 2005

3.3 Drilling Induced Tensile Fractures

3.3.1 Theory

Drilling induced tensile fractures (DITF) are frequently identified on image logs. They form when circumferential stress around borehole is smaller than the tensile strength of the rock (Reynolds, 2001). When formation is penetrated by drill bit, stress in the formation is disturbed. However DITF is not formed until the pressure of fluid in borehole exceed the minimum principal stress causing lost circulation. In a vertical borehole DITF form in the orientation of maximum principal stress while in a deviated well DITF can occur in an en echelon pattern (Barton and Zoback, 2002).

Fig 3.3 shows a number of DITF. As mentioned in section 3.2, breakouts are in the direction of minimum principal horizontal stress (σ_{hmin}). Brudy and Zoback (1999) imply that it provides direct

evidence that DITF are oriented in the direction of maximum principal stress (σ_{Hmax}). DITF are abundant and it is unlikely to encounter a number of fractures parallel to wellbore axis.

3.3.2 Interpretation

DITF can be easily interpreted from image logs acquired through borehole televiewer, Formation microscanner and formation microimager. DITF can determine the orientation of maximum horizontal stress accurately. Fig 3.3shows an image log illustrating DITF in dark colours. During drilling mud penetrated into the fractures which show high electrical conductivity as compare to the surrounding rock matrix.

3.4 Hydraulic Fracturing

3.4.1 Theory

Hydraulic fracturing is considered to be a successful treatment to produce economically from low permeability reservoirs by connecting natural fractures and cleats within a reservoir. Since 1957, after first hydraulic fracturing treatment, it has become a regular practice for stimulating reservoirs to produce at best possible rates (Holditch, 2007). Minifrac test is a type of hydraulic fracture treatment carried out at smaller scale utilized to determine the magnitude of minimum horizontal stress. It has subsequently become a reliable method to determine in situ stress at depths in a sedimentary basin. The process involves injection of high pressure fluids in a test interval creating a fracture that is in the direction of maximum horizontal stress (σ_{Hmax}) and opens in orientation of minimum horizontal stress (σ_{hmin}). Natural fracture impact the propagation of fractures but it is mainly controlled by stress field (Zoback, 2007). Therefore, knowledge of localised stress field is vital to effective fracture treatment. Poroelastic model is usually used to estimate magnitude of minimum horizontal stress.

$$\sigma_{\min} \cong \frac{v}{1-v}(\sigma_1 - \alpha p_p) + \alpha p_p + \sigma_{ext}$$

Equation 3.1, Mathematical form of poroelastic model. Minimum horizontal stress is correlative to closure pressure.

σ_{hmin} = minimum horizontal stress
v = poisson's ratio

P_p = Pore pressure

σ_{ext} = tectonic stress

3.4.2 Operational procedure

Hydraulic fracturing is a process in which fluids are injected into reservoir at high rate that is impossible for formation to accept in a radial pattern (Holditch, 2007). This leads the pressure to increase in the borehole until the tensile strength of rock is overcome resulting a fracture through the rock. As soon as fracture is formed, fluids injected begin to move into the fracture. Theoretically, the fracture in the formation is vertical that propagate in two opposite directions away from the well bore; the fracture wings being 180 apart and identical in shape, size and length (Holditch, 2007). Fluids injected during the treatment contain "propping agent" that prop open the facture after injection is ceased. Normally sand grains or ceramic beads are used as propping agent.

The basic equipment used for fracture treatment is shown in Fig 3.4. The interval that is to be fractured is sealed off using packers. If any natural fracture already exists in the interval, it will open when pressure in well bore rises and avoid the formation of induced fracture. This will invalidate the in situ stress assessment; therefore care should be taken while selecting a candidate interval.

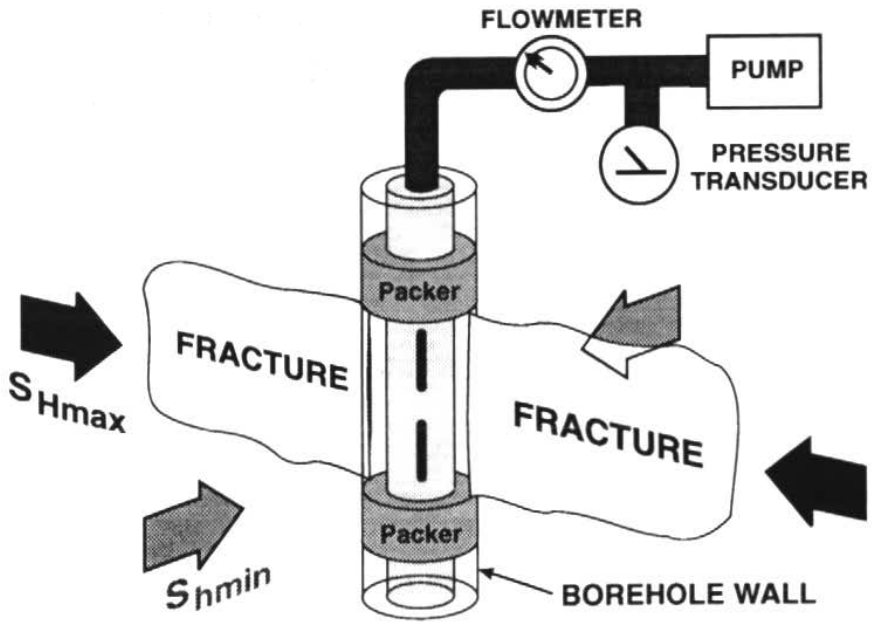

Figure 3.4 Equipment for Hydraulic fracturing from Bell (1996)

A fracture is created when circumferential stress exceeds tensile strength of the rock. The basic difference between hydraulic fracture and drilling induced tensile fractures is that during hydraulic fracturing the magnitude of fluid pressure in borehole is greater than minimum principal stress so the fracture can propagate away from the borehole (Zoback, 2007).

Rock mechanics

Besides *in situ stress* field, mechanical rock properties also affect a successful hydraulic fracture treatment. "Ratio of lateral expansion to longitudinal contraction" is defined as Poisson's ratio. The amount of Poisson's ratio is used in determining the closure pressure (Cooke, 2011). Similarly Young's modulus controls the fracturing ability. Therefore, data regarding the elastic moduli of the rock to be fractured should be determined.

Injection test

Minifrac test is a reliable technique to measure *insitu* stress field. A time-pressure plot is used to estimate the closure pressure. The term closure pressure corresponds to minimum horizontal stress (Holditch, 2007). The test is carried out by injecting small volumes of same fluids used in the main treatment. The purpose of the test is to create similar fracture but of small height. As soon as fracture is created pumping is stopped leading to a decrease in pressure. The decline curve is used to estimate minimum horizontal stress.

3.4.3 Interpretation

The stresses are calculated using pressure-time plot (Fig 3.5). Fracture breakdown, shut in and reopening pressures are used for computation. A sharp peak followed by quick decline determines the pressure at which fracture is created and fluids enter into fracture (Bell, 1996). After the fracture is created pumping is stoped (shut in), but the fracture growth continues until fracture fluid pressure is equal to stress intensity factor (Hayashi and Haimson, 1991). This phenomenon causes the pressure to decline leading the fracture to close. This pressure is termed as fracture closure pressure. Rapid decline in pressure gradient changes to relatively stable decline because of closing of pressure (Bell, 1996). Facture closure pressure can be used in determining measurement of minimum horizontal stress (S_{hmin}).

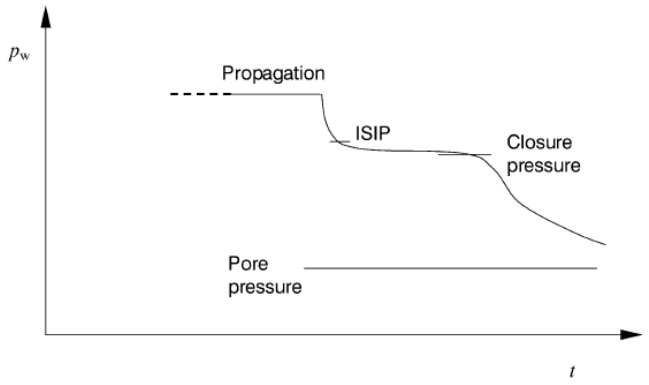

Figure 3.5 Pressure -Time plot representing closure pressure estimated to determine magnitude of minimum horizontal stress.

The instantaneous shut in pressure (ISIP) is always higher than the closure pressure and is considered to be upper bound for closure pressure. Rocks with low permeability have sharp shut in curve due to minimal fluid leak-off, while rocks with higher permeability have large curvature of shut-in pressure that make identification of closure pressure vague (Reynolds, 2001).

3.4.4 Impact of stress on fracture stimulation

The magnitude and direction of stress around borehole and well trajectory may affect the way in which the fractures may initiate and propagate away from the borehole (Hossain et al., 2000). Some fracture stimulation treatments don't undergo ideally. A number of fractures convert into torturous pathways (Fig 3.6b) as they grow away from the wellbore, this result in limited fracture growth (Nelson *et al.*, 2007; Reynolds *et al.*, 2004). Restricted connectivity limits the possible drainage area for production. Fig 3.6 shows difference between torturous and ideal fractures created during a fracture treatment.

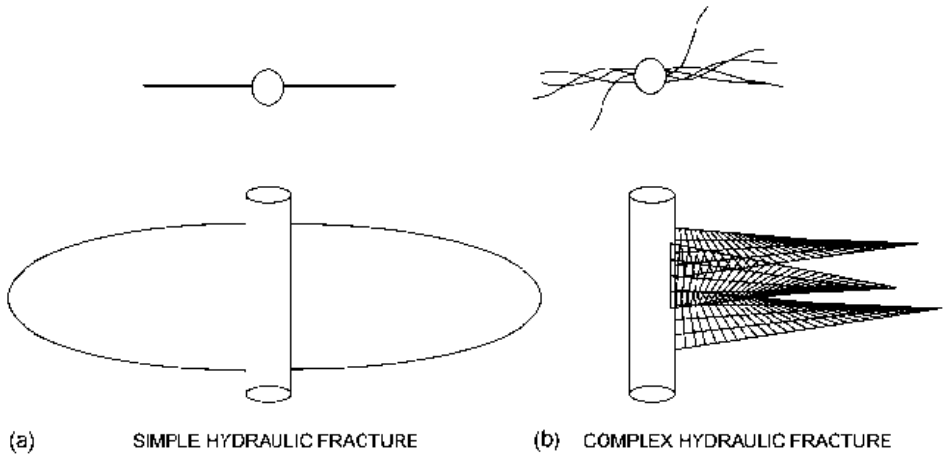

Figure 3.6 Schematic representation of variation in fracture propagation in a well against theoretical approach. From Nelson *et al.* (2007)

Fracture development is mainly controlled by stress field around well bore; however it is also regulated by natural fractures in reservoir which determine failure planes in the rock body. (Zoback, 2007).

3.5 Overcoring measurements

3.5.1 Theory

Overcoring is a term used to describe a number of measurement techniques that involves cutting core with stress measuring instruments attached, for example doorstopper, USBM guage. This technique involves measuring three-dimensionl stress tensor by estimating strain relief when a rock sample is isolated from surrounding rocks (Ljunggren et al., 2003). When rock is isolated, amount of expansion is directly proportional to the stress within the rock (Engelder, 1993). The in situ stress can be estimated using elastic modulus.

Each overcoring technique has its own methodology and is applied at various stages (Ljunggren et al., 2003; McGarr and Gay, 1978).

3.5.2 Interpretation

Each technique is interpreted in a separate fashion. Reynolds (2001) has summarized generalized assumptions considered for the analysis of overcoring measurements in a borehole.

- Stresses that are relieved are equal to the stresses when rock was in situ.
- Diameter of overcoring has no influence on stress measurements.
- Rock response in a linear elastic manner when unloaded during overcoring.
- Rock is assumed to be isotropic.
- Borehole is circular with no rugosity.
- In situ field is three dimensional.
- Rock deforms in plane stress or strain.

3.6 Earthquake focal mechanism

Earthquake focal mechanism (fault plane solution) involves measurement of deformation stimulated by large volume of rocks at great depths (Zoback and Zobak, 1991; Zoback, 2007). If sufficient seismic acquisition seismographs are available, it can help to continuous change as earthquake occurs (Ljunggren *et al.*, 2003). The beach balls in Fig 3.7 denote normal, strike slip and reverse fault regimes. Earthquake focal mechanism contains two orthogonal nodal planes one of which is termed as fault plane and other is referred as auxiliary plane which bound the compressional and extensional quadrants of focal mechanism. These planes define the orientation of P (compressional), B (intermediate) and T (extensional) planes and are sometimes misinterpreted as orientation of S_1, S_2 and S_3. (Zoback and Zoback, 2002).

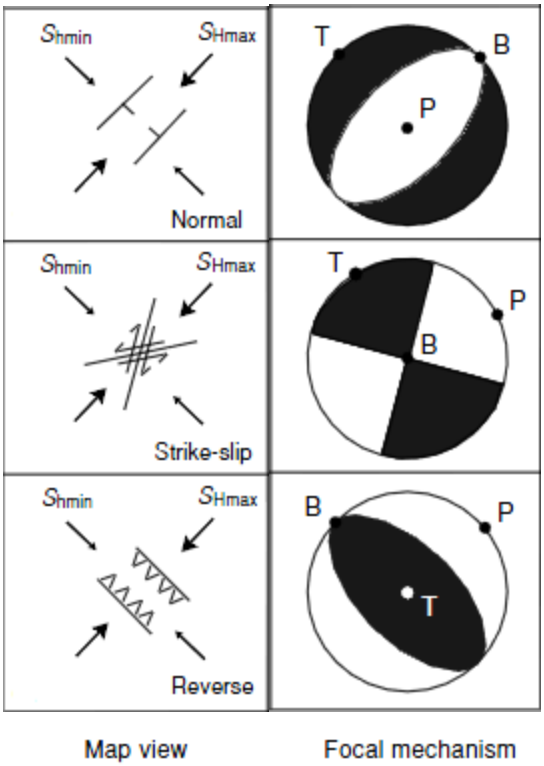

Figure 3.7 Representation of Anderson's classification in the form of earthquake focal mechanism on right. From Zoback (2007)

P and T axes are at 45˚ from the fault plane and B-axis. In a frictionless fault, seismic propagation is not controlled by *insitu* stress but by the orientation of fault (Zobak and Zoback, 2002). Therefore, plate boundary strike-slip faults do not allow determination of principal stress orientation. Stress field can be determined from earthquake focal mechanism using inversion techniques (Reynolds, 2001; Zobzck and Zoback, 2002). Seismic waves radiating as a result of an earthquake can be used to estimate the relative magnitude of stress.

3.7 Seismic (AVO)

`

Principal stresses (S_{Hmax}, S_{hmin} and S_v) and elastic properties of rock can be estimated from investigation of azimuthal velocity and AVO analysis of conventional 3D seismic data (Schmid and Gray, 2011; Gray *et al.*, 2012). Borehole derived measurements provide information of stress change in the vicinity of well and does not propose the lateral and temporal changes. Therefore it is necessary to develop techniques to assess and predict stress regimes with non destructive qualities.

As seismic waves propagate through the rock volume, they cause some strain within elastic limits. Young's modulus and poisson's ratio can be calculated using assumptions described by Gray *et al.*, (2012). These moduli are illustrated as dynamic because they are estimated by high frequency measurement of velocities of elastic waves (Gray *et al.*, 2012). AVO inversion can be used to calculate vertical stress (S_v), through integration which can lead in estimating minimum and maximum horizontal stress. However these calculations should be calibrated with log data, microseismic and regional knowledge (Schmid and Gray, 2011). The combination of these estimates allows for evaluation for hydraulic fractures and geomechanical issues before drilling any well.

Chapter 4

In situ stress of the Cooper Basin

4.1 Introduction

The Cooper Basin is Australia's most proficient onshore basin Fig (4.1). It is northeast-southwest trending basin located in the central Australia, with major part lying in Queensland and other portion lying in South Australia. Since 1963, 229 x 10^9 m^3 (8.2 tcf) of recoverable gas and 6.9*10^6 kL (43.9 mmstb) of recoverable oil have been found in the Cooper basin (Laws and Gravestock, 1998). Largest reserves of Cooper basin are accumulated in the Moomba and Big lake fields. Cooper basin lie beneath the Eromanga basin (Great Artesian Basin) which is Jurasssic to cretaceous in age. Fig 4.1 outlines the boundaries of Cooper and Eromanga basin.

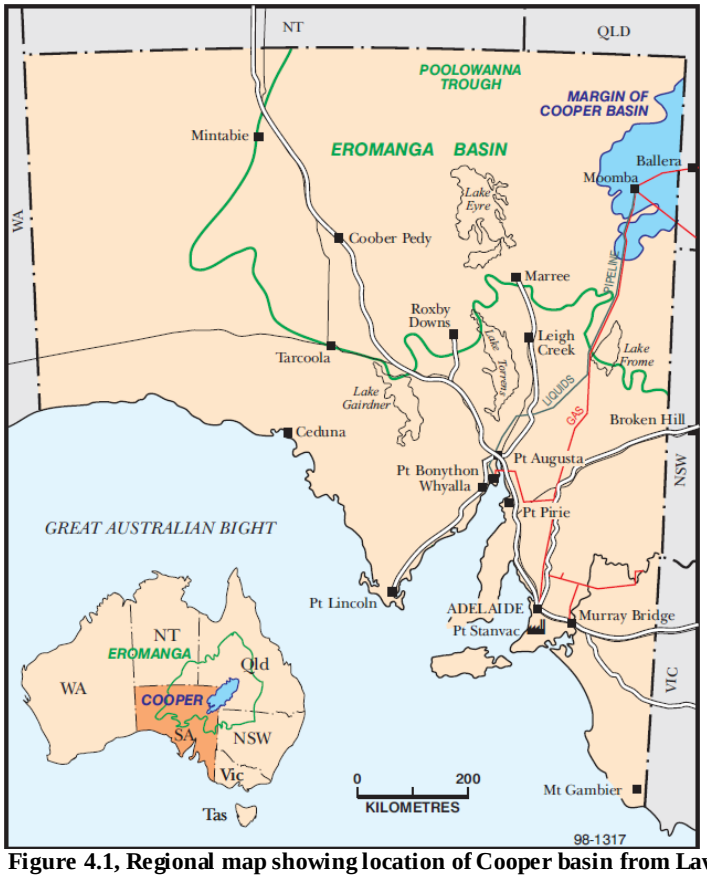

Figure 4.1, Regional map showing location of Cooper basin from Laws and Gravestock (1998).

Exploration history of Cooper basin is more than 40 years, therefore, extensive database is available from Queensland and South Australian sectors of the basin. A significant number of image logs and dipmeter data can be used to interpret stresses in the basin (Reynolds, 2004). The study of *in situ* stress in Cooper basin is very important as many of the hydrocarbon bearing formations are of low permeability therefore need to fracture stimulate to produce at economic rates. The author has used stress magnitude measured by Reynolds *et al.*, (2006) for the well Dullingari North-8 for geomechanical modelling. Hence, this chapter will provide an overview of the stress orientation and magnitude to help the reader understand the change in fracture pattern during hydraulic fracturing.

4.2 Tectonic evolution

Apak *et al.*, (1997) explains tectonic development involves varying amount of uplift and erosion, resulting in major depocenters and ridges. The northwest oriented Karmona-Naccowlah feature divides the cooper basin into southern and northern portions. Prominent northeast trending structures exist in South Australian part of the basin. These structures include two intrabasins highs, the Gidealpa-Merrimelia Innamincka (GMI) and the Nappacoongee Murteree (NM) trends, additionally three main depocenters, the patchwarra, Nappamerri and Tenappera troughs (Fig 4.2).

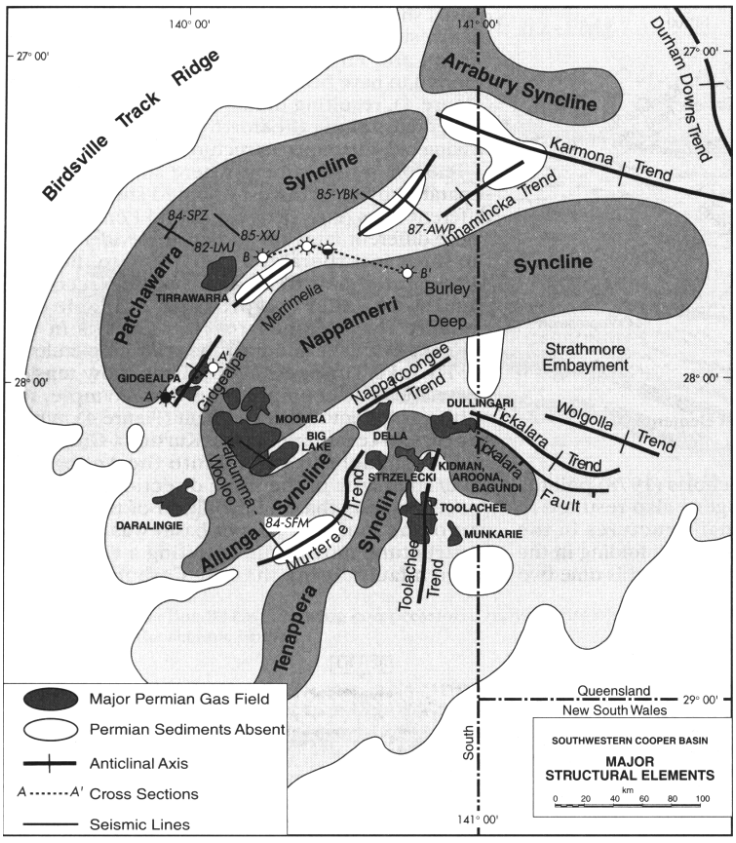

Figure 4.2, prominent structures of Cooper Basin. From Apak *et al.* (1997)

Prior to the formation of Cooper basin, a number of orogenies resulted in intense deformation in the region causing crustal shortening over south-eastern Australia and eastern central Australia, Moreover, stresses were transmitted to the basin area (Apak *et al.*, 1997). The Cooper basin was developed under gentle compressional regime evident from the compressional folds thrust faults, strike-slip movements and inversions within the Permian-Triassic sequences (Apak *et al.*, 1997).

Major structural trends are underlain by features initiated by basement related compresssional regime. Orientation of a number of faults and folds in cooper basin suggest that northeast trending structures were developed in Permian sequence as a result of northwest-southeast or an east-west oriented stress regime (Apak *et al.*, 1997). According to Apak *et al.*, 1997 reactivation of structural lineaments in pre Cambrian had strong influence on basin configuration. Gravestock and Jensen-Schmidt (1998) has divided structural evolution of cooper basin into Pre Permian and late Permian-Triassic with a long period of non deposition after deposition of Daralingie formation.

Apak *et al.*, 1997 propose that Cooper basin is described by high geothermal gradient while basement structures partially controlling the evolution of the basin. Same authors suggest two episodes of tectonic uplift headed by 'gentle down wrapping' followed by tectonic stability.

4.3 *In situ* stress field of Cooper basin

4.3.1 Overview

Extensive drilling in the Cooper basin has provided substantial amount of stress data. Orientation of maximum horizontal stress is approximately east-west in direction with azimuth of ˚108. Stress magnitudes have been calculated by Reynolds *et al.*, (2006). Vertical stress magnitude (σ_v) is equivalent to the overburden of the rock at a particular depth; it is truer for rocks at greater depths (Zoback, 2007). σ_v has been calculated using density and checkshot velocity survey. Minifrac test provide for the magnitude of minimum horizontal stress (σ_{hmin}) indicating magnitude approximately equal to the magnitude of σ_v. Due to variability of σhmin and σv estimates, maimum horizontal stress magnitude can be loosely confined regionally (Reynolds *et al.*, 2006). However it is important to determine stress magnitudes locally (Reynolds *et al.*, 2006). Stress magnitudes in Cooper basin are very complex which vary with depth in subsurface and location in the basin. Reynolds *et al.* (2006) constrains magnitude of principal stresses in Bulyeroo-1 and Dullingari North-8 that illustrate a predominant strike slip-stress regime ($\sigma_{Hmax}>\sigma_v>\sigma_{hmin}$) at depth ranghing from 1 to 3 km. At greater depths strike slip stress regime change into reverse fault stress regime ($\sigma_{Hmax}> \sigma_{hmin}> \sigma_v$) with minimum horizontal stress magnitude reaching equal to the magnitude of vertical stress magnitude. Lateral variation in stress regime is illustrated by Reynolds *et al.* (2004) which depict reverse fault stress regime at shallower depths and strike slip stress regime at greater depths (Fig 4.3).

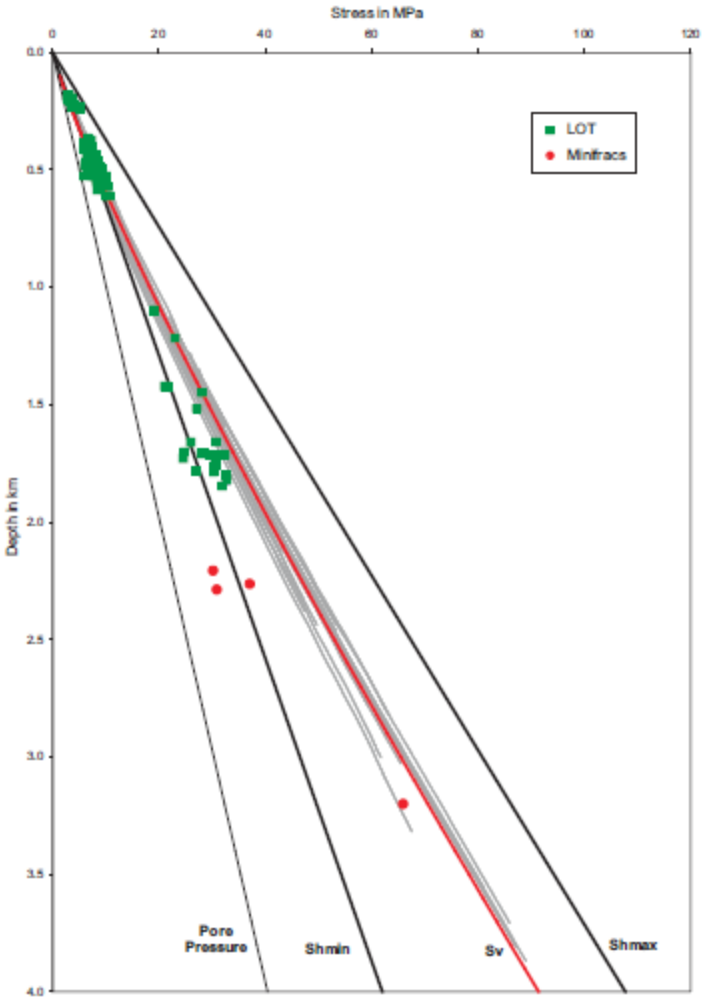

Figure 4.3, Depth Stress plot explaining change in stress regime. From Reynolds *et al*. (2004)

Variation in stress regime can be a serious problem to produce from tight reservoirs of Cooper basin, where a number of hydraulic fractures treatments have failed to provide significant results. The fracture propagation is controlled by stress regime and the perturbation in stress field due to fractures and faults.

4.3.2 Stress Orientation

Reynolds *et al.,* (2005) used datasets from 61 wells to interpret the orientation of maximum horizontal stress. It uses wells ranked A to C quality determined by World Stress Map (WSM) project ranking scheme. The average σ_{Hmax} orientation from all wells determined by borehole breakouts and Drilling induced tensile fractures (DITF) is 101. Geologic and geomorphologic features also affect trend of σ_{Hmax}. Stress data from Patchawarra trough indicate southeast-northwest orientation. σ_{Hmax} direction at GMI rigde is west-northwest which changes to east-west at Nappamerri trough (Fig 4.2).

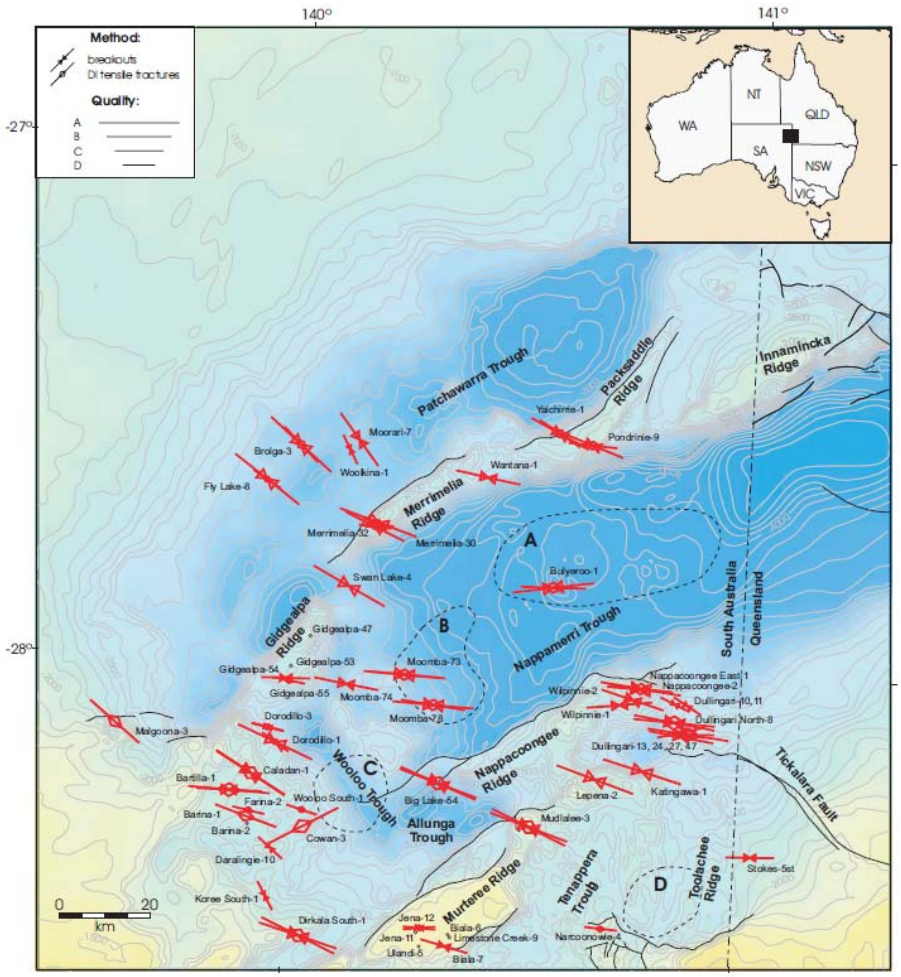

Figure 4.4, Map representing orientation of maximum horizontal stress in th Cooper basin.

The systematic clockwise rotation of $\sigma_{H\,max}$ orientation is part of regional rotation across the Australian continent (Reynolds *et al.*, 2005; Hills *et al.*, 1998). North-south oriented maximum horizontal stress in the Amadeus basin corresponds to the Tennant Creek earthquake. In the north-east of Cooper basin, σ_{Hmax} is north-northwest to south-southeast in Bowen basin which is consistent for 500 km (Reynolds *et al.*, 2005). Therefore, Cooper basin appears to be at the apex of the regional $\sigma_{H\,max}$ rotation which provides an evidence for regional rotation of stress field across the continent.

4.3.3 Stress Magnitudes

Vertical stress magnitude

A stress from the weight of overlying rock is directed in a vertical direction due to gravity. It is known as overburden stress or vertical stress. Density log can be used to determine vertical stress (σ_v). Fig 4.3 shows vertical stress magnitude calculated by Reynolds *et al.*(2004). This data gives an average

approximate of vertical stress across the basin and show no unusual deviation from the trend (Reynolds *et al.,* 2004; Reynolds *et al.,* 2006).

Vertical stress gradient in Cooper-Eromanga basin is around 20MPa/Km (Hills *et al.,* 1998). As shown in Fig 4.3, vertical stress is intermediate stress at greater depth but at shallow depth minimum horizontal stress approach the magnitude of vertical stress causing the stress regime to change from strike slip to reverse fault stress regime.

Minimum horizontal stress magnitude

The minimum horizontal stress in a basin can be determined by minifrac and leak-off tests. Minifrac, which is a type of hydraulic fracture, is more authentic method to determine minimum horizontal stress in a basin. A fracture is created pumping fluids at high pressure, causing the fracture to propagate in the direction of minimum horizontal stress. Details of the process are provided in section 3.4.

Reynolds *et al.* (2006) illustrates two minifrac tests conducted in Daralingie formation and one each in Toolachee formation and Nappameri Group. The minimum horizontal stress magnitude is estimated by a linear relationship, 20.5 MPa/Km. Similar authors propose that the magnitude of minimum horizontal stress is controlled by lithology and the mechanical stratigraphy of the basin effects stress magnitudes.

In Dullingari North-8 and Bulyeroo-1, minifrac tests elucidate that minimum horizontal stress is less than the vertical stress defining stike slip stress regime ($\sigma_{Hmax}>\sigma_v>\sigma_{hmin}$) at a depth of 1 to 3 km. Minifrac tests also indicate that minimum horizontal stress may be as high as vertical stress such that stress regime is at the border of strike slip and reverse fault stress regime ($\sigma_{Hmax}> \sigma_{hmin=} \sigma_v$). Differential stress ($\sigma_{Hmax} - \sigma_{hmin}$) in Cooper basin is high (50 MPa at 2.8 km).

Maximum horizontal Stress

Reynolds *et al.,* (2004 and 2006), estimate magnitude of maximum horizontal stress using frictional limit to stress with hydrostatic pressure being constant. Variation in the amount of minimum horizontal stress (σ_{Hmax}) and vertical stress limits the calculation of maximum horizontal stress on the basin scale (Reynolds *et al.,* 2006). σ_{Hmax} is the highest principal stress throughout the basin and is not affected by either stress regimes (strike-slip and reverse fault).

As vertical stress does not have a linear relationship with depth, estimation of maximum horizontal stress is also not linear (Reynolds *et al.,* 2006). The upper bound magnitude of $\sigma_{H\,max}$ in Dullingari North-8 is 41.1 MPa/Km and 38.6 Mpa/Km in Bulyeroo-1 using friction limit Reynolds *et al.* (2006).

The *insitu* stress field of Cooper basin is considered to be as a result of complex interaction of tectonic elements surrounding the Australian plate transmitted to the Cooper basin through high strength upper crust (Reynolds *et al.,* 2006). However, stress field is disturbed by local geologic features (Reynolds *et al.,* 2006) which can change the magnitude and orientation of principal stresses locally and affect the final result.

Chapter 5

Geomechanical modelling

5.1 Introduction

Unlike Indo-Australian plate, most continental areas such as Western Europe, South America and North America exhibit $\sigma_{H\,max}$ orientation parallel to the absolute plate velocity (Zoback *et al.,* 1989; Reynolds; 2001; Reynolds, 2005). Most researchers believe that plate boundary forces are the primary control on the character of the first order intra plate stress field (Zoback *et al.,* 1989). A brief explanation of *insitu* stress field in Cooper basin in the previous chapter suggest that plate boundary forces put forth first order control on the intraplate stress field, however; local geologic structures such as faults, fractures and salt domes highly perturb the stress patterns around (Luo *et al.,* 2012). Knowledge of disturbance in stress field around these structures is vital for stability of the well and economic production from reservoir.

Tight reservoirs need to be hydraulically fractured to flow at economic rate. For a successful fracture treatment, fractures may grow tens of meters and perhaps encounter a natural fracture. The fracture stimulation treatment may cause shear movement on the natural fracture if the natural fracture is critically stressed. Shear movement on natural fractures can be associated with an increase in production. Therefore, understanding these stress perturbations is very important. Geomechanical modelling of such geologic structures can reveal important information helpful to develop an oil and gas field more competitively. Finite element modelling (FEM) and boundary element modelling (BEM) are two approaches used for the purpose.

This thesis uses *Poly 3D* software which is based on the boundary element method. This chapter provides an introduction to BEM and includes stress modelling results in the form of plane view and line plots. The modelling results represent that the local stress perturbation can be a function of fault size, lithology and $\sigma_{H\,max}$ azimuth. This approach allows evaluation of a very large number of models and quantitative assessment of stress disturbance around the fault tips. It is worth emphasizing that the primary aim of the project is to predict and quantify abnormal stress change at the fault tips using the limited knowledge of stress. The study also presents extent of fault size after which stress perturbation is negligible. The conclusions from the study are limited to the average rock properties of rocks such as Poisson's ratio and young's modulus. Poisson's ratio and young's modulus vary laterally and vertically which will affect the ability of a fracture to propagate during hydraulic fracturing.

Geomechanical modelling helps to understand fluctuation in magnitude at the fault tips and facilitate predicting the orientation of possible shear fractures in the zone of concentration of stress.

5.2 Modelling Approach

5.2.1 Boundary element method (BEM)

The possible magnitude of minimum horizontal stress was predicted using Schlumberger's stress simulation package *Poly 3D* based on boundary element method (BEM). BEM is a numerical method used by engineers for modelling purposes. It is prominent that BEM offers distinctive advantages in simulation. For example it lessens the spatial dimension of the problem, preserving high accuracy (Pecher and Stanislav, 1996; Fu, 2006). It provides much better results compared to other numerical modelling methods (Pecher and Stanislav, 1996). Furthermore, it represents a quasi-infnite domain in terms of internal surface geometry and boundary conditions; hence, we can model rock volume as an infinite or semi-infinite elastic mass (Lorig and Brady; Thomas, 1993).

The boundary element method has been part of mathematical literature for a long time but had never applied to computer geomechanical simulation until research efforts at Stanford University (Pecher and Stanislav, 1996). The study was formulated in form of a computer program namely Poly 3D by Thomas (993) which helps to get precise solution of stress and strain estimated at observation points in the surrounding volume using linear elastic properties (Swyer and Davatzes, 2012).

It efficiently computes 3D loading conditions representing any tectonic regime.

5.2.2 Poly 3D

Thomas (1993) states, "*Poly3D is a C language computer program that calculates the displacements, strains and stresses induced in an elastic whole- or half-space by planar, polygonal-shaped elements of displacement discontinuity*." A geological surface is divided into small polygonal elements across which the discontinuity is in displacement is assumed constant (Thomas, 1993). Polygonal elements may have minimum of 3 sides as used in this thesis (Fig 5.1). The user can select the number of elements to divide a fault or fracture. These polygonal elements can be used to model complex geologic structures with bending surfaces (Thomas, 1993). Faults having different strike and slip can be modelled without gaps. The surface of the fracture as a result of hydraulic fracturing can also be meshed using *Poly 3D* (Thomas, 1993). The sensitivity to results is achieved due to individual role of the polygonal elements.

In *Poly 3D*, traction on an element is defined through determining any remote stress in addition to the total stress field induced by all polygonal planes on the element plane (Thomas, 1993). The element

plane collectively forms an observation grid, which is defined as a series of equally spaced observation points and instructs Poly 3D to estimate stress, strain and displacement at individual points.

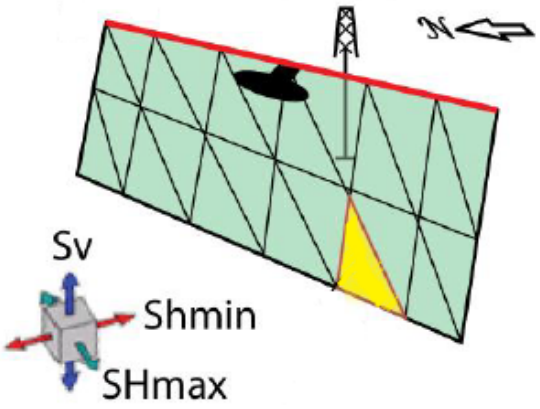

Figure 5.1 Modified from Swyer and Davatzes (2012). A geological surface divided into triangular polygonal elements

.

5.2.3 Model information

A significant number of simulations were created using Poly 3D with varying fault size ranging from 100 to 2000 meters. Each model consists of constant volume and rock properties with varying length of faults. To prevent any perturbation of stress due to model edges, the edge of the model was kept 200 meters from the fault top. Therefore, models with fault length 1900 and 2000 meters have model length of 2100 and 2200 meters.

The simulation grid is divided into small triangular segments, each segment acting as individual element when running the simulation. Each model consists of a near vertical strike-slip fault and two observation grids (Fig 5.3a). One encompassing the fault; displays stress change across the entire fault length while second observation grid depicts stress variation at the fault tips (Fig 5.3a). The former observation grid consists of 400 nodes and later is composed of 40 nodes, while both having similar number of nodes (20) on X axis. Change of fault size does not affect the model as the number of nodes on horizon is always constant.

The far field stress magnitude used for the simulation purpose was extracted from Reynolds *et al.* (2006). In the Cooper basin a strike-slip stress regime prevails from 1 to 3 km. Therefore, the magnitude of stresses used in simulations represent strike-slip stress regime. Three depth points models magnitude of $\sigma_{H\,max}$, σ_{hmin}, σ_v and pore pressure (Pp) taken from Reynolds *et al.* (2006) as per

table 5.1. Separate models using similar amount of stress data were created for Sandstone, Shale and Coal.

Each model with different lithology was further with the azimuth between fault and $\sigma_{H\,max}$ of 0˚, 5˚, 15˚, 30˚, 45˚, 60˚ and 90˚. All models were assigned an average Young's modulus and Poisson's ratio as per lithology assuming no change in elastic properties of rocks throughout the model. Simulation results vary not only with lithology but also as we change the angle between the fault and $\sigma_{H\,max}$. A comprehensive tree explaining the structure of model formulation is described in Fig 5.2.

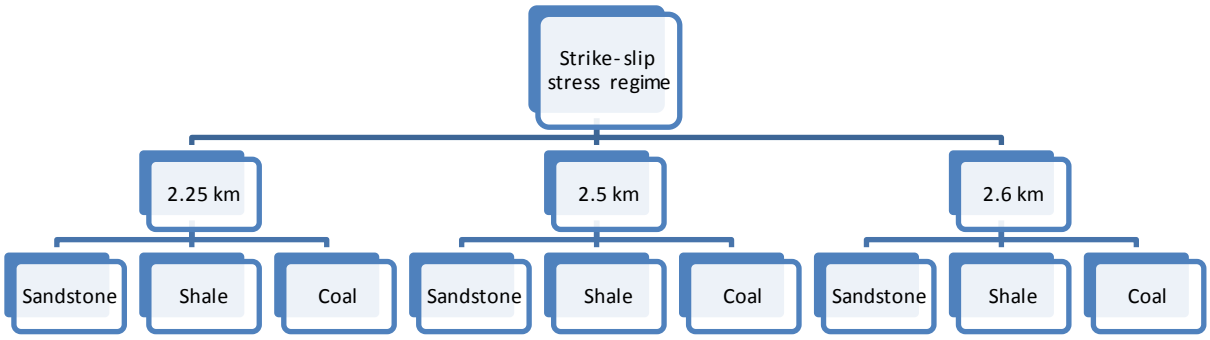

Fig 5.2, Tree representation of modelling paradigm. N.B each lithology is further divided into seven different models with 0, 5, 15, 30, 45, 60 and 90 as σ_H azimuth.

Stress magnitude for each depth is compiled in table 5.1. The stress magnitude in the Cooper basin has high differential stress, around 50 MPa (Reynolds *et al.*, 2006). Data represented in table 5.1 is evident of elevated stress in the upper crust responsible for the transfer of stress intraplate (Reynolds, 2001; Reynolds *et al.*, 2006). Poisson's ratio for Sandstone, Shale and Coal is 0.24, 0.14 and 0.35 respectively while Young's modulus used in these simulations for Sandstone, Shale and Coal is $2.2*10^{6,}$, $2.8*10^{6}$ and $5*10^{9}$ Pascals respectively.

Depth (Km)	**Stress Magnitude (MPa)**			
	Maximum horizontal stress	Minimum Horizontal stress	Vertical stress	Pore pressure
2.25	62	32	47	20
2.5	100	50	55	22
2.6	110	52	58	24

Table 5.1, Tabulation of stress magnitudes utilized in the simulations.

It should be noted that the faults in these simulations are hypothetical, but certainly realizable. Use of fault is intended is to understand the abrupt change of stress across the fault. Therefore, these models are not only applicable in the Cooper basin but may also serve as analogue to understand stress behaviour across faults worldwide.

5.3 Modelling Results

Examination of results from the model runs indicated that stress variation is the function of lithology, σ_H azimuth and fault size. Each of the factors has its impacts on stress perturbation. Therefore, the impact of each of these properties is presented in a separate section.

According to Gudmundsson (2000), stress concentrates in two quadrants on the opposite ends of fault tips. Simulation results presented in this thesis align with the hypothesis of Gudmundsson (2000). The *Poly 3D* results are displayed in two forms. One, map view of minimum horizontal stress magnitude (S_{hmin}) depicted in colour with vectors determining the orientation of S_1. Second, a graphical representation in the form of line plot explaining abrupt change in stress magnitude across fault tips. The dark line passing through fault tip is the smaller observation grid. Following sub sections represent outcomes of the model run on the basis of above give criteria.

5.3.1 Lithology

Each Lithology used in modelling has average elastic modului. Therefore, no lateral variation due to change in rock properties is expected. Fig 5.3a, 5.4a and 5.5a represent model run with Sandstone, Shale and Coal as the candidate for hydraulic fracture treatment. Each model is composed of an absolute scale representing minimum horizontal stress (Shmin).For the sake of demonstrating the variation due to litholgy; fault size and stress magnitude is kept constant. Models 5.3a, 5.4a and 5.5a represent minimum horizontal stress at 2.5 km depth and fault size 600 meters.

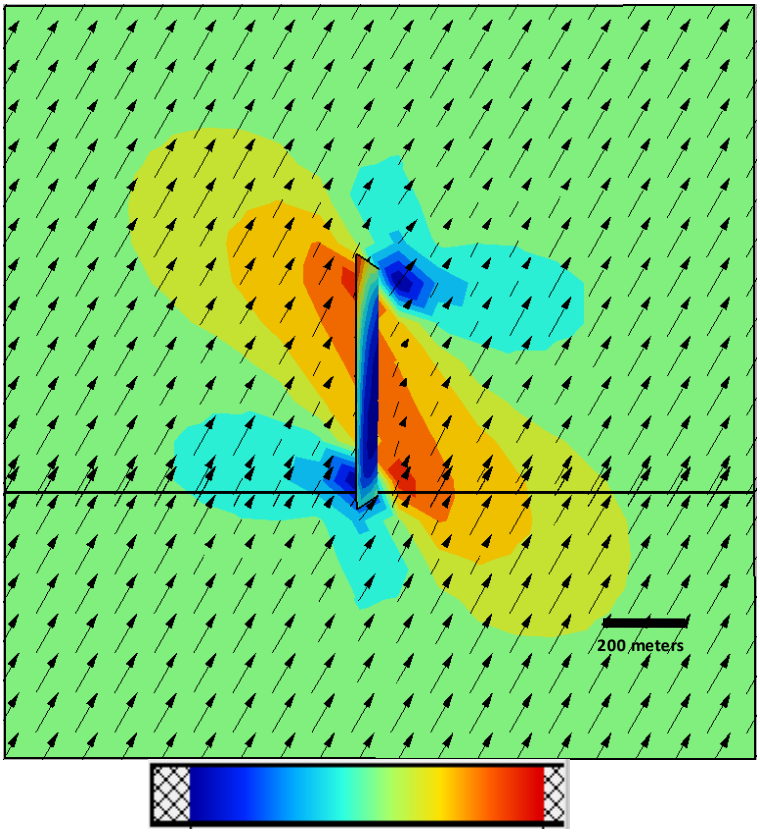

Fig 5.3 Plane view near of vertical fault representing minimum horizontal stress (S_3) in colour contours, with vectors depicting orientation of S_1 shale at 2.5 km azimuth 30° fault 600.

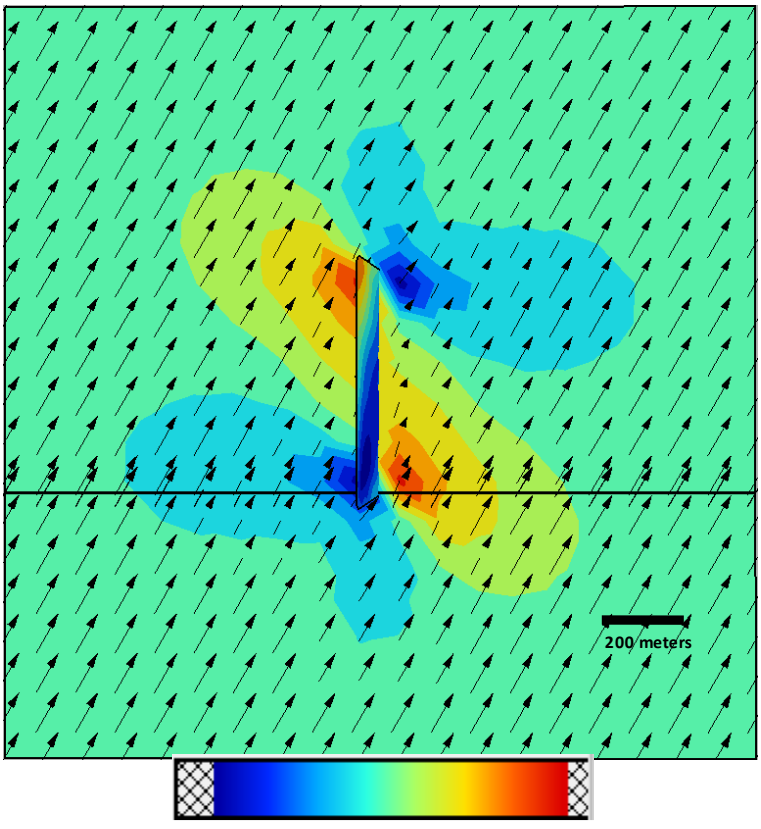

Fig 5.4 Plane view near of vertical fault representing minimum horizontal stress (S_3) in colour contours, with vectors depicting orientation of S_1 for Coal at 2.5 km σ_H azimuth of 30° and fault length of 600 meters.

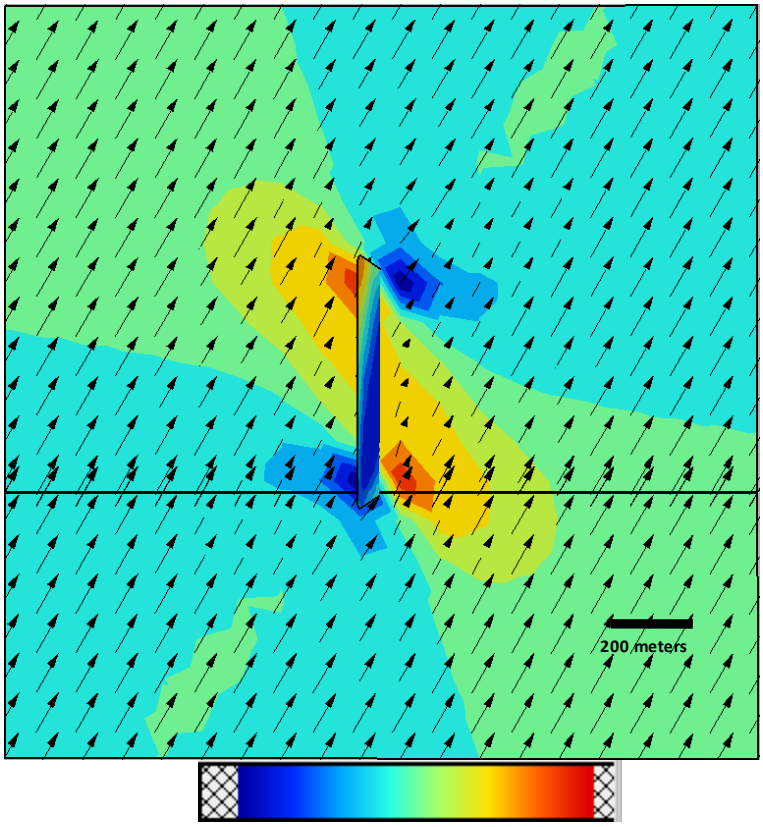

Fig 5.5 Plane view near of vertical fault representing minimum horizontal stress (S_3) in colour contours, with vectors depicting orientation of S_1 for Sandstone at 2.5 km σ_H azimuth of 30° and fault length of 600 meters.

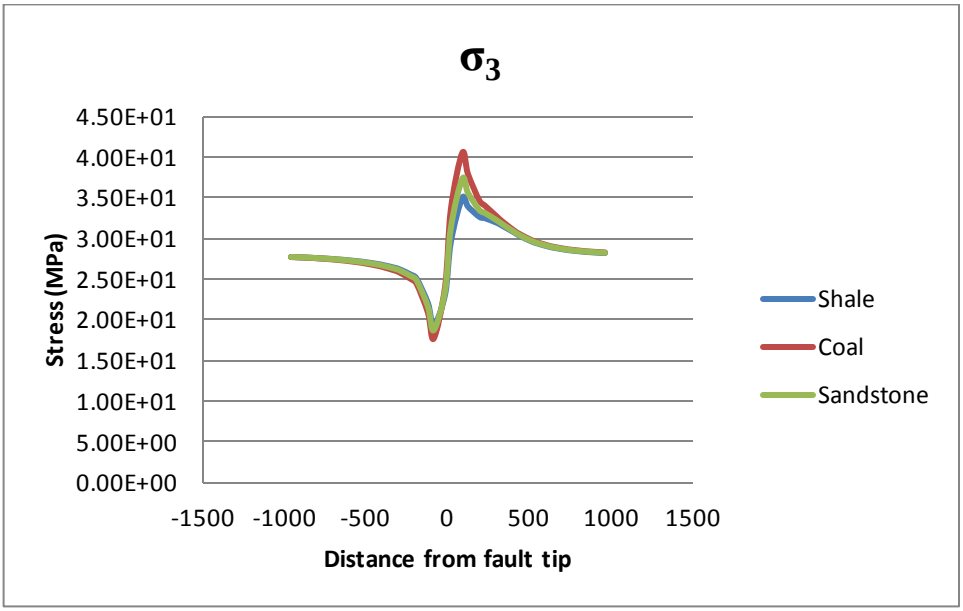

Fig 5.6, graphical representation of rapid change in stress magnitude of minimum horizontal stress (S3) at the fault tip for Shale, Coal and Sandstone at 2.5 km σ_H azimuth of 30° and fault length of 600 meters.

These results indicate prominent change in stress across the model with change in lithology. Difference in distribution of stress field is observed clearly, sandstone being able to distribute stress far away from the fault compare to Coal and Shale. Similar simulations with different lithology and stress magnitudes are compiled in Appendix A.

Fig 5.6 is line plot for Shale, Coal and Sandstone that correspond to smaller observation grid (black line in simulation model crossing through the fault tip).

5.3.2 σ_H azimuth

Tectonic stresses influence the orientation of geologic structures, therefore effect of direction of maximum horizontal stress is analysed by changing σ_H azimuth. Fig 5.7, 5.8 and 5.9 represent simulations with orientation of maximum horizontal stress (σ_{Hmax}) of 5, 45˚and 90˚. To purely explain the effect of angle change, presented simulations utilize magnitude to stresses at 2.5 km depth within shale with fault size 1000 m.

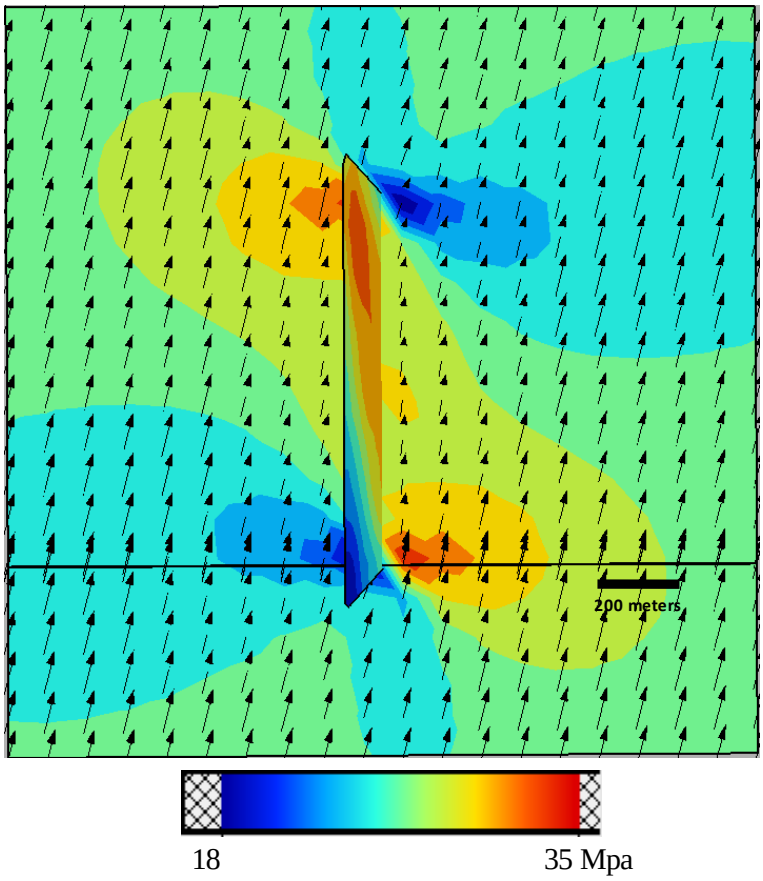

Fig 5.7 Plane view near of vertical fault representing minimum horizontal stress (S_3) in colour contours, with vectors depicting orientation of S_1 for Shale at 2.5 km σ_H azimuth of 15˚ and fault length of 1000 meters.

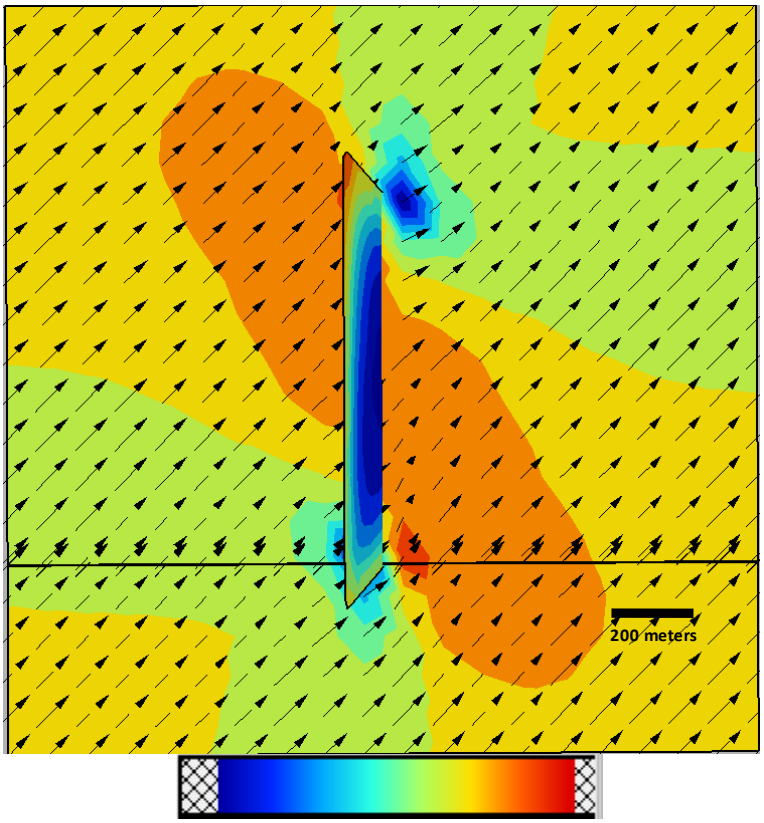

Fig 5.8 Plane view near of vertical fault representing minimum horizontal stress (S_3) in colour contours, with vectors depicting orientation of S_1 for Shale at 2.5 km σ_H azimuth of 45° and fault length of 1000 meters.

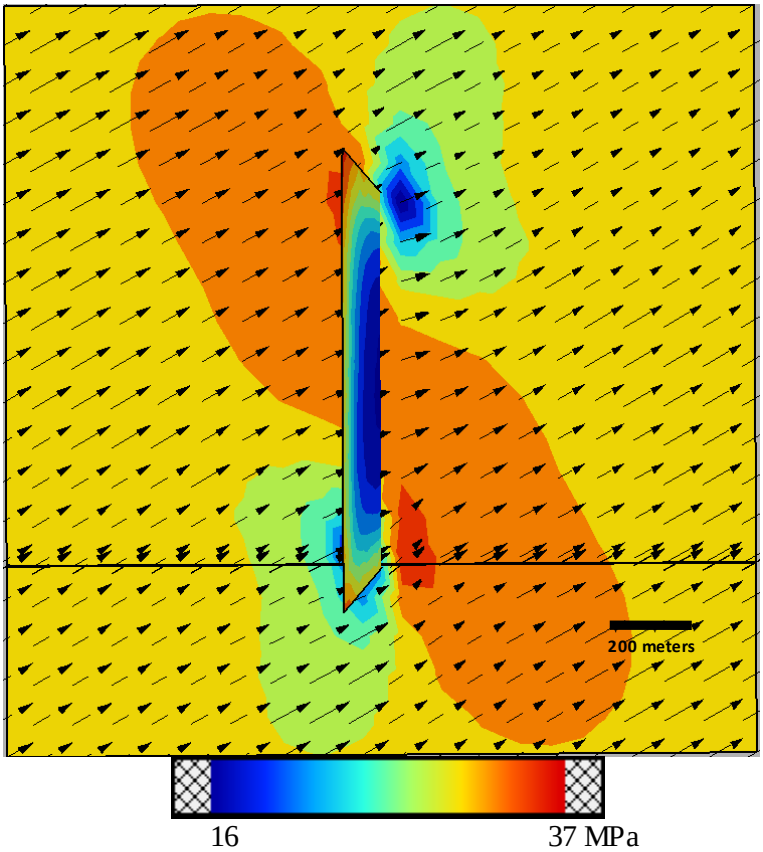

Fig 5.9 Plane view near of vertical fault representing minimum horizontal stress (S_3) in colour contours, with vectors depicting orientation of S_1 for Shale at 2.5 km σ_H azimuth of 60° and fault length of 1000 meters.

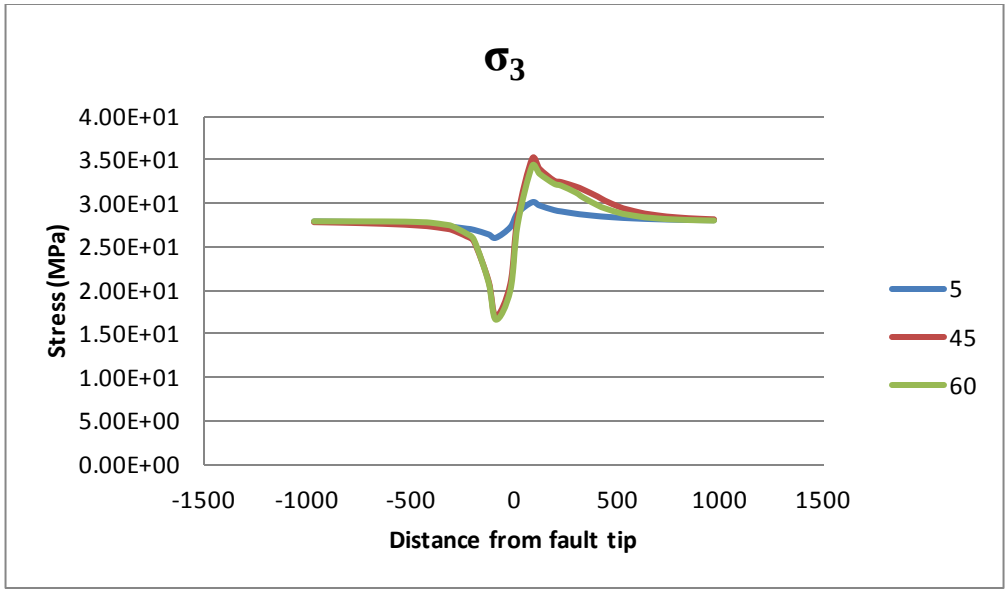

Fig 5.10, graphical representation of rapid change in stress magnitude of minimum horizontal stress (S_3) at the fault tip for σ_H azimuth of 5˚, 45˚ and 60˚ at 2.5 km in Shale and fault length of 600 meters.

Fig 5.10 correspond to simulations anticipating stress varaition at the fault tips. It was observed that maximum stress perturbation exist when σ_H angle is 45˚. Similar reseults were observed at different depths within Sandstone and Coal. Graphical representation of these results is compiled in Appendix.

5.3.3 Fault size

Fault size with fault poulation in a reservoir control the orientation of fracture development (Zoback, 2007). Therefore, a detailed analysis is carried out estimating stress perturbation due to change in fault size. As demonstrated in the previous sub sections, litholgy and σ_H azimuth influence the stress disturbance around fault tips; both parameters are reserved stable. Fig 5.11, 5.12 and 5.13 represent change in stress magnitude at 2.25 km depth within shale at σ_H angle of 0˚, 30˚ and 60˚.

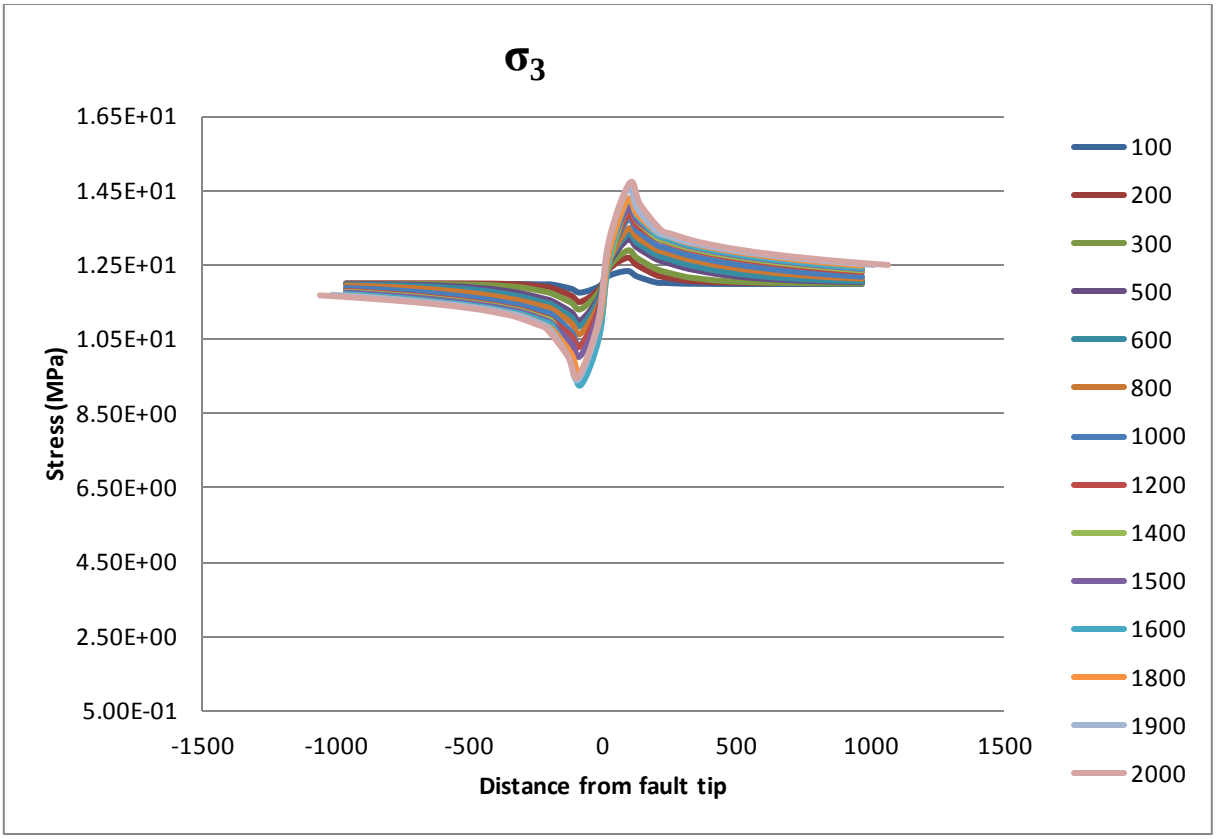

Fig 5.11, Stress concentration at fault tips in Shale at 2.25 km depth, σ_H azimuth 5°

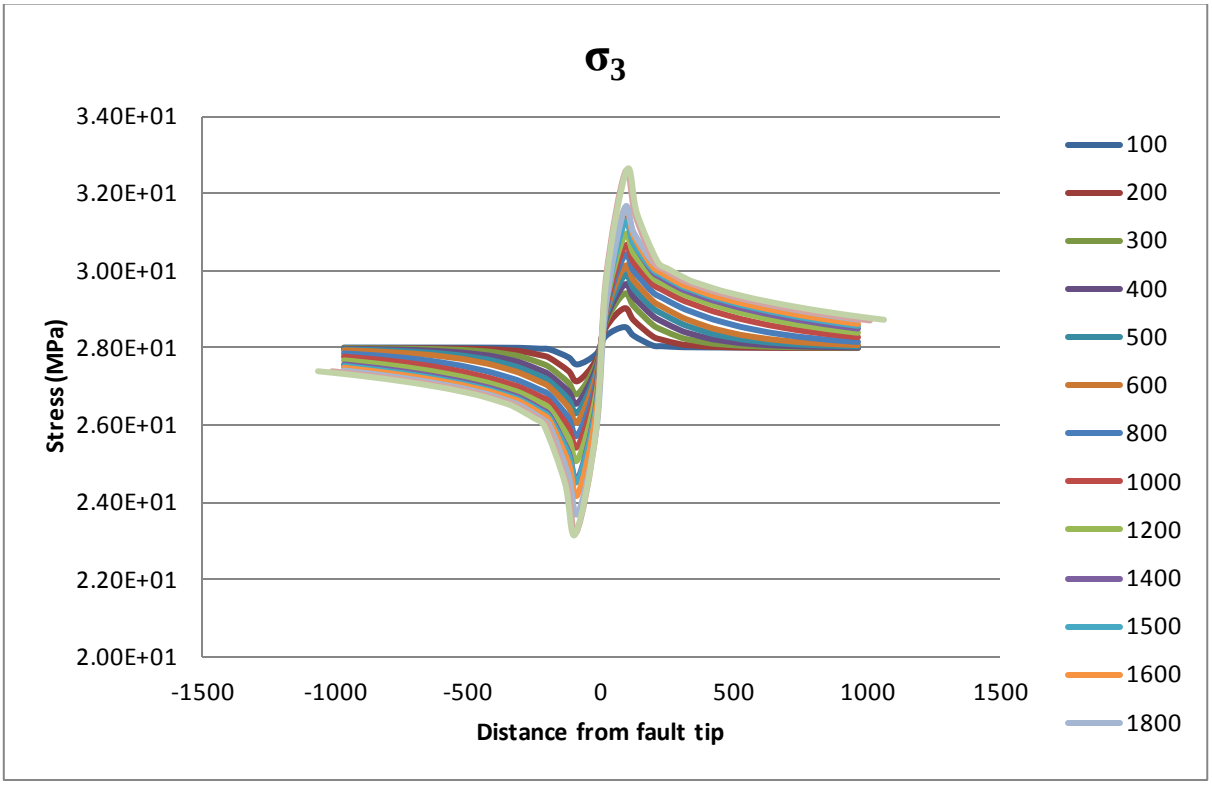

Fig 5.12, Stress concentration at fault tips in Shale at 2.5 km depth, σ_H azimuth 5°

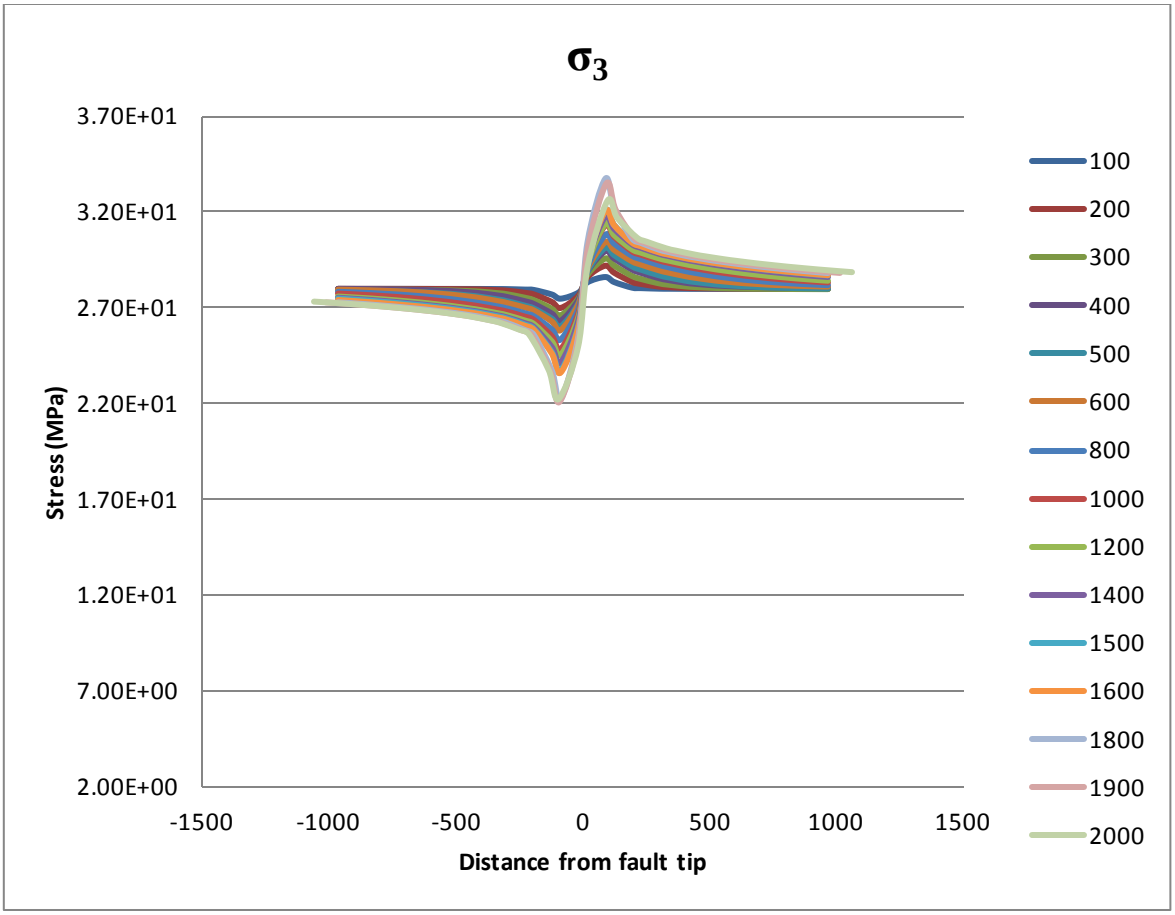

Fig 5.13, Stress concentration at fault tips in Shale at 2.6 km depth, σ_H azimuth 5°

5.4 Discussion

Results presented in this thesis are broadly similar to previous studies (Nicol *et al.*, 1996; Homberg *et al.*, 1997; Gudmundsson, 2000; Bourne and Willemse, 2001; Kattenhorn and Marshall, 2005). However significant differences also exist, that are discussed in this section. Orientation of principal stresses can be affected by local geologic structures and rock properties (Reynolds *et al.*, 2005; Zoback, 2007). If no shear stress exists at the boundary, principal stress may align themselves parallel or perpendicular to the orientation weak planes (Zoback, 2007). Re-orientation of maximum horizontal stress vectors (S_1) near the fault can be observed from the simulation results (Fig 5.14). Therefore, fractures as a result of hydraulic fracturing treatment will change their orientation affecting production from the well bore.

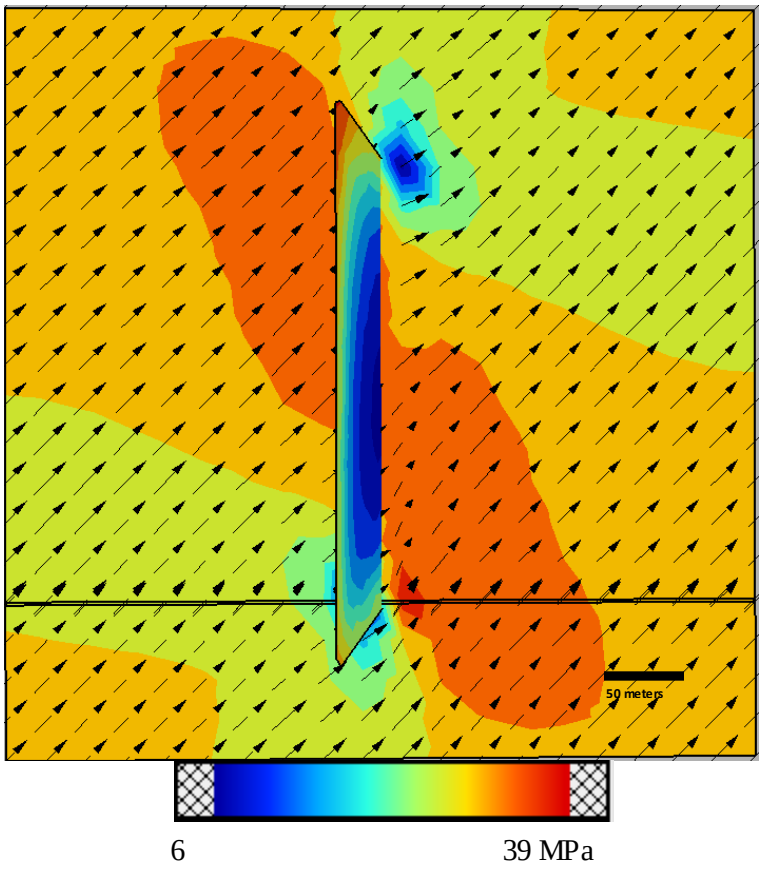

Fig 5.14, Stress concentration at fault tips in Shale at 2.5 km depth, σ_H azimuth 45° with horizon length of 500 meters fault size 300 meters

A general observation in all models is the concentration of stress at the fault tips in opposite quadrants of the fault. Therefore, fault tips can be divided into four quadrants; two compressional and two extensional (Fig 5.3). Near the fault tips, stress vectors appear to align in a different orientation compare to the far field stress direction. According to Kattenhorn and Marshall (2005) stress field at the fault tip is greater than the magnitude and different in orientation than regional stress and may lead to fractures if tensile strength of rock is reached. . Vectors in Fig 5.3 do not appear to diverge from the trend because spacing between two observation points is 200 meter. However, in fig 5.14 spacing in observation points is 25 meter, therefore; S_1 vectors show a prominent change in orientation. Deviation of stress orientation is consistent in every model and is influenced by the orientation of far field stress. Failure planes indicated in the simulations represent points where faults may initiate. However, the orientation of fractures is a function of σ_H azimuth and elastic properties of rock matrix.

Each lithology has different elastic moduli that affect the magnitude of closure pressure. Cooke (2011) explains the importance of Poisson's ratio in measuring the magnitude for closure pressure. Change in magnitude of $\sigma_{h\,min}$ can affect the propagation of fractures. Hence, elastic moduli affect the ability of rock to transfer stress, thus orientation of fractures. Moreover, more brittle lithologies tend

to fracture easily compare to relatively ductile formations (Lorenz *et al.*, 1991). *Poly 3D* models possible orientation of shear fractures. Sandstone being most brittle of the presented lithologies, fractures more easily with high number of fractures compare to shale and Coal. Coal usually have weak planes (cleats) and has some influence on the fractures during fracture stimulation treatment. Though the orientation of fracture created during the treatment is mainly controlled by *insitu* stress. Coloured contours in figures represent minimum horizontal stress while the vectors determine the orientation of maximum horizontal stress. S_1 vectors indicate propagation in the direction of σ_{Hmax} while the fractures open in the direction of S_3. Elastic moduli used in these models are static but this is not the case in actual practice. Rock properties vary laterally and vertically (King, 2010). However, for the purpose of developing understanding of the behaviour of stress static properties can be used. A number of authors (Reynolds, 2001; Cooke, 2011; Swyer and Davastez, 2012) have utilized averagerock properties for geomechanical modelling.

Homberg *et al.* (1997) explains the relation of σ_H azimuth and strike of geologic structure. As the orientation of maximum horizontal stress is changed, it influences the concentration of stresses at the fault tips. Stress distribution illustrated in Figures 5.7, 5.8, 5.9 and 5.10 are in good agreement with those predicted by Homberg *et al.* (1997). For the sake of argument σ_H azimuth of 15˚, 45˚ and 60˚ are presented in the figures. It should be noted that stress perturbation is symmetrical relative to the centre of fault. The vectors for maximum horizontal stress appear to align themselves according to the orientation of the fault. Largest perturbation is encountered at the angle of 45˚. If a faulted reservoir is hydraulically fractured, σ_H azimuth shall change locally with pre existing faults and fractures which will serve as barrier for economical production. Thus, fracture stimulation will not be considered to be successful.

The third criteria used for simulation purpose the fault size (5.11, 5.12 and 5.13). Detailed analysis of faults depicts rapid change in stress magnitude at fault tips as proposed by previous authors. However, author has made an attempt to predict the fault size in a given geologic condition after stress perturbation is constant and is not the function of fault size. Figure represents line plots for stress perturbation with fault sizes ranging from 100 meters to 2000 meters. It was observed; increase in size of fault results in increase in perturbation of stress at the fault tips. The fluctuation is prominent in the models with smaller size of faults (100-1000 meters). Line plots start to come close after 1000 meters and the amplitude of stress change is not very significant after fault size of 1500 meters (Fig 5.15 Fault vs stress).

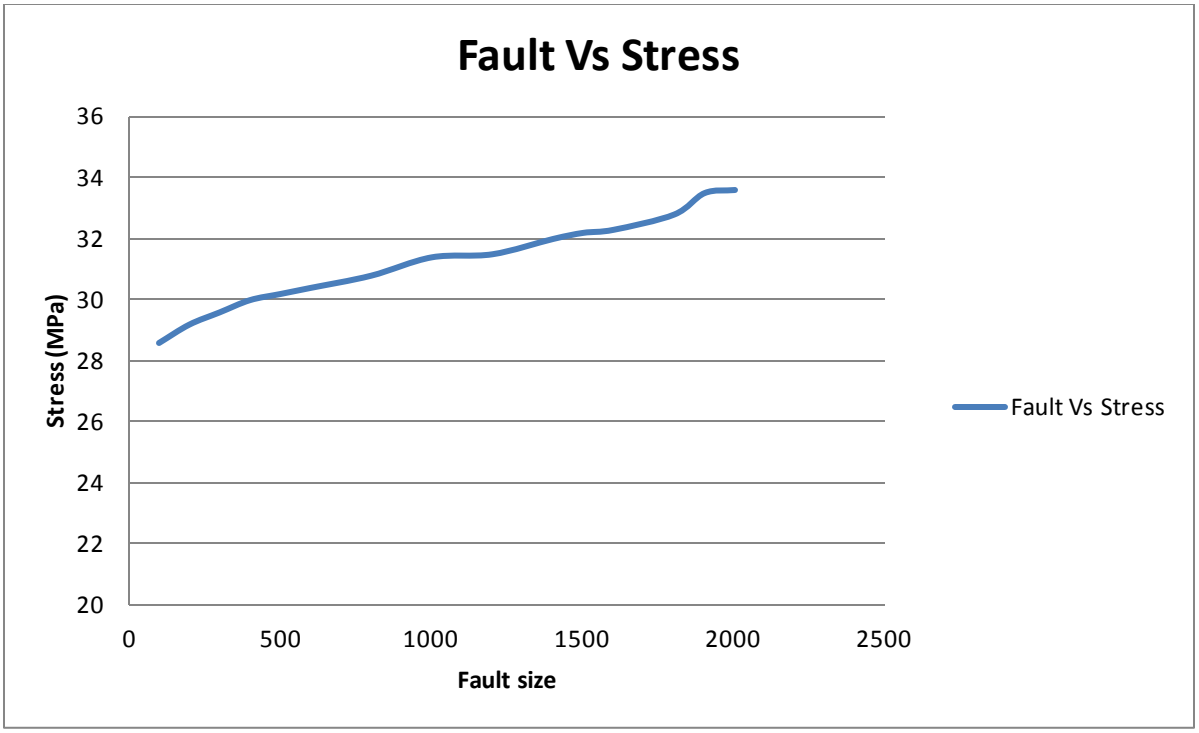

Fig 5.15, An analysis of Fault size with Stress.

Similar trend was observed in all models. However, the magnitude of stress perturbation is function of lithology and orientation of maximum horizontal stress. Fault size can be predicted from the seismic survey and using that fault size in such models can help to determine critically stressed areas around the fault. This practice may help fracking engineer to develop a good understanding of local stress disturbance in subsurface leading to a successful fracture treatment. It is obvious that fractures created due to fracture stimulation will intersect such faults in a reservoir. Critically stressed faults may aid to the production, therefore, such models allow.

Chapter 6

Concluding statement and recommendation

6.1 Concluding Statement

A number of studies have been carried out to understand the variation in production resulting from not so successful hydraulic fracturing treatments. Production from unconventional reservoirs particularly shale gas from world's known reservoirs is unpredictable due to various factors explained by (King, 2010; Cooke, 2011). Shale gas targets in Cooper basin are also subjected to similar problems like Barnett Shale and Haynsville Shale.

The detailed analysis of models has led to greater understanding of distribution and abrupt change in stress field at the fault tips. The simulation uses real stress magnitudes estimated by Reynolds *et al.* (2006). This study represents few of the geomechanical factors responsible that can affect the variation in production from a faulted reservoir. Fractures resulting from hydraulic fracture treatment have height of several hundred feet; therefore, it is obvious to encounter faults.

Stress is concentrated in two opposite quadrants of the fault at the fault tips. Abrupt change in magnitude can influence the orientation of fracture during fracture treatment. Fault size play an important role in determining change in magnitude. Stress perturbation increases with increase in fault size. However, line plots depict that stress magnitude is not large when fault size reaches around 1500 meters.

6.2 Recommendations

This study of stress distribution leads to following recommendations

- Actual subsurface rocks have varying elastic properties. An analysis using dynamic rock properties should be carried out to mimic the subsurface more accurately.

- Layered models with different combination of lithologies need to be modelled.

References

APAK, S. N., STUART, W. J., LEMON, N. M. & WOOD, G. 1997. Structural Evolution of the Permian–Triassic Cooper Basin, Australia: Relation to Hydrocarbon Trap Styles. *AAPG Bulletin,* 81**,** 533-555.

BAIHLY, J. D., MALPANI, R., EDWARDS, C., HAN, S. Y., KOK, J. C. L., TOLLEFSEN, E. M. & WHEELER, C. W. 2010. Unlocking the Shale Mystery: How lateral Measurements and well placement impact completions and resultant production.

BARTON, C. A., MOOS, D. & ZOBACK, M. D. November 1997. In-situ stress measurements can help define local variations in fracture hydraulic conductivity at shallow depth. *The leading edge.,* November.

BARTON, C. A. & ZOBACK, M. D. 2002. Discrimination of Natural Fractures From Drilling-Induced Wellbore Failures in Wellbore Image Data—Implications for Reservoir Permeability. *SPE Reservoir evaluation and engineering*.

BELL, J. S. June 1996. Petro Geoscience 1. In Situ Stress in Sedeimentary rocks (Part 1): Measurement Techniques. *Geoscience Canada* 23**,** 85-100.

BELL, J. S. September 1996. Petro Geoscience 1. In Situ Stress in Sedeimentary rocks (Part 2): Measurement Techniques. *Geoscience Canada,* 23**,** 135-153.

BELL, J. S. & GOUGH, D. I. 1979. NORTHEAST-SOUTHWEST COMPRESSIVE STRESS IN ALBERTA EVIDENCE FROM OIL WELLS. *Earth and Planetary Science Letters,* 45.

BOURNE, S. J. & WILLEMSE, E. J. M. 2001. Elastic stress control on the pattern of tensile fracturing around a small fault network at Nash Point, UK. *Journal of structure Geology.***,** 1753-1770.

BRECKELS, I. M. & EEKELEN, H. A. M. V. September 1982. Relationship Between Horizontal Stress and Depth in Sedimentary Basins

BRUDY, M. & ZOBACK, M. D. 1999. Drilling-induced tensile wall-fractures: implications for determination of in-situ stress orientation and magnitude. *International Journal of Rock Mechanics and Mining Sciences,* 36**,** 191-215.

BRUDY, M., ZOBACK, M. D., FUCHS, K., RUMMEL, F. & BAUMG'ARTNER, J. 1997. Estimationo f the completes tresst ensort o 8 km depthi n the KTB scientificd rill holes'I mplicationsf or crustals trength. *JOURNAL OF GEOPHYSICAL RESEARCH,,* 102**,** 18,453-18,475.

CAMAC, B. A. & HUNT, S. P. 2004. Application of Stress Feld Modelling Using the Distinct Element Method for Petroleum production.

CHIPPERFIELD, S. T. & BRITT, L. K. 2000. Application of After-Closure Analysis for Improved Fracture Treatment Optimisation: A Cooper Basin Case Study.

COOKE, D. DECEMBER 2011. The production rate variability problem with shale reservoirs: what we know and what we don't know.

CRAMER, D. D. 2008. Stimulating Unconventional Reservoirs: Lessons Learned, Successful Practices, Areas for Improvement.

DAS, I. & ZOBACK, M. D. 2011a. Long Period Long Duration Seismic Events During Hydraulic Stimulation of a Shale Gas Reservoir.

DAS, I. & ZOBACK, M. D. 2011b. Long period, long-duration seismic events during hydraulic fracture stimulation of a shale gas reservoir. *The leading edge*.

DOE, T., KJELL INGEVALD, L. S., HAIMSON, B. & CARLSSON, H. HYDRAULIC FRACTURING AND OVERCORING STRESS MEASUREMENTS IN A DEEP BOREHOLE AT THE STRIPA TEST MINE, SWEDEN.

ENGELDER, T. 1993. Stress regimes in the Lithosphere.

FU, L.-Y. 2006. 3-D Boundary element seismic modeling in complex geology.

GARR, M. & GAY, M. 1978. State of Stress in the earth's crust.

GRAVESTOCK, D. I. & JENSEN-SCHMIDT, B. 1998. STRUCTURAL SETTING: Petroleum geology of Cooper basin 4.

GRAY, D., ANDERSON, P., LOGEL, J., DELBECQ, F., SCHMIDT, D. & SCHMID, R. 2012. Estimation of stress and geomechanical properties using 3D seismic data. *first break,* 30.

GROB, M. & BAAN, M. V. D. 2011. Inferring in-situ stress changes by stastical analysis of microseismic event characteristics. *The leading edge.***,** 1296-1301.

GUDMUNDSSON, A. 2000. Active fault zones and ground water flow. *Geophysical research letters,* 27**,** 2993-2996.

HART, B., SAYERS, C. M. & JACKSON, A. 2011. An introduction to this special section:Shales. *The leading edge*.

HAYASHI, K. & HAIMSON, B. C. 1991. Characteristics of Shut-in Curves in Hydraulic Fracturing Stress Measurements and Determination of in Situ Minimum Compressive Stress. *JOURNAL OF GEOPHYSICAL RESEARCH,* 96**,** 18,311-18,321.

HICKMAN, P. A. 1985. STRESS-INDUCED BOREHOLE ELONGATION.

HILL, T. 2010. UNCONVENTIONAL OIL AND GAS OPPORTUNITIES IN SOUTH AUSTRALIA. *DMITRE*.

HILLS, R. R., MEYER, J. J. & REYNOLDS, S. D. 1998. The Australian Stress map. *Exploration Geophysics*.

HOLDITCH, S. A. 2007. Hydraulic fracturing: Petroleum Engineering Handbook. 4.

HOMBERG, C., ANGELIER, J., BERGERAT, F. O. & LACOMBE, O. 2004. Using stress de£ections to identify slip events in fault systems. *Earth and Planetary Science Letters*, 409-424.

HOMBERG, C., HU, J. C. & ANGLIER, J. 1997. Characterization of stress perturbations near major fault zones: insights from 2-D distinct-element numerical modelling and field studies (Jura mountaines). *Journal of structure Geology.*, 19.

HOSSAIN, M. M., RAHMAN, M. K. & RAHMAN, S. S. 2000. Hydraulic fracture initiation and propagation: roles of wellbore trajectory, perforation and stress regimes. *Journal of Petroleum Science and Engineering*, 27, 129–149.

KATTENHORN, S. A. & MARSHALL, S. T. 2006. Fault-induced perturbed stress fields and associated tensile and compressive deformation at fault tips in the ice shell of Europa: implications for fault mechanics. *Journal of structure Geology.*, 2204-2221.

KING, G. 2010. Thirty years of Gas Shale fracturing: What have we learned? *SPE 133456*.

LAWS, R. A. & GRAVESTOCK, D. I. 1998. INTRODUCTION: Petroleum geology of Cooper basin.

LJUNGGREN, C., CHANG, Y., JANSON, T. & CHRISTIANSSON, R. 2003. An overview of rock stress measurement methods. *International Journal of Rock Mechanics & Mining Sciences*, 40, 975–989.

LORENZ, J. C., TEUFEL, L. W. & WARPINSKI, N. R. 1991. Regional Fractures I: A Mechanism for the formation of Regional Fractures at Depth in Flat-Lying Reservoirs. *AAPG Bulletin*, 75, 1991.

LORIG, L. J. & BRADY, B. H. G. A hybrid discrete element-boundary element method of stress analysis. *Chapter 65*.

LUO, G., NIKOLINAKOU, M. A., FLEMINGS, P. B. & HUDEC, M. R. January 2012. Geomechanical modeling of stresses adjacent to salt bodies: Part 1—Uncoupled models. *AAPG Bulletin*, 96, 43–64.

MAERTEN, L., GILLESPIE, P. & DANIEL, J.-M. 2006. Three dimensional geomechanical modeling for constraint of subseismic fault simulation. *AAPG Bulletin*, 90, 1337-1358.

MAERTEN, L. & MAERTEN, F. August 2006. Chronologic modeling of faulted and fractured reservoirs using geomechanically based restoration: Technique and industry applications. *AAPG Bulletin*, 90, 1201–1226.

MAXWELL, S. 2011. Microseismic hydraulic fracture imaging: The path toward optimizing shale gas production. *The leading edge.*, 340-346.

NELSON, E., HILLIS, R., SANDIFORD, M., REYNOLDS, S. & MILDREN, S. 2006. PRESENT-DAY STATE-OF-STRESS OF SOUTHEAST AUSTRALIA. *AAPEA Journal*.

NELSON, E. J., CHIPPERFIELD, S. T., HILLIS, R. R., GILBERT, J. & MCGOWEN, J. 2007a. Using geological information to optimize fracture stimulation practices in the Cooper Basin, Australia. *Petroleum Geoscience,* 13**,** 3–16.

NELSON, E. J., CHIPPERFIELD, S. T., HILLIS, R. R., GILBERT, J., MCGOWEN, J. & MILDREND, S. D. 2007b. The relationship between closure pressures from fluid injection tests and the minimum principal stress in strong rocks. *International Journal of Rock Mechanics & Mining Sciences,* 44**,** 787–801.

NICOL, A., WALSH, J. J., WATYERSON, J. & GILLESPIE, P. A. 1996. Fault size distributions m are they really power-law? *Journal of structure Geology.*, 18.

NORMAN R. WARPLNSKL February 1991. Hydraulic Fracturing in Tight, Fissured Media. *Journal of Petroleum Technology*.

PAUL, P., NEELY, T., ALLWARDT, T., HENNINGS, P., MCLENNAN, J., REID, R. & BROWN, D. 2011. Geomechanical Controls on the Gas Production in the North Parachute Area, Colorado.

PECHER, R. & STANISLAV, J. F. 1997. Boundary element techniques in petroleum reservoir simulation. *Journal of Petroleum Science and Engineering,* 17**,** 353-366.

PESKA, P. & ZOBACK, M. D. 1995. Compressive and tensile faliure of inclined well bores and determination of in situ stress and rock strength. *JOURNAL OF GEOPHYSICAL RESEARCH,* 100**,** 12,791-12,811.

PLUMB & HICKMAN 1985. Stress -induced borehole elongation.

REYNOLDS, S. 2001. Characterization and modelling of the regional insitu stress field of continental australia. *A Ph.D. dissertation*.

REYNOLDS, S. D., COBLENTZ, D. D. & HILLIS, R. R. 2002. Tectonic forces controlling the regional intraplate stress field in continental Australia: Results from new finite element modeling. *JOURNAL OF GEOPHYSICAL RESEARCH,* 107.

REYNOLDS, S. D., MILDREN1, S. D., HILLIS, R. R. & MEYER, J. J. 2004. The in situ stress field of the Cooper Basin and its implications for hot dry rock geothermal energy development.

REYNOLDS, S. D., MILDREN, S. D., HILLIS, R. R. & MEYER, J. J. 2006. Constraining stress magnitudes using petroleum exploration data in the Cooper–Eromanga Basins, Australia. *Tectonophysics* 123–140.

REYNOLDS, S. D., MILDREN, S. D., HILLIS, R. R., MEYER, J. J. & FLOTTMANN3, T. 2005. Maximum horizontal stress orientations in the Cooper Basin, Australia: implications for plate-scale tectonics and local stress sources.

RIDER, M. 2002. Geological interpretation of the well logs. *Cambridge university press.*

SAYERS, C. M. & SCHUTJENS, P. M. T. M. 2007a. An introduction to reservoir geomechanics. *The leading edge.***,** 597-601.

SAYERS, C. M. & SCHUTJENS, P. M. T. M. 2007b. Introduction to this special section: Geomechanics. *The leading edge*.

SCHMID, R. & GRAY, D. 2011. Principal Stress Estimation in Shale Plays Using 3D Seismic.

SWYER, M. W. & DAVATZES, N. C. February 2012. USING BOUNDARY ELEMENT MODELING OF FAULT SLIP TO PREDICT PATTERNS OF STRESS PERTURBATION AND RELATED FRACTURES IN GEOTHERMAL RESERVOIRS AND EXPLORE PARAMETER UNCERTAINTY.

THOMAS, A. L. 1993. Poly 3D: A Three-Dimensional, Polygonal element, displacement discontinuity boundary element computer program with applications to fractures, faults cavities in the earth's crust. *A thesis submitted to the department of Geology and the committee on graduate studies of Stanford University*.

TINGAY, M., MÜLLER, B., REINECKER, J., HEIDBACH, O., WENZEL, F. & FLECKENSTEIN, P. 2005. Understanding tectonic stress in the oil patch:The World Stress Map Project. *The leading edge*.

TINGAY, M. R. P., HILLIS, R. R., MORLEY, C. K., KING, R. C., SWARBRICK, R. E. & DAMIT, A. R. January 2009. Present-day stress and neotectonics of Brunei: Implications for petroleum exploration and production. *AAPG Bulletin*, 93**,** 75–100.

WARPINSKI, N. R., SCHMIDT, R. A. & NORTHROP, D. A. March 1982. In-situ stresses: The predominant influence on hydraulic fracture Containment. *Journal of Petroleum Technology*.

WATTERSON, J. 1986. Fault Dimensions, Displacements and Growth.

WATTERSON, J. 1999. The future of faliure: stress or strain? *Journal of structure Geology.*, 21**,** 939-948.

ZOBACK, M. D. 2007. Reservoir Geomechanics. *Cambidge University press*.

ZOBACK, M. D., BARTON, C. A., BRUDY, M., CASTILLO, D. A., FINKBEINER, T., GROLLIMUND, B. R., MOOS, D. B., PESKA, P., WARD, C. D. & WIPRUT, D. J. 2003. Determination of stress orientation and magnitude in deep wells. *International Journal of Rock Mechanics & Mining Sciences*, 40**,** 1049–1076.

ZOBACK, M. D. & HAIMSON, B. C. 2001. STATUS OF THE HYDRAULIC FRACTURING METHOD FOR IN-SITU STRESS MEASUREMENTS.

ZOBACK, M. D., MOOS, D., MASTIN, L. & ANDERSON, R. N. 1985. Well Bore Breakouts and in Situ Stress.

ZOBACK, M. D. & ZOBACK, M. L. 2002. State of Stress in the Earth's Lithosphere.

ZOBACK, M. L. 1992. First- and Second-Order Patterns of Stress in the Lithosphere' The World Stress Map Project. *JOURNAL OF GEOPHYSICAL RESEARCH*, 97**,** 11,703-11,728.

ZOBACK, M. L. & ZOBACK, M. D. 1991. Tectonic stress fied of North America and relative plate motion.

ZOBACK, M. L., ZOBACK, M. D., ADAMS, J., ASSUMPCAO, M., BELL, S., BERGMAN, E. A., BLUMLING, P., BRERETON, N. R., DENHAM, D., DING, J., FUCHS, K., N.GRAY, GREGERSEN, S., GUPTA, H. K., GVISHIANI, A., JACOB, K., KLIEIN, R., KNOLL, P., MAGEE, M., MERCIER, J. L., MULLER, B. C., PAQUIN, C., RAJENDRAN, K., STEPHANSSON, O., SUAREZ, G., SUTER, M., UDIAS, A., XU, Z. H. & ZHIZHIN, M. 1989. Global patterns of tectonic stress. *Nature*.

Appendix A

Raw data

This appendix presents models with fault length of 600meters with σ_H azimuth of 0˚, 5˚, 15˚, 30˚, 45˚, 60˚ and 90˚. Sandstone, Shale and Coal are included in the section. A number of models are included in the DVD attached with the thesis.

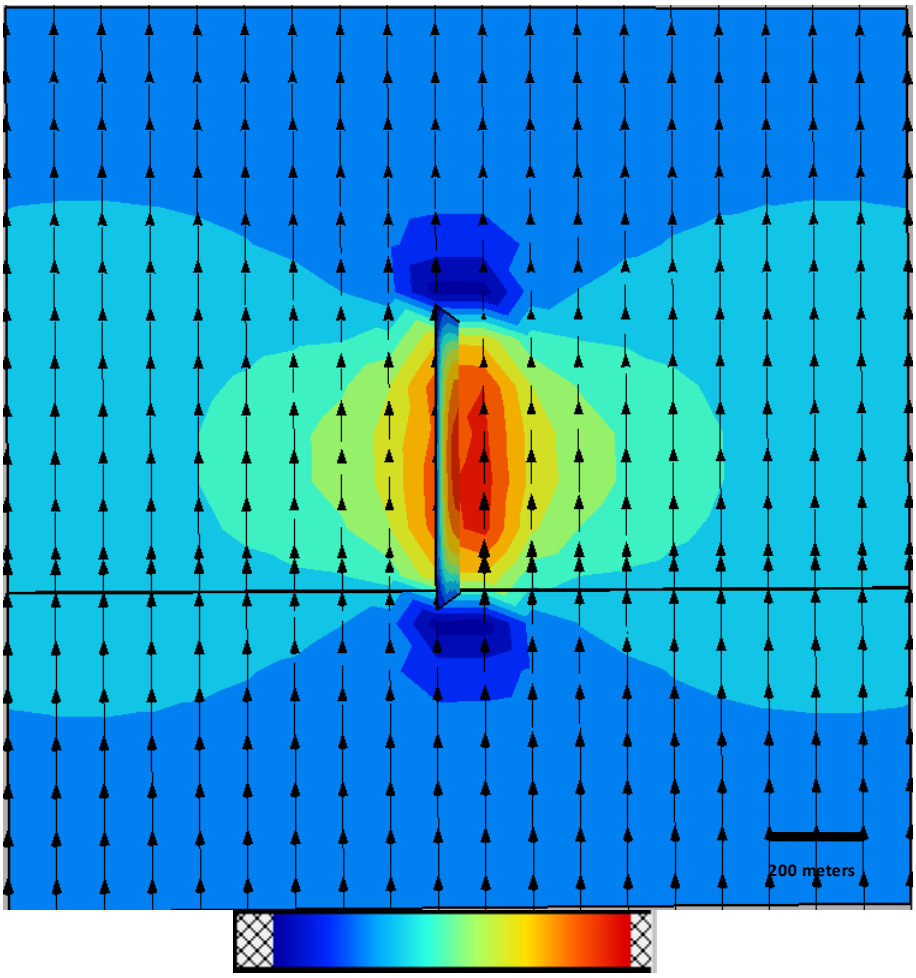

12.1 12.1 MPa

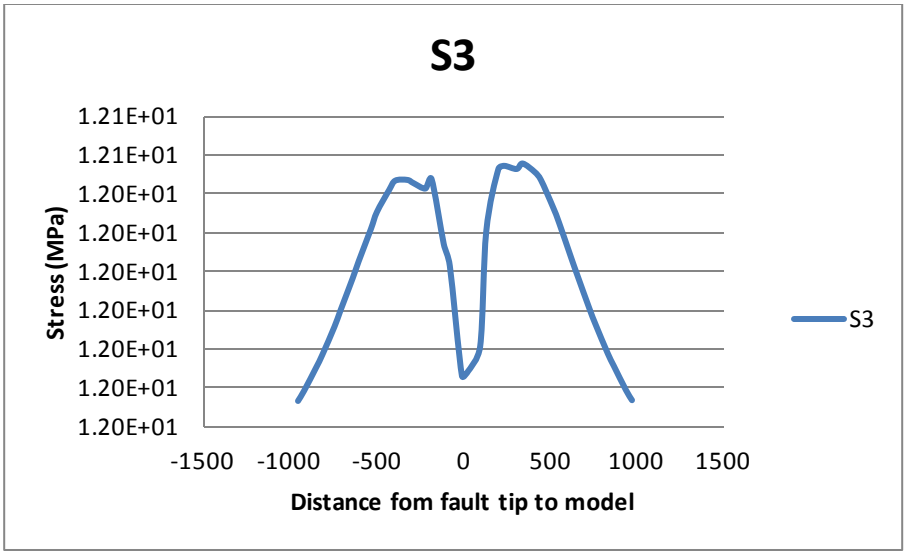

Fault 600 meter, Shale 0˚ at 2.25 km

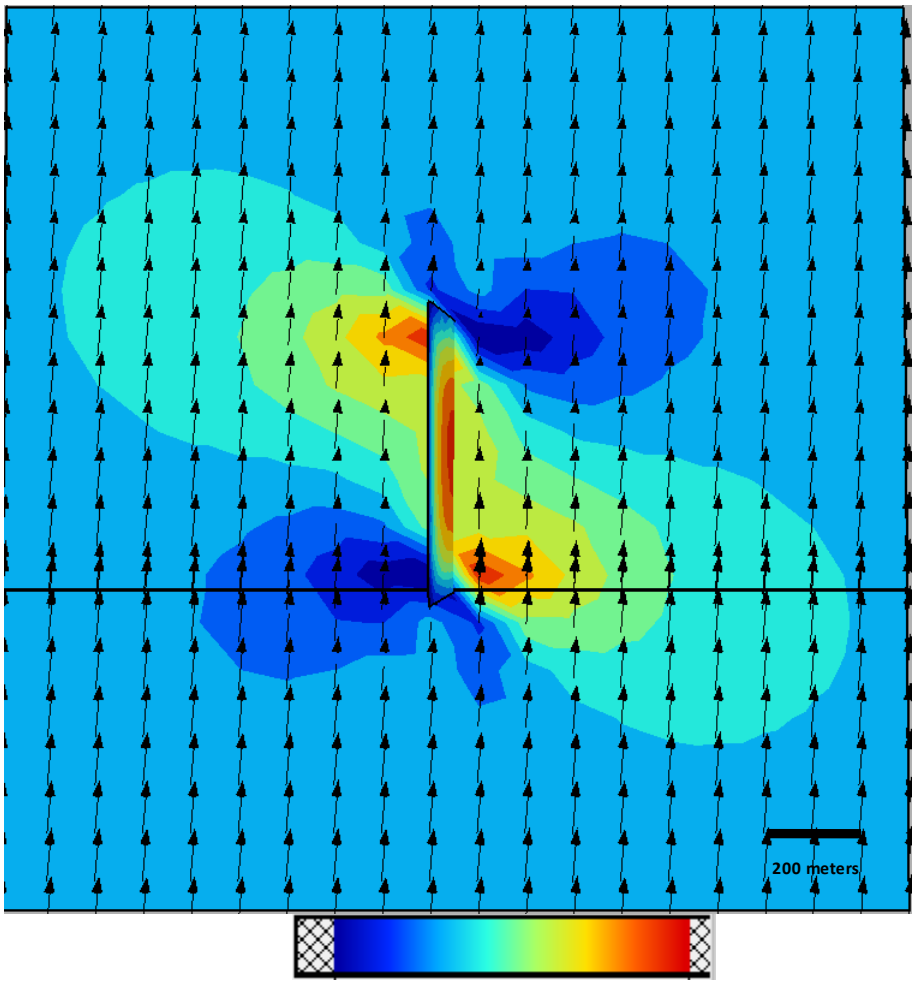

10.6 13.5 MPa

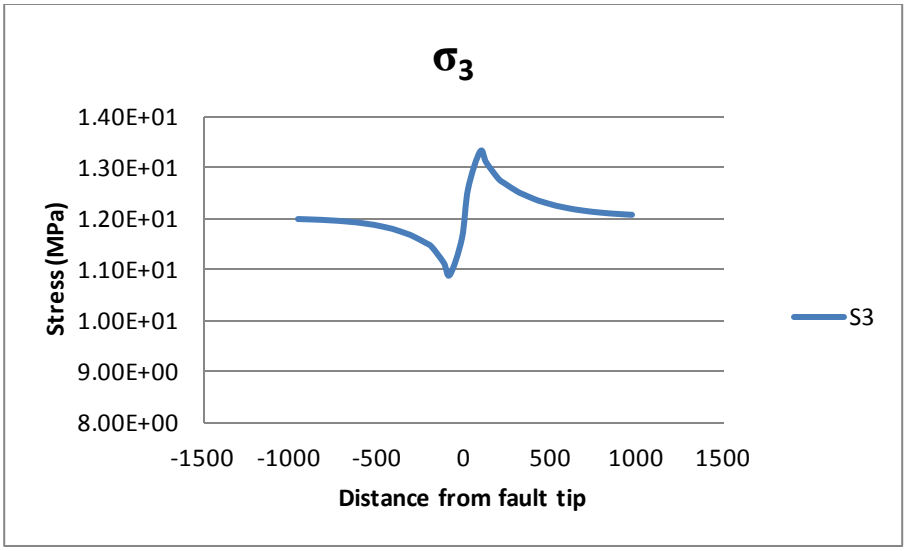

Fault 600, Shale 5 at 2.25 km

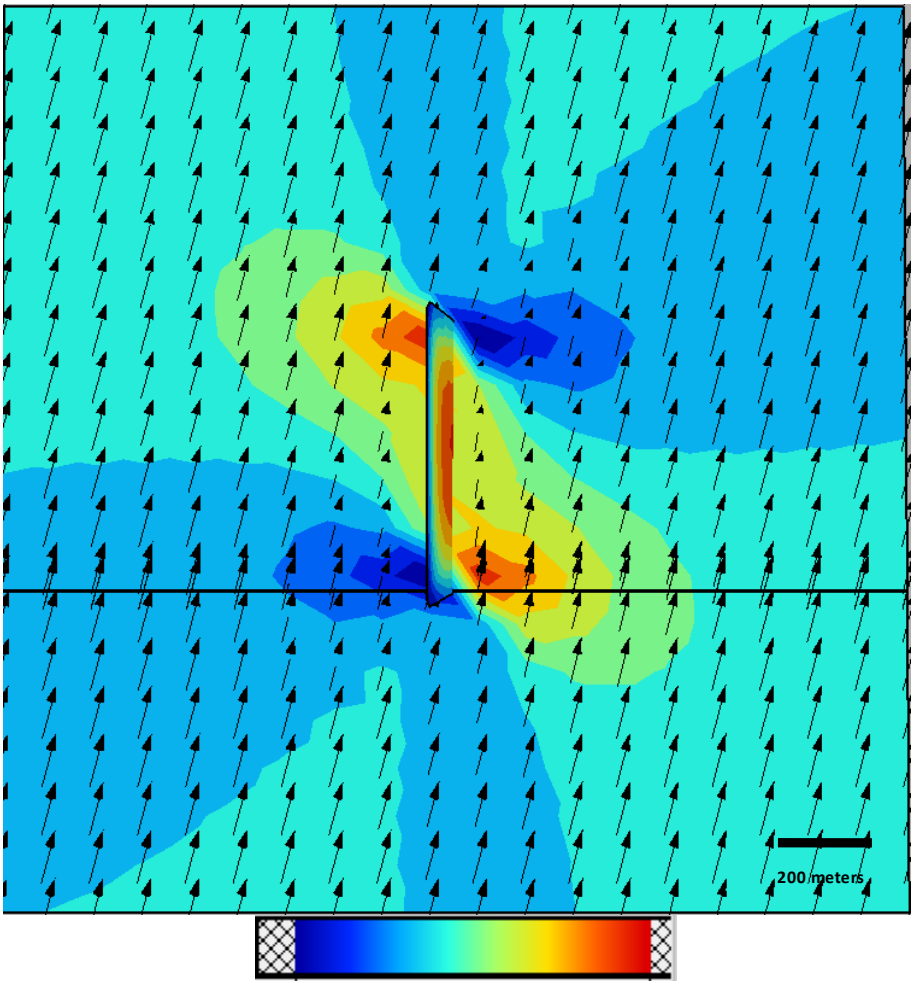

8 16.7 MPa

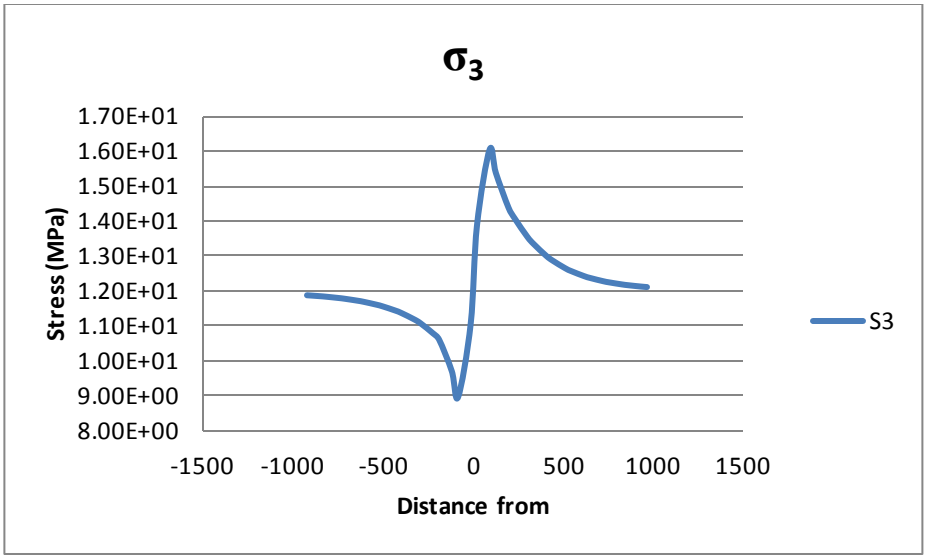

Fault 600 meters, Shale 15˚ at 2.25 km

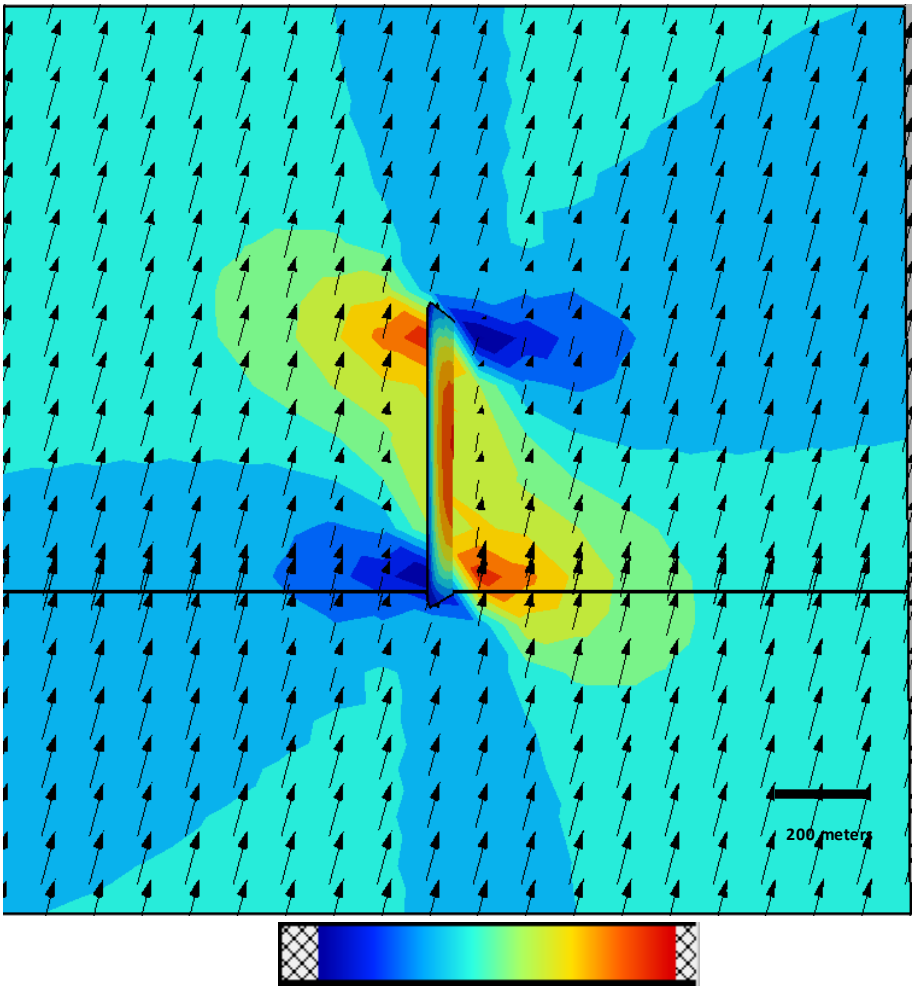

5.0 21.0 MPa

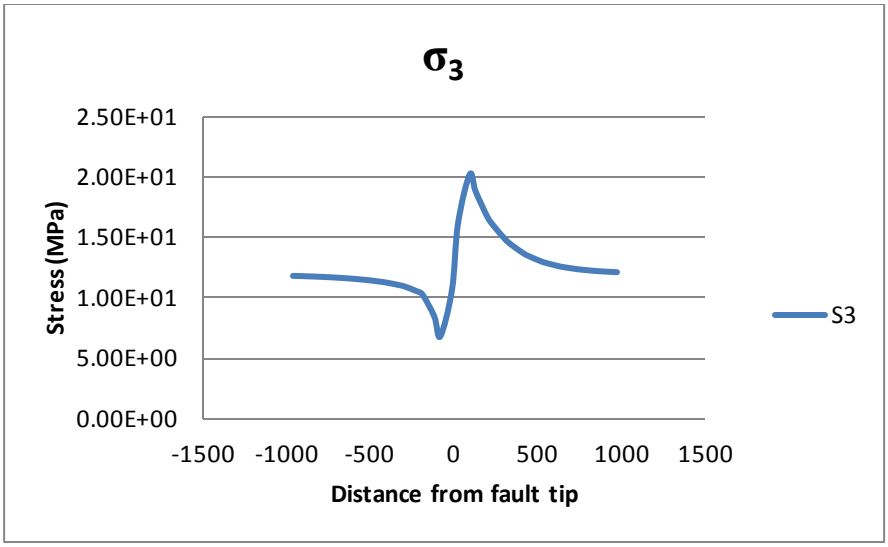

Fault 600 meters, Shale 30˚ at 2.25 km

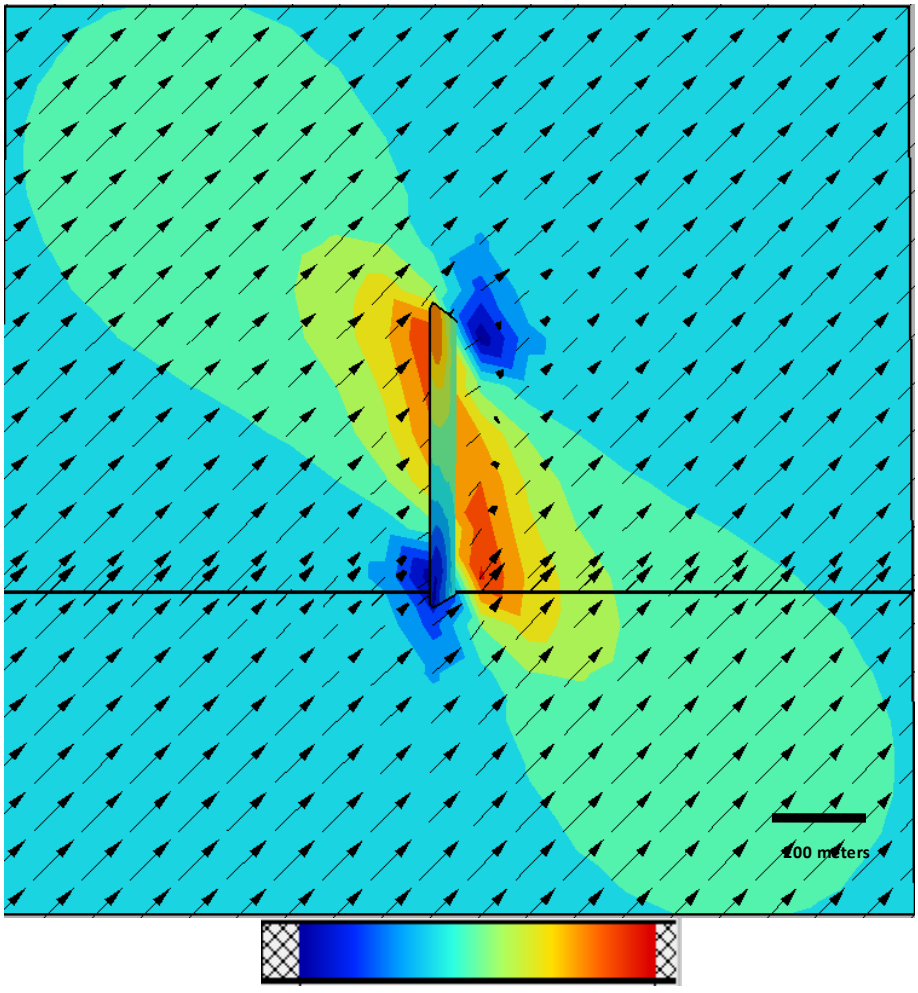

3.0 24.0 MPa

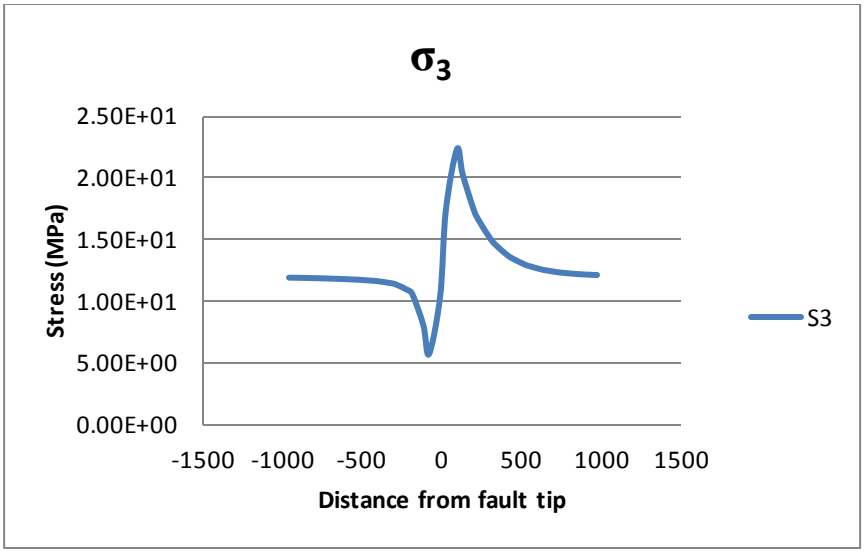

Fault 600 meters, Shale 45˚ at 2.25 km

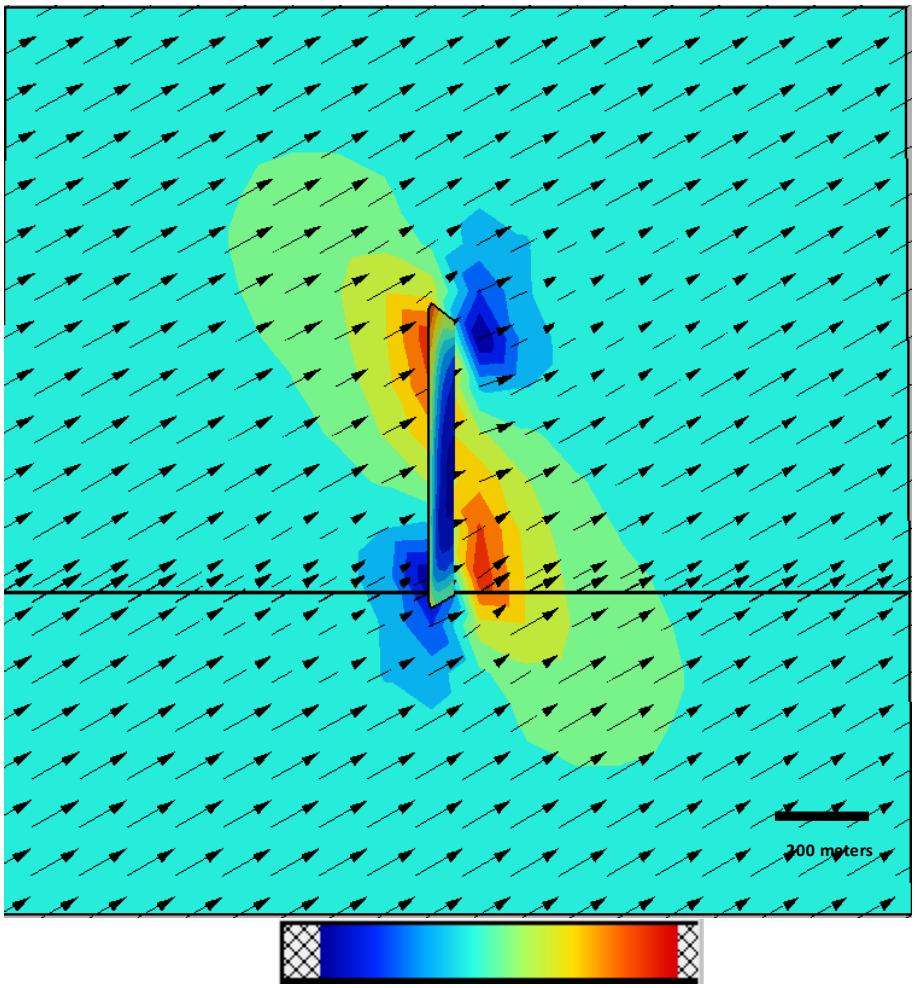

5.0 23.0 MPa

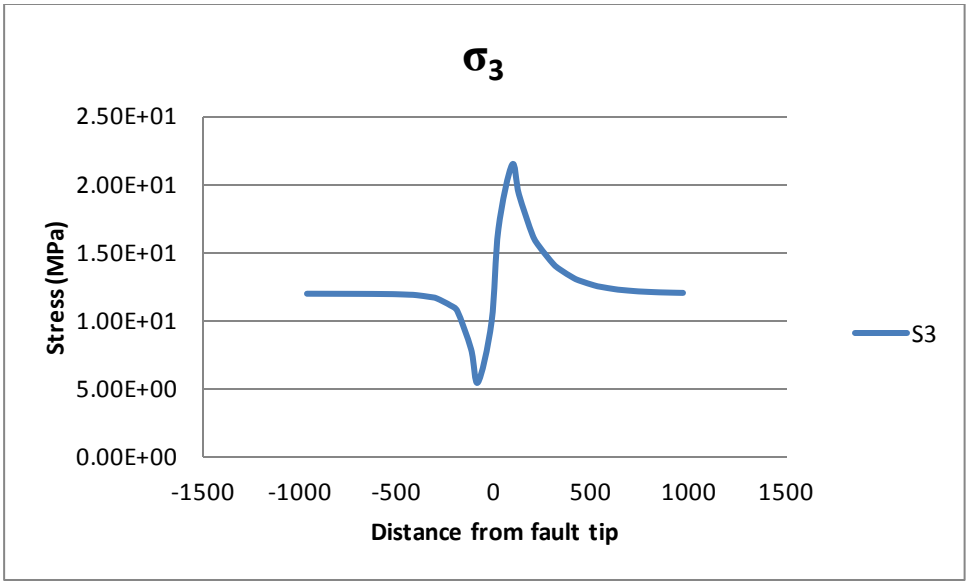

Fault 600 meters, Shale 60˚ at 2.25 km

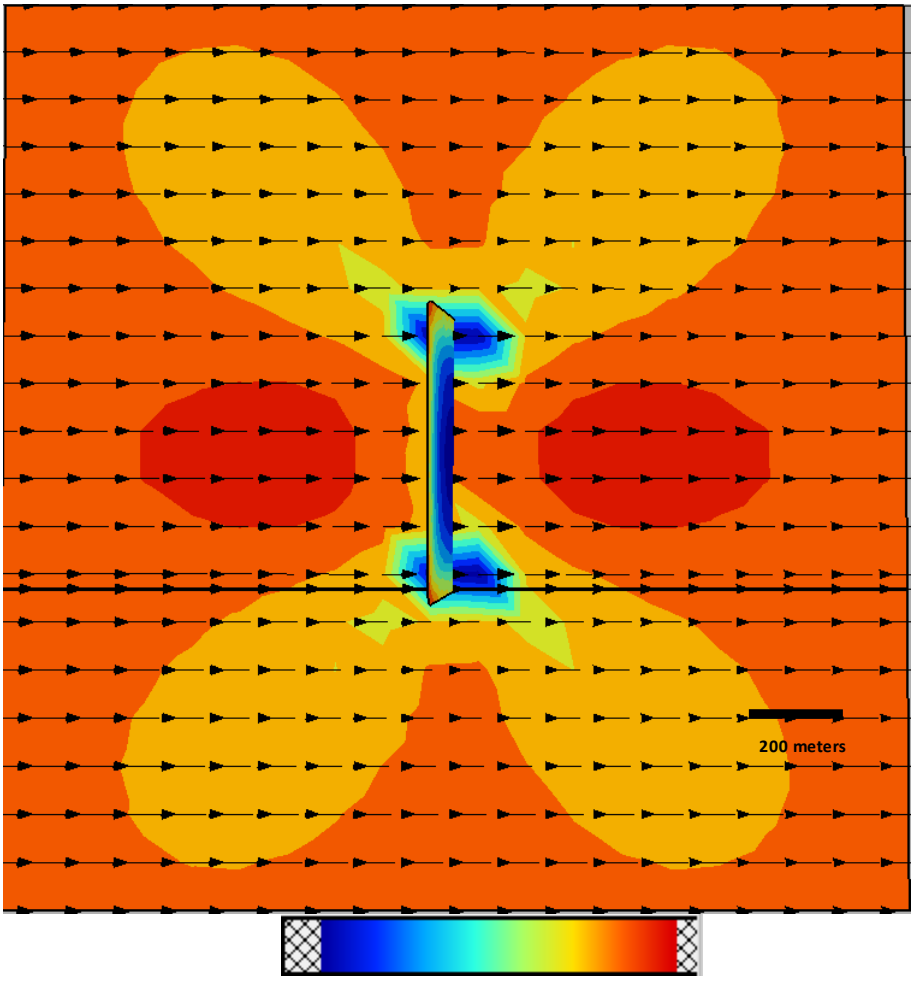

11.8 12.1 MPa

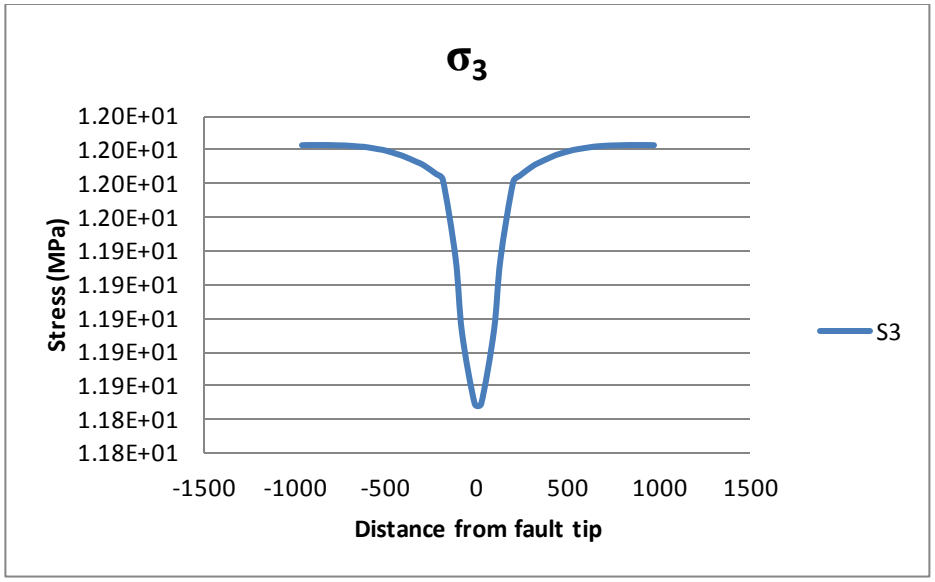

Fault 600 meters, Shale 90˚ at 2.25 km

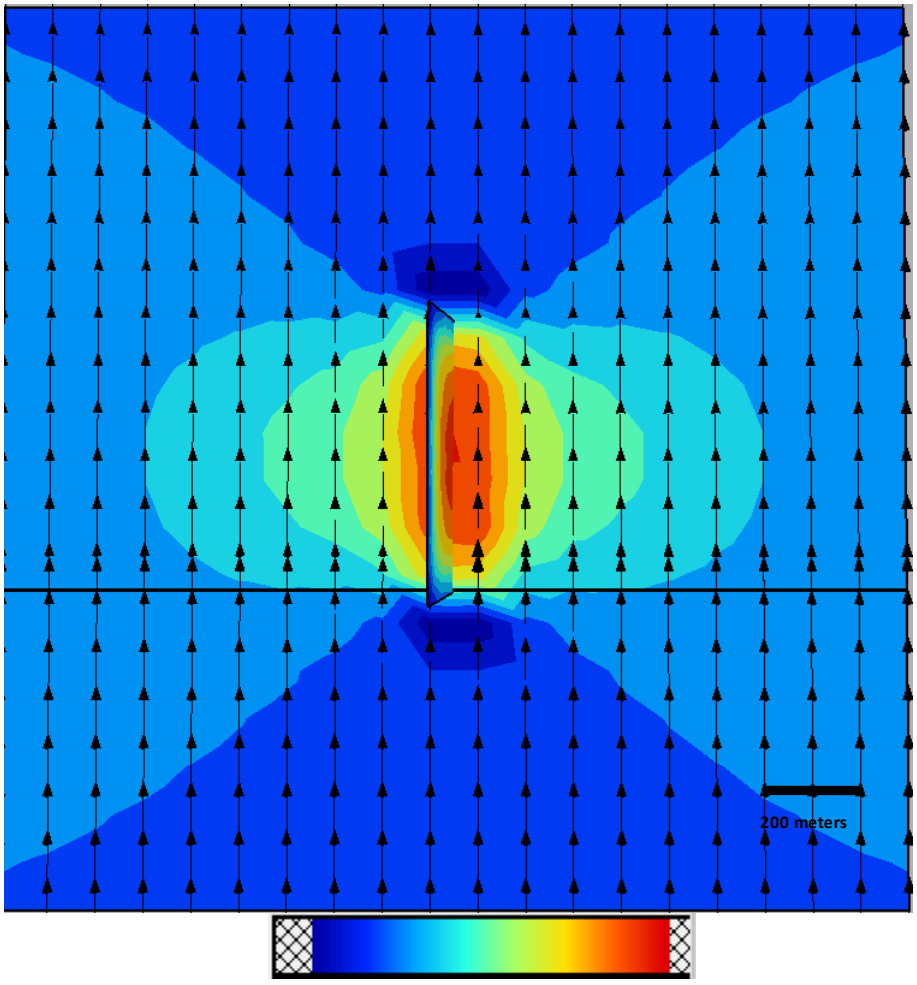

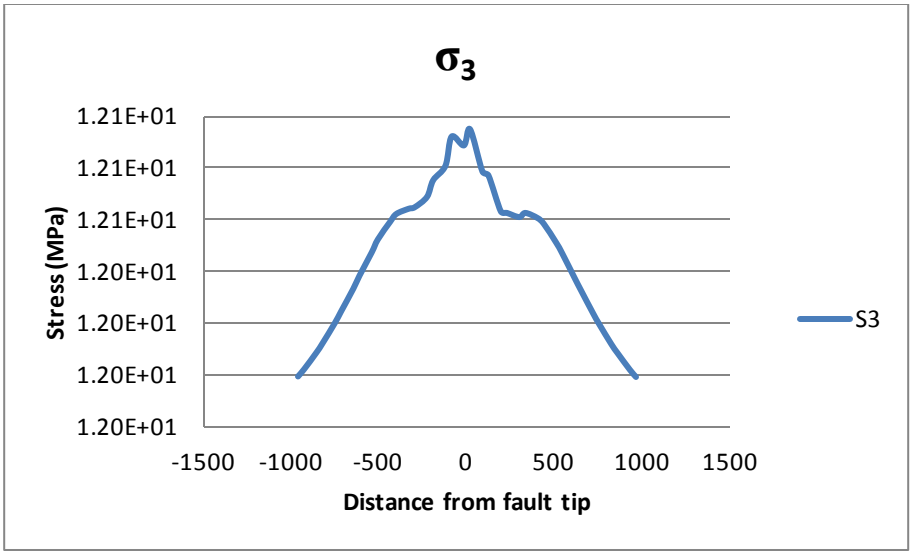

Fault 600 meters, Coal 0˚ at 2.25 km

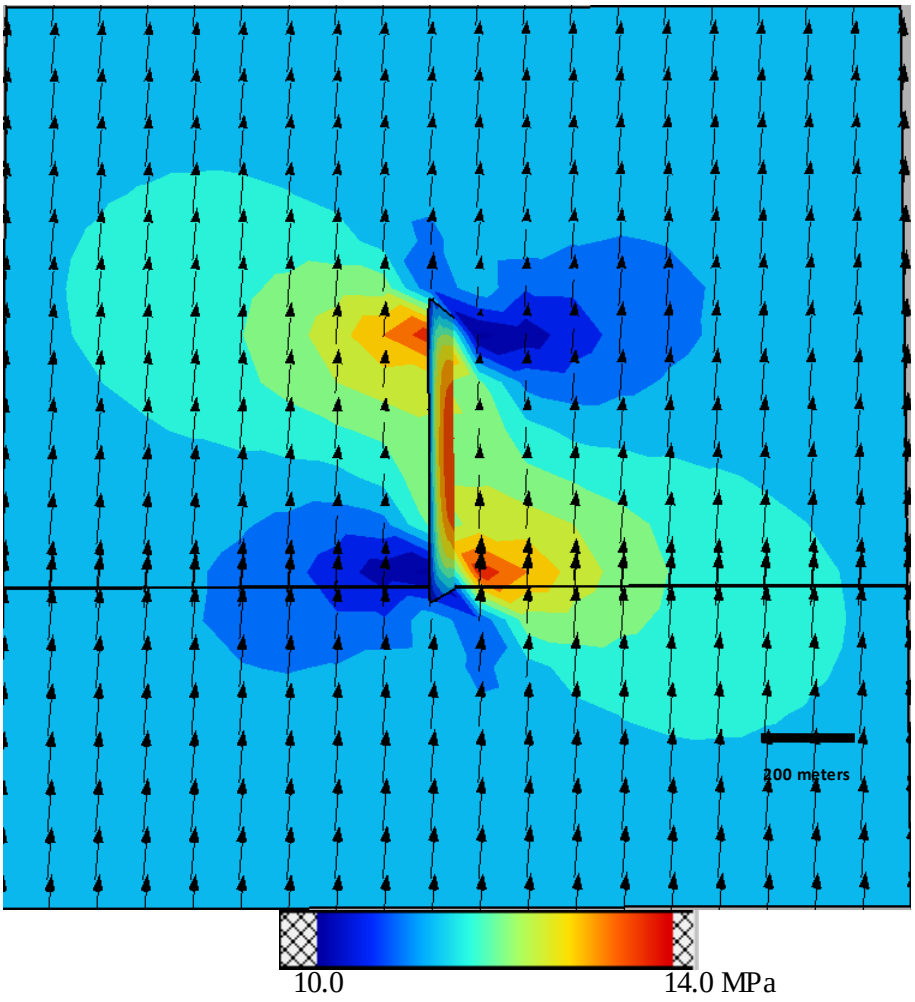

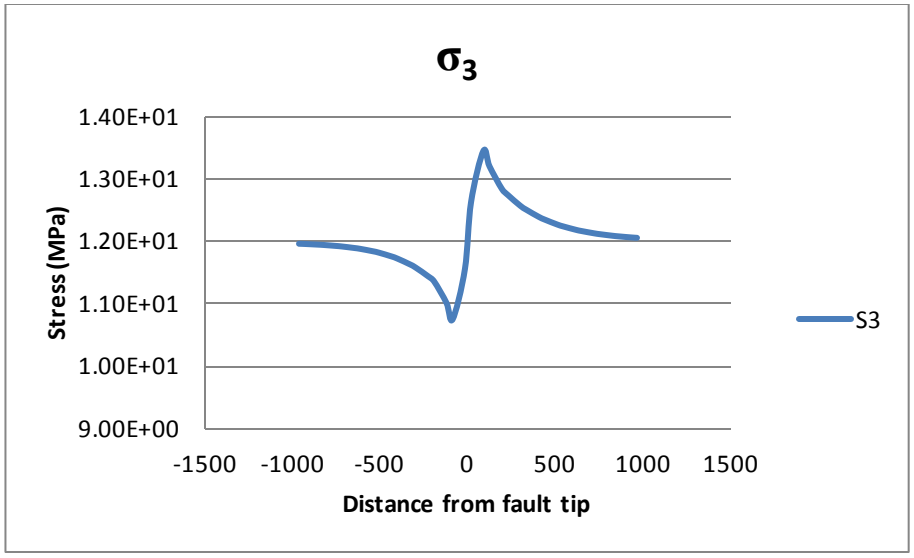

Fault 600 meters, Coal 5˚ at 2.25 km

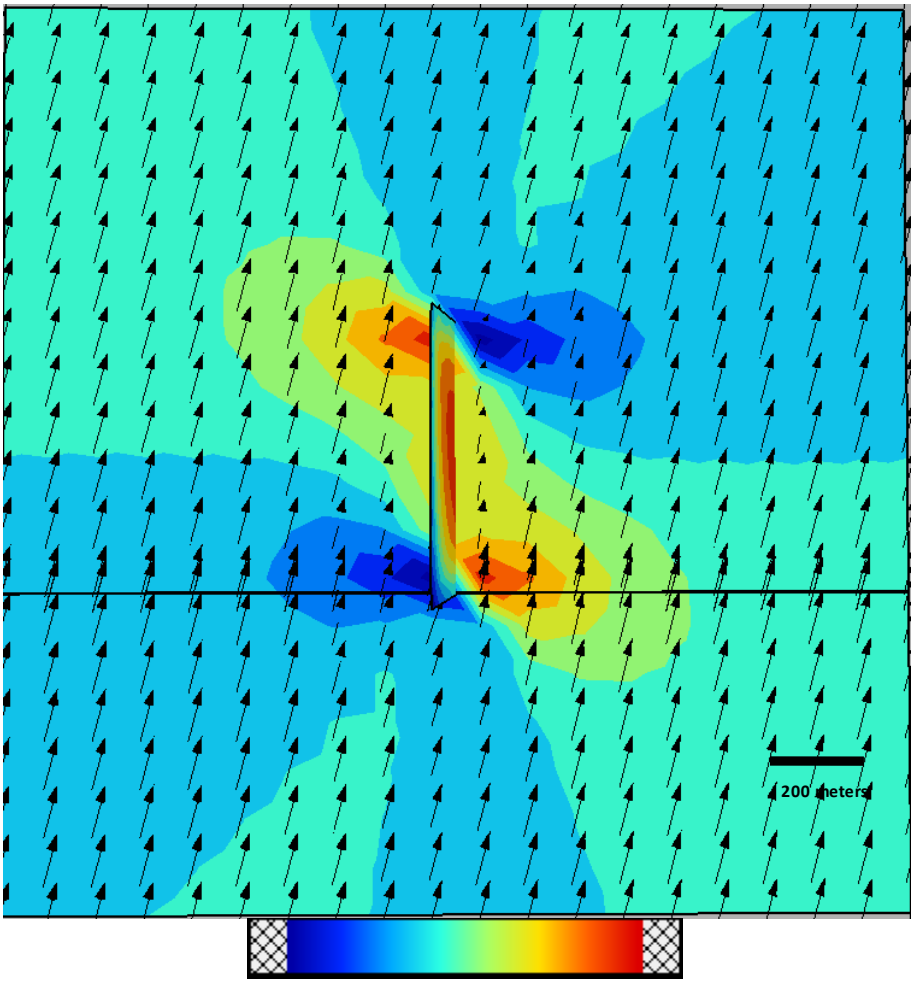

7.0 17.0 MPa

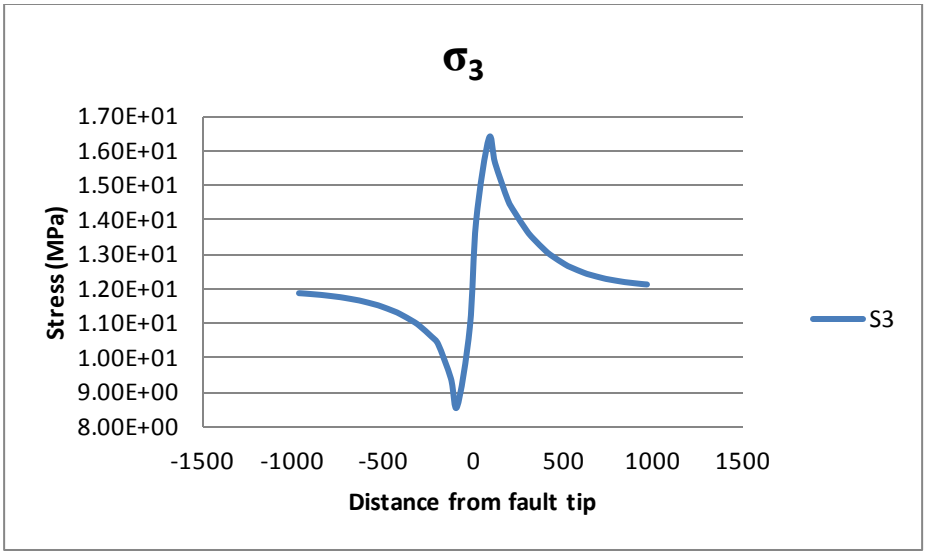

Fault 600 meters, Coal 15˚ at 2.25 km

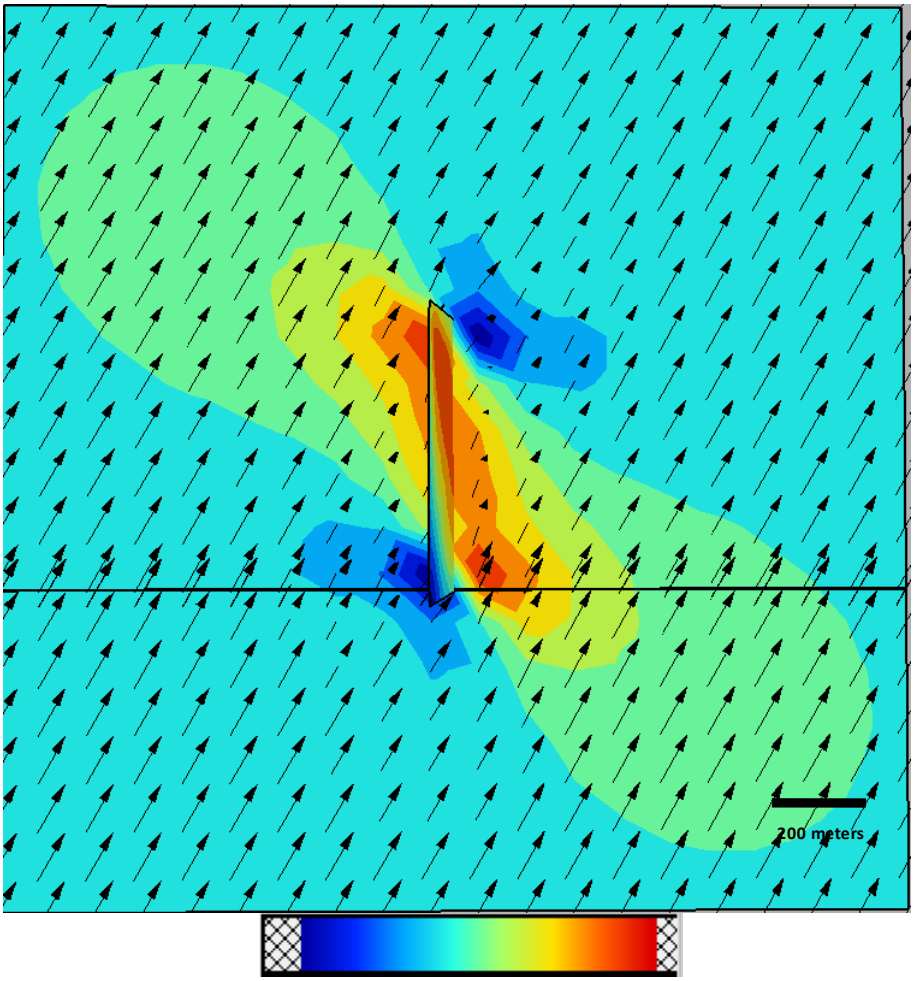

4.0 22.0 MPa

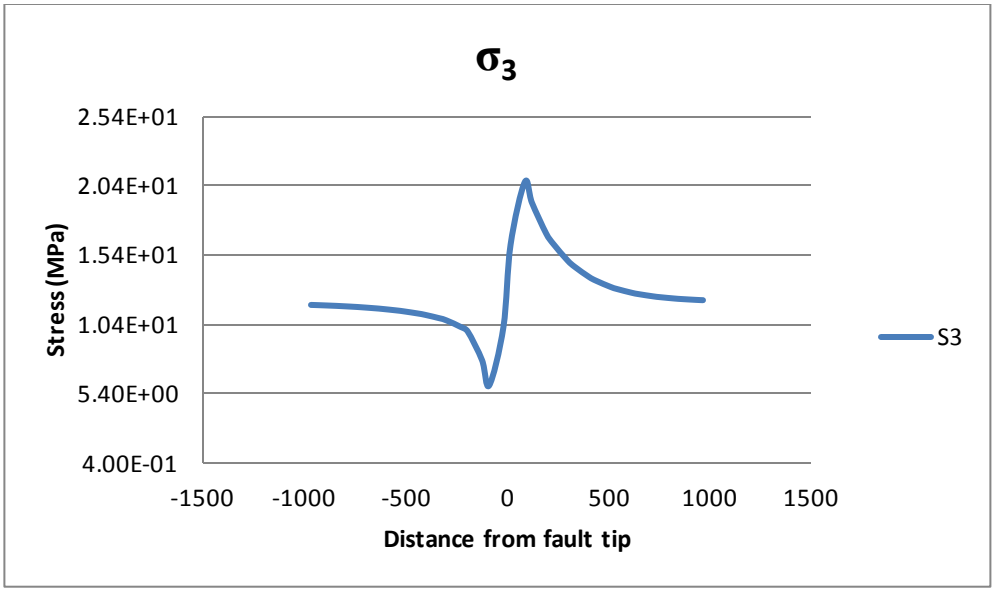

Fault 600 meters, Coal 30˚ at 2.25 km

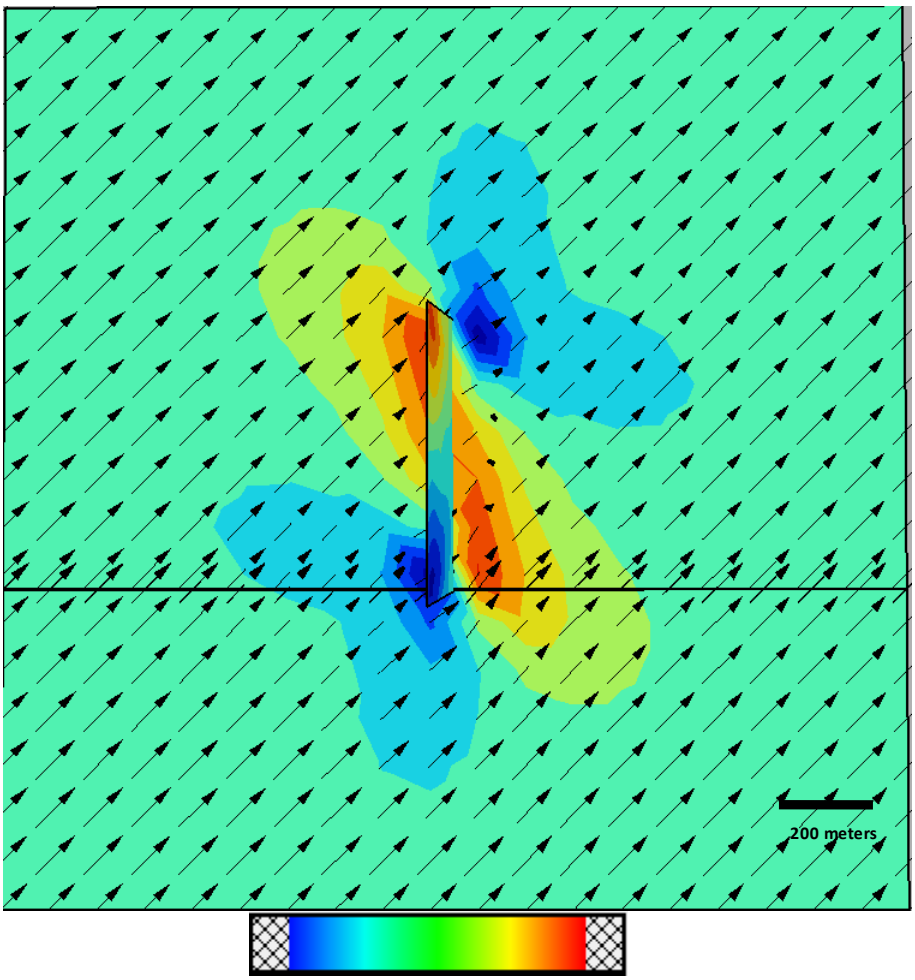

4.0 25.0 MPa

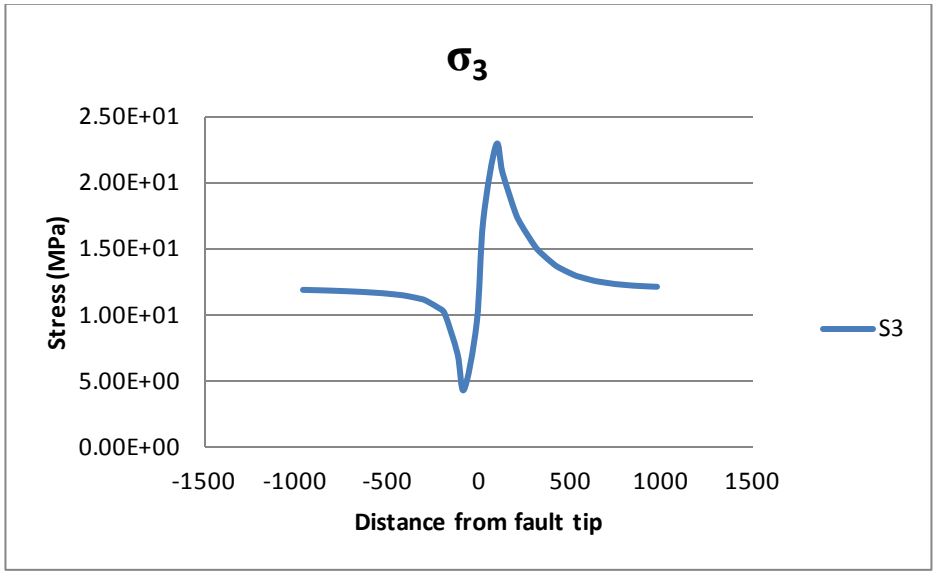

Fault 600 meters, Coal 45˚ at 2.25 km

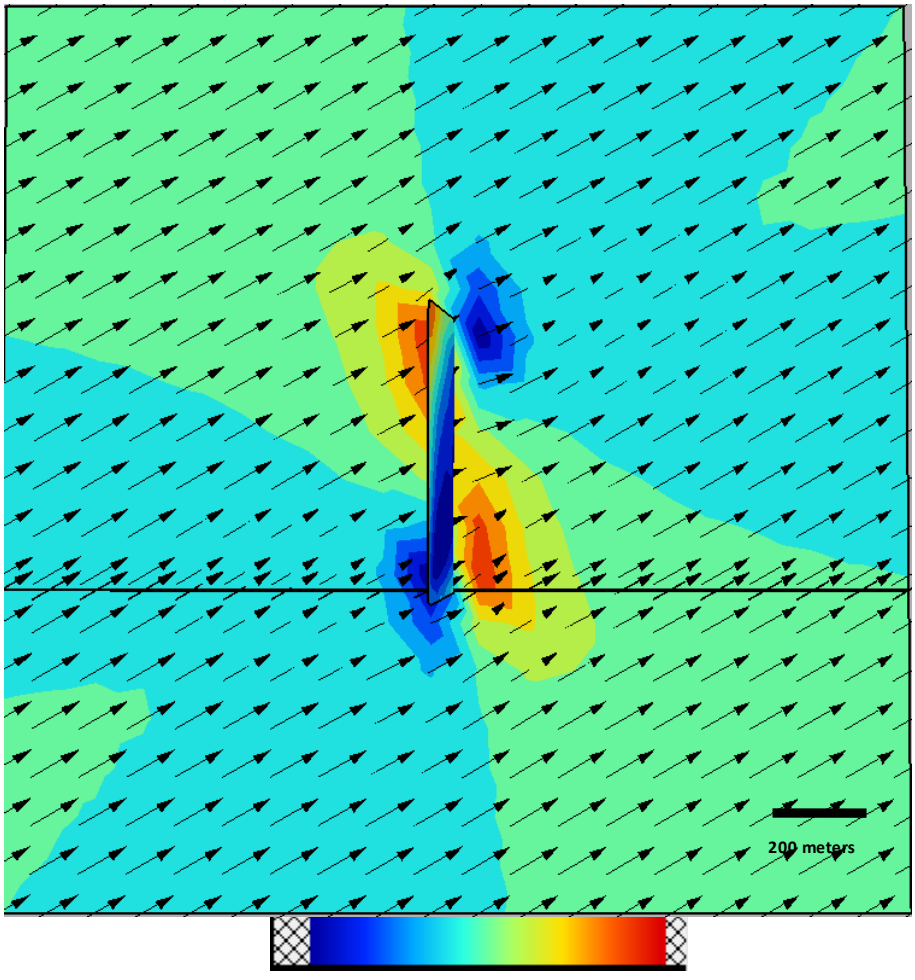

4.0 24.0 MPa

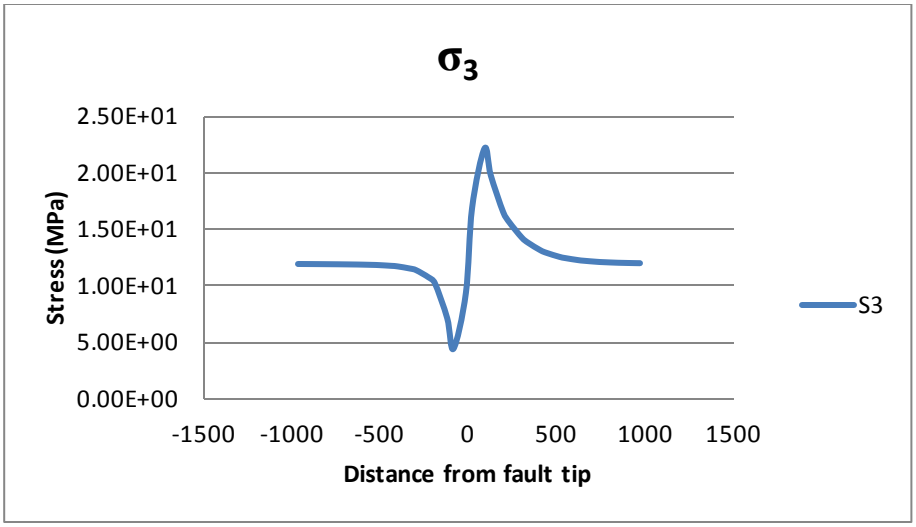

Fault 600 meters, Coal 60˚ at 2.25 km

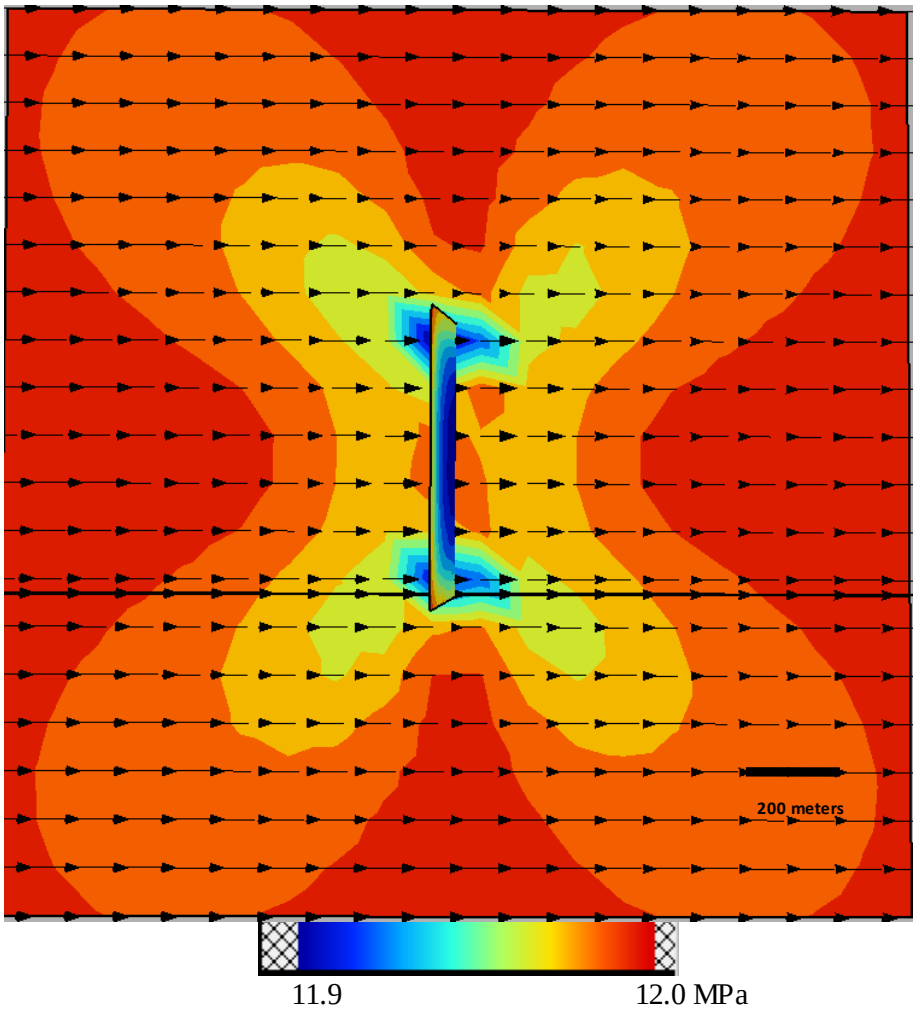

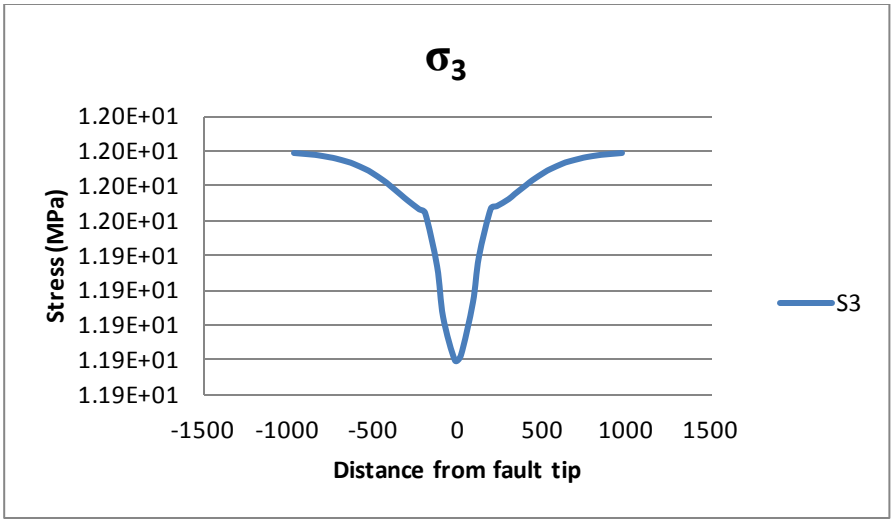

Fault 600 meters, Coal 90˚ at 2.25 km

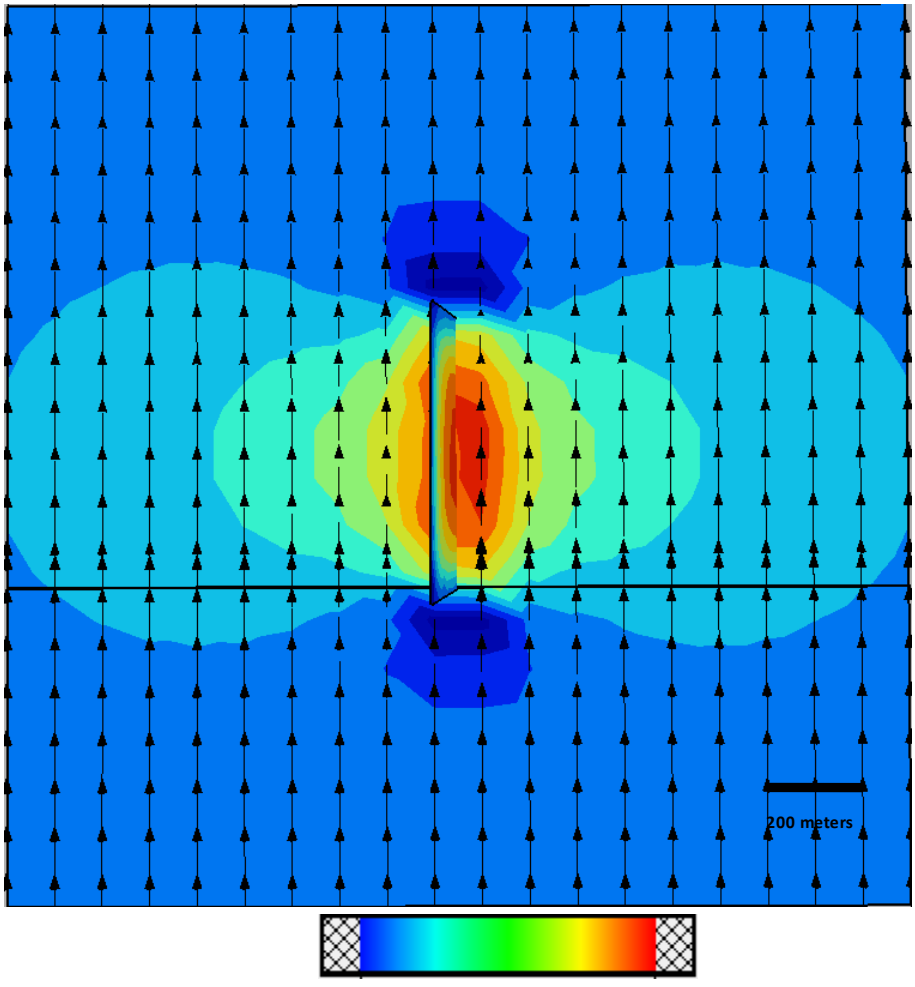

12.0 12.1 MPa

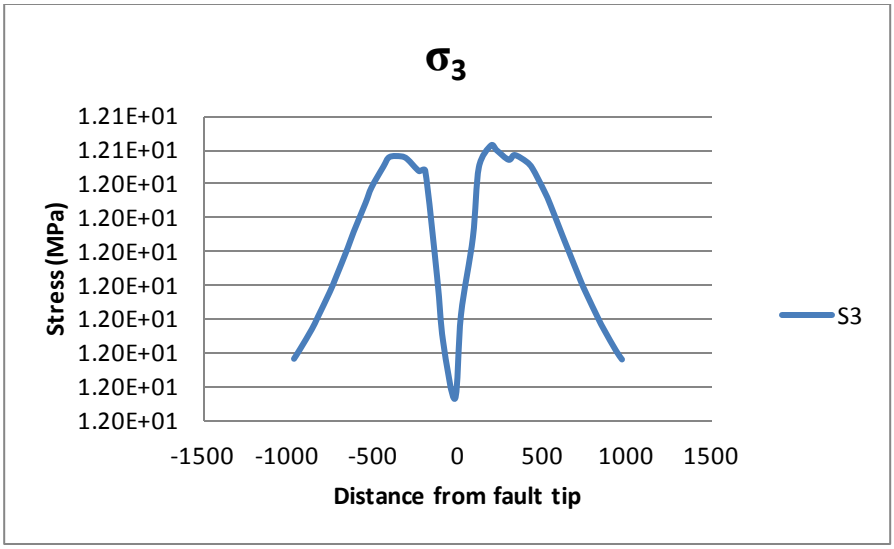

Fault 600 meters, Sandstone 0˚ at 2.25 km

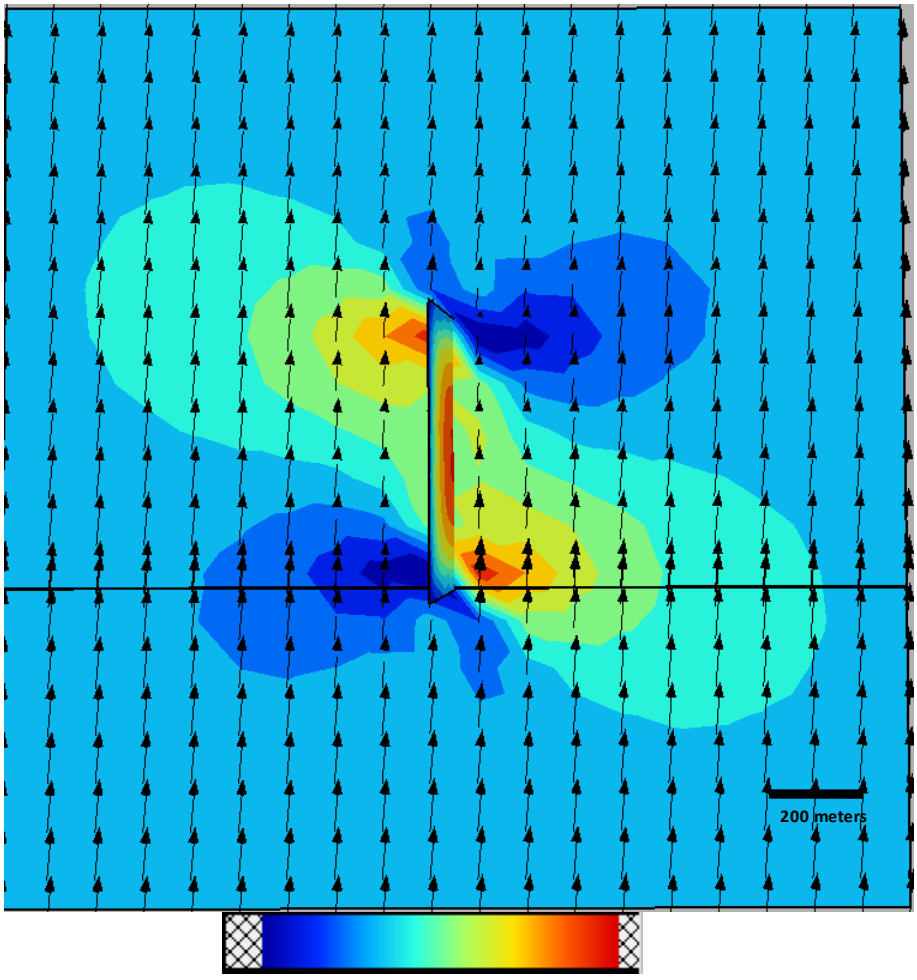

10.5 13.5 MPa

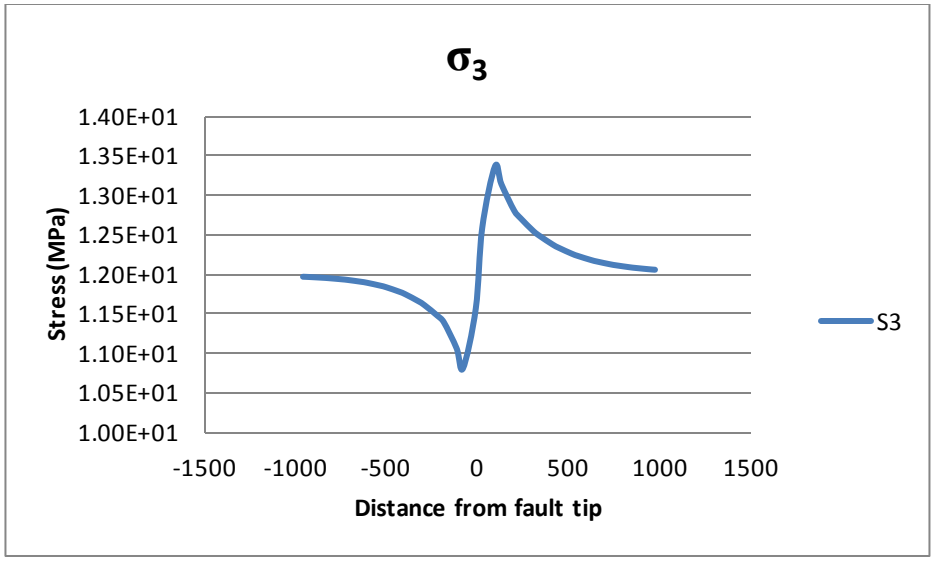

Fault 600 meters, Sandstone 5˚ at 2.25 km

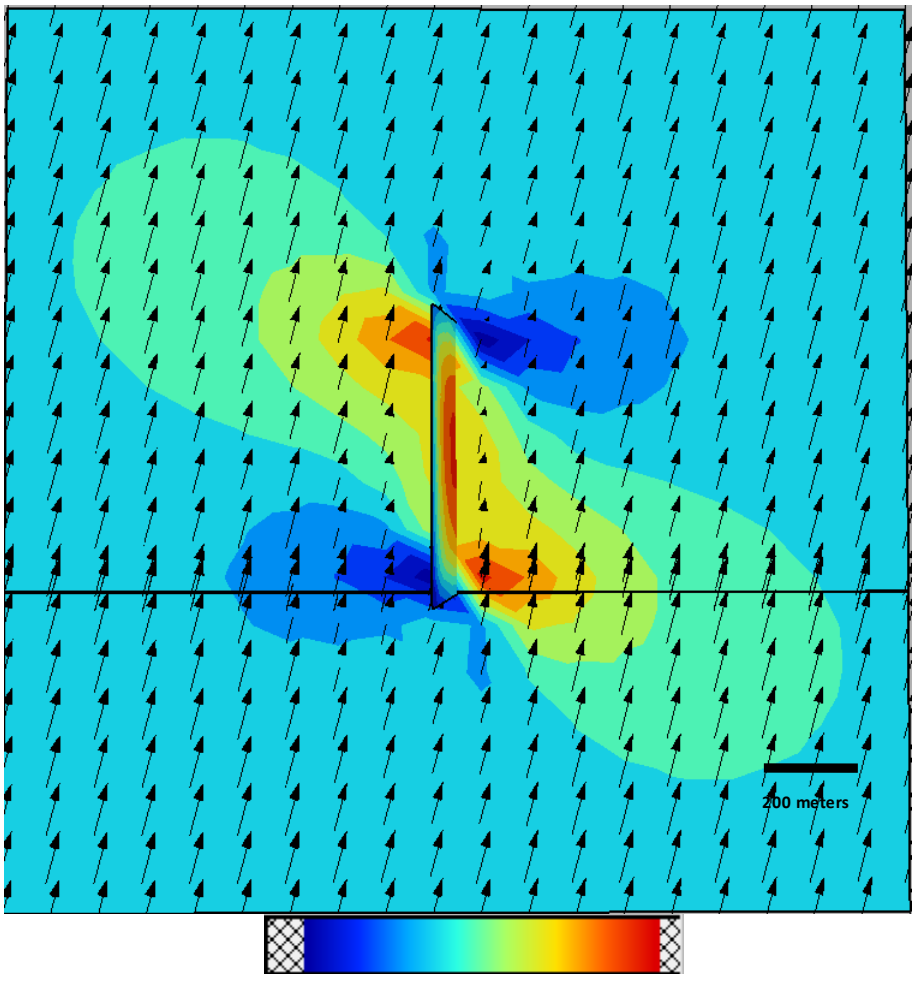

8.0 17.0 MPa

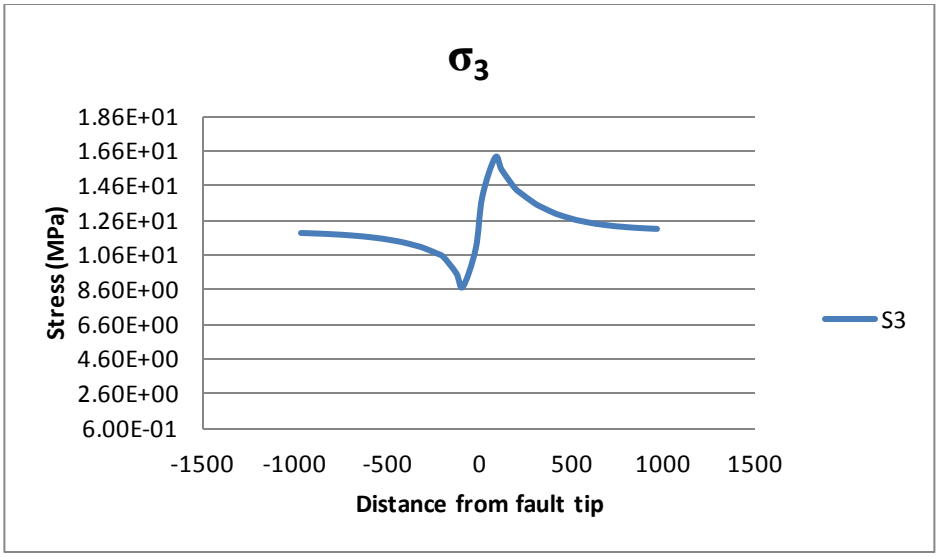

Fault 600 meters, Sandstone 15˚ at 2.25 km

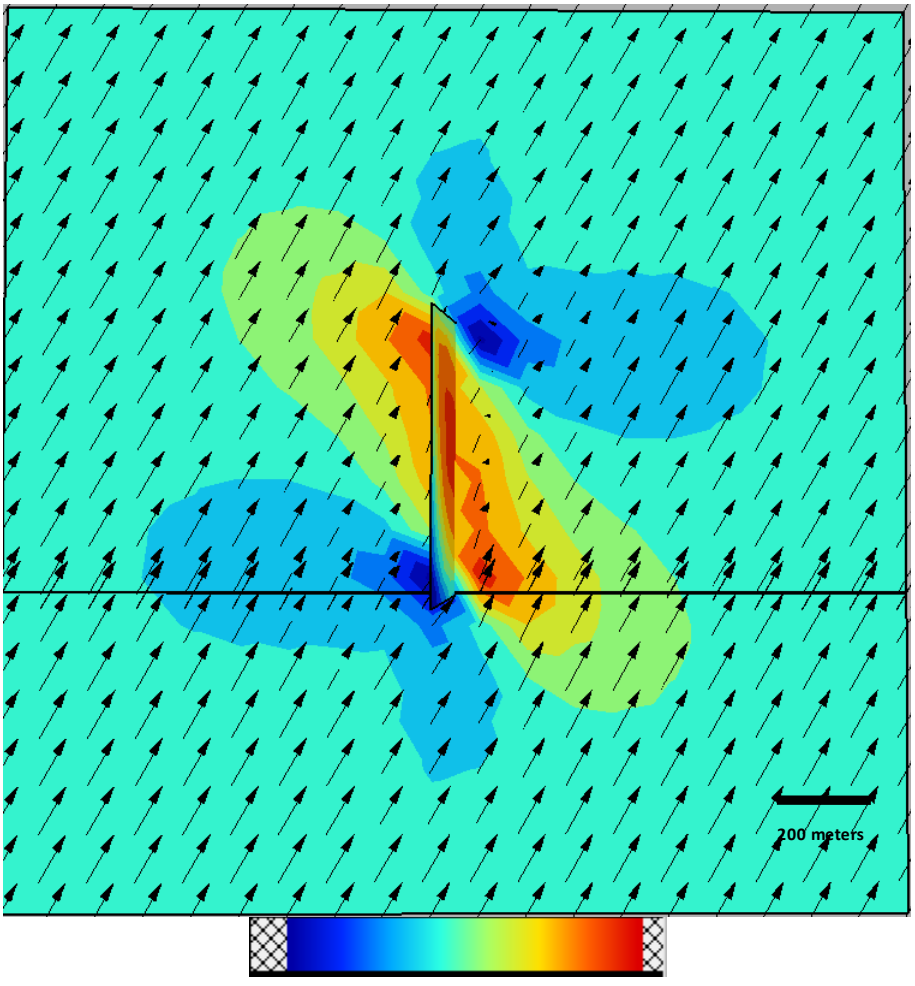

5.0 22.0 MPa

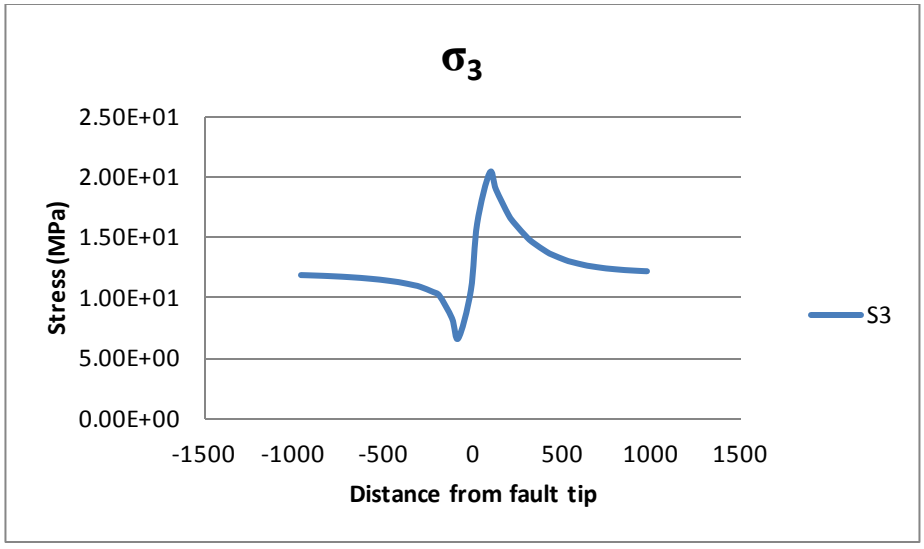

Fault 600 meters, Sandstone 30˚ at 2.25 km

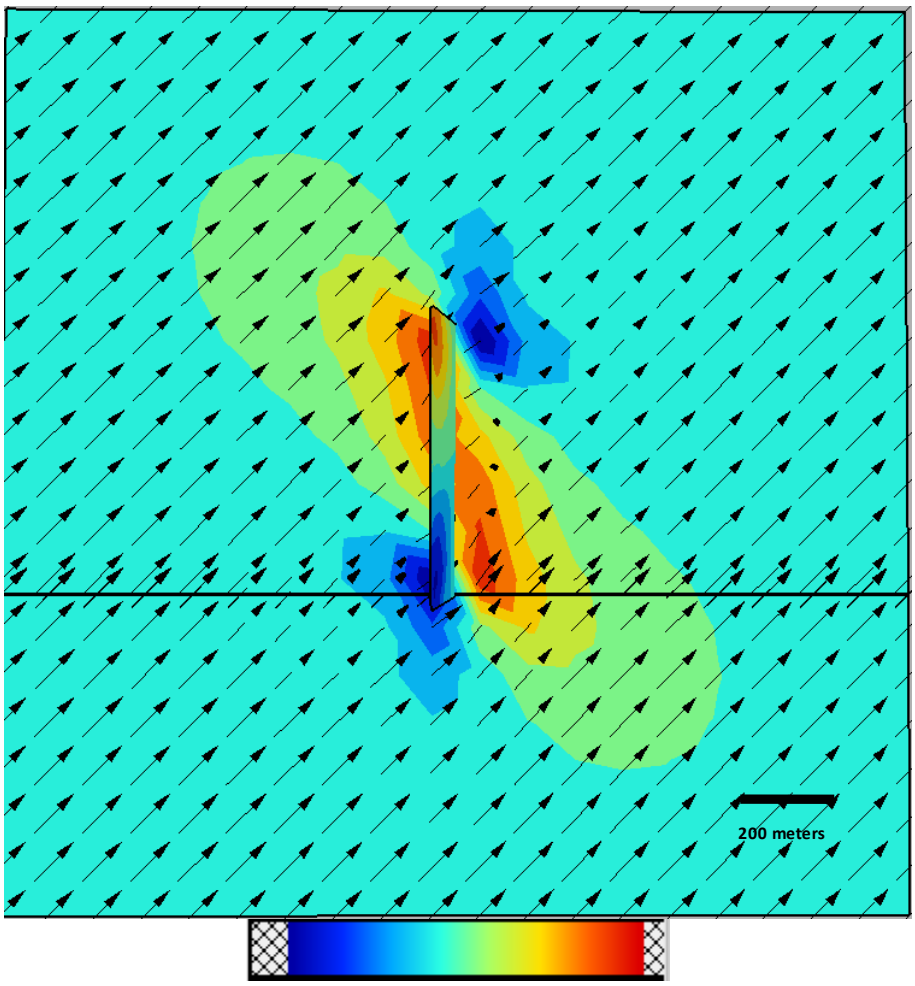

4.0 25.0 MPa

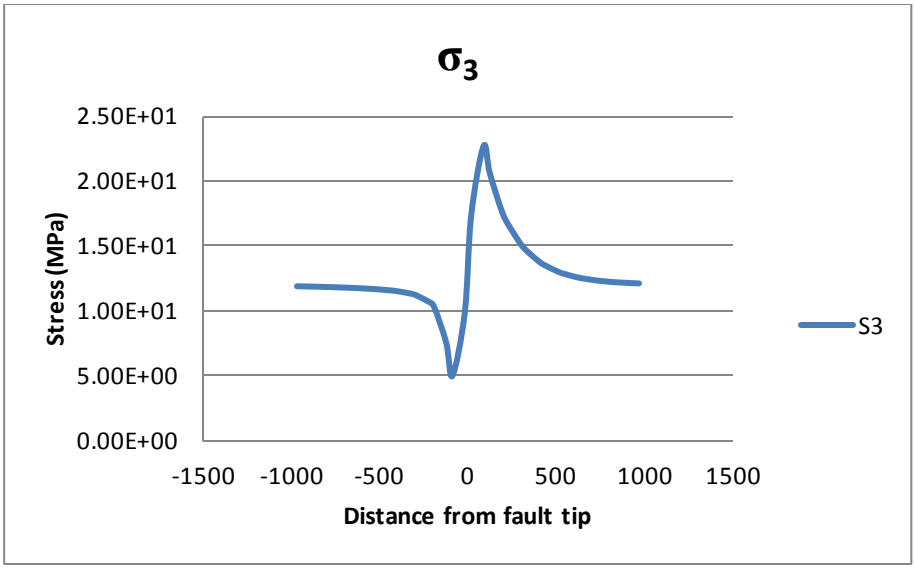

Fault 600 meters, Sandstone 45˚ at 2.25 km

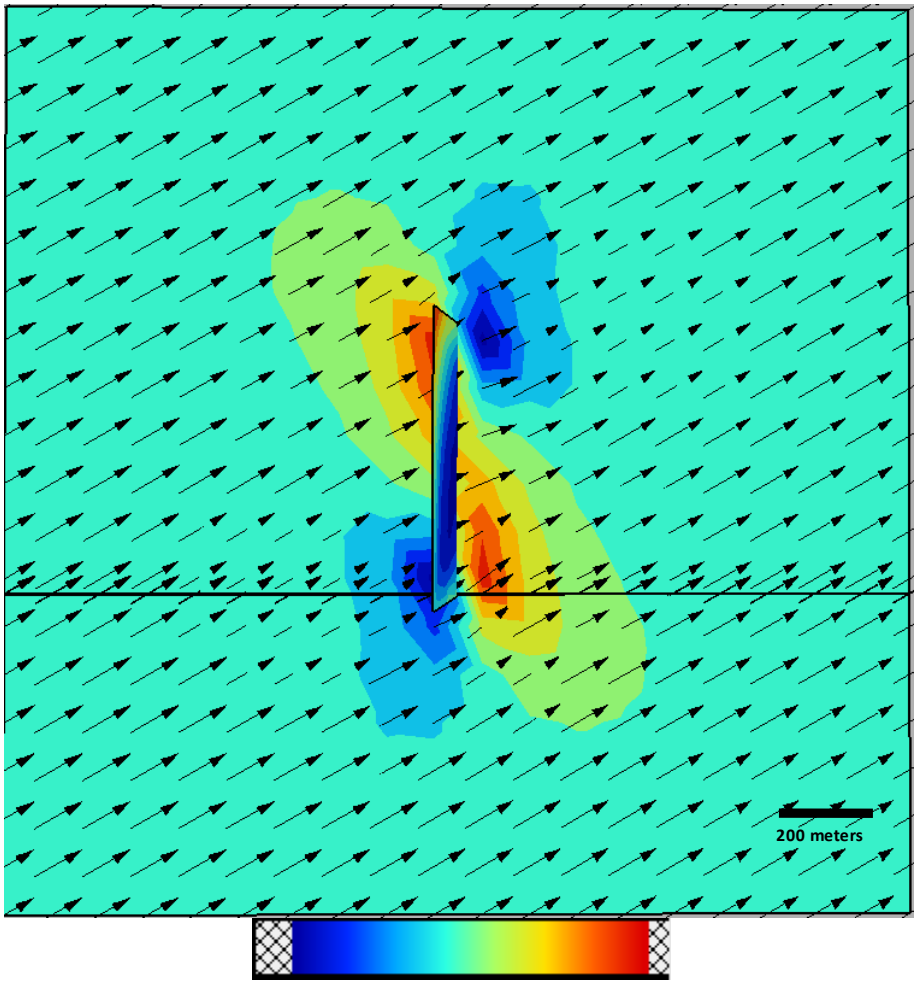

4.0 24.0 MPa

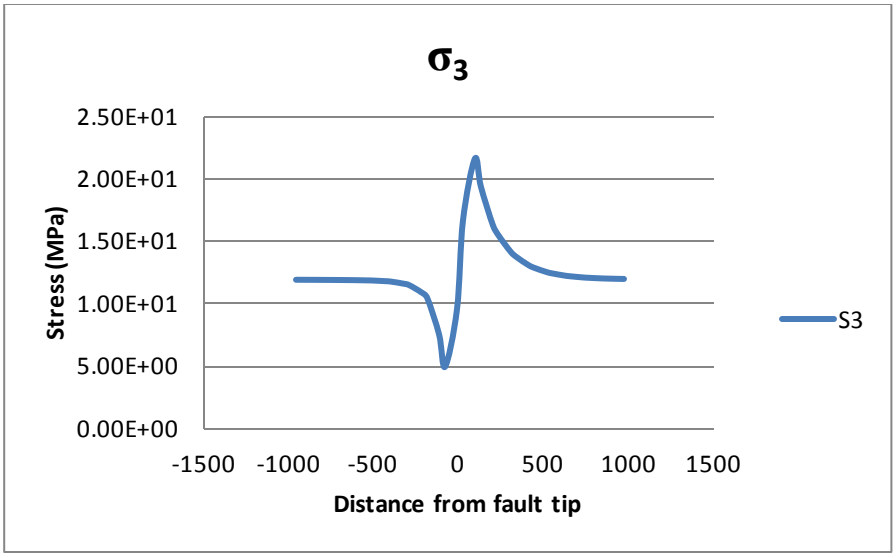

Fault 600 meters, Sandstone 60˚ at 2.25 km

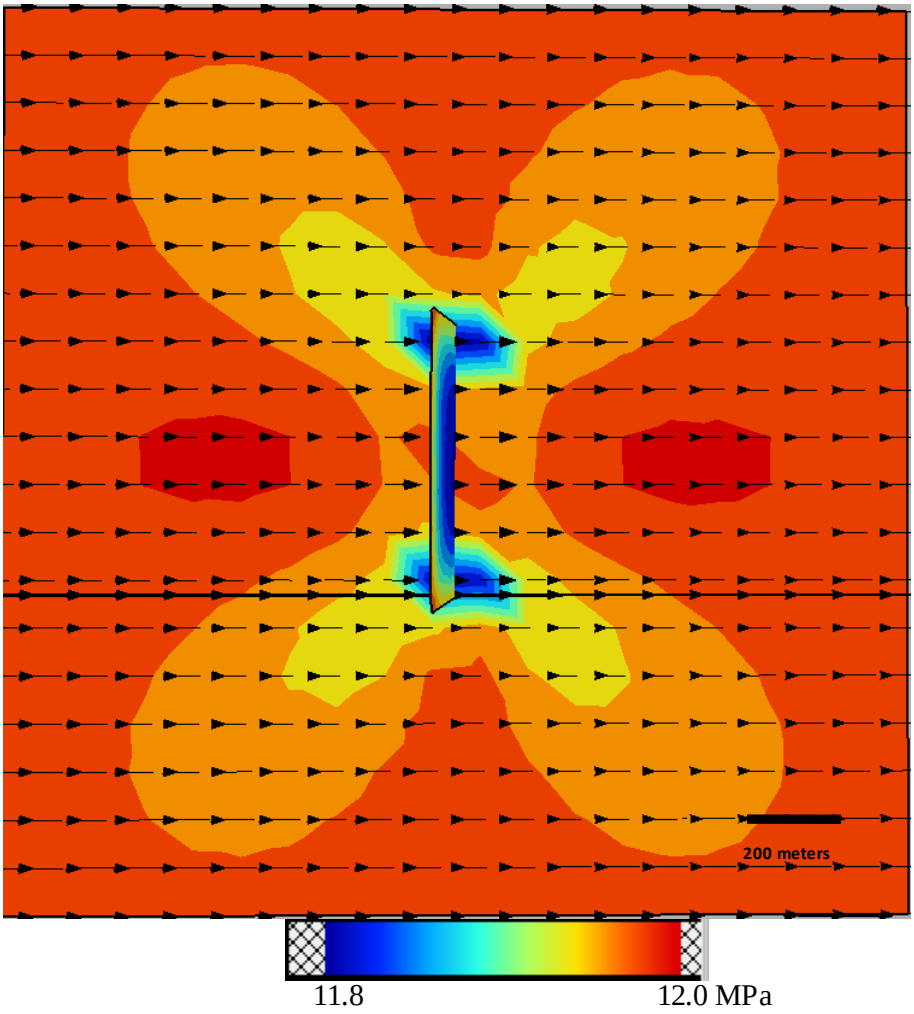

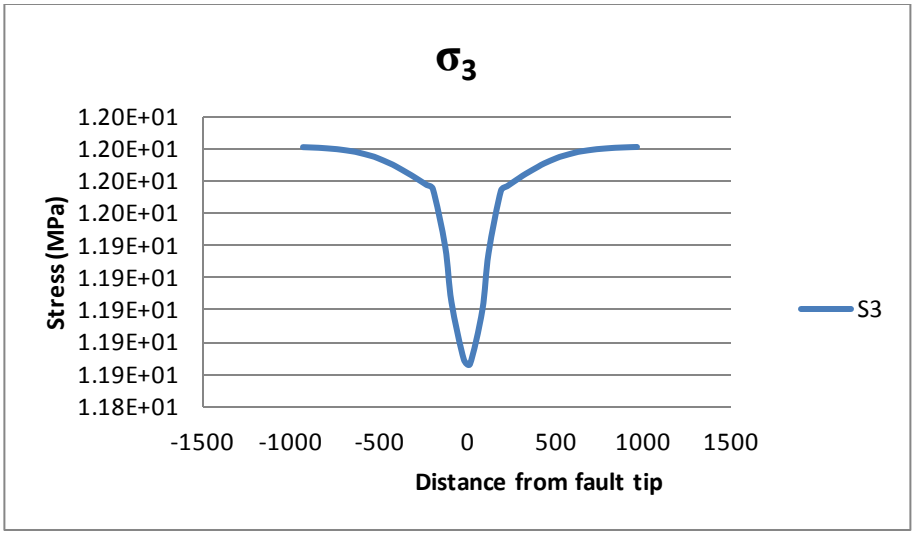

Fault 600 meters, Sandstone 90˚ at 2.25 km

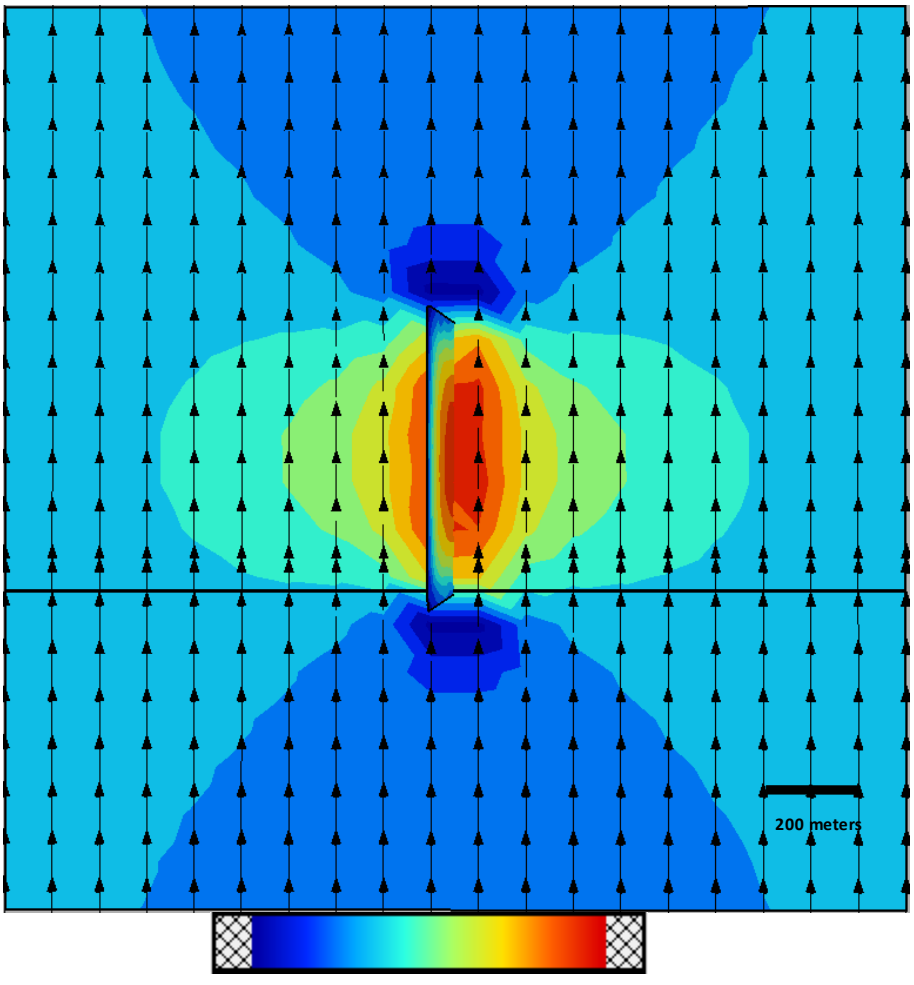

2.8 2.8 MPa

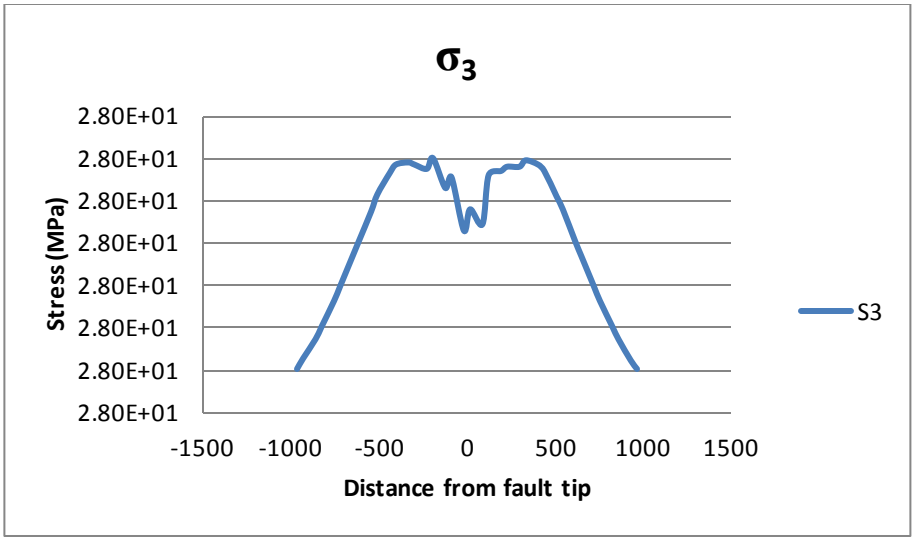

Fault 600 meters, Shale 0˚ at 2.5 km

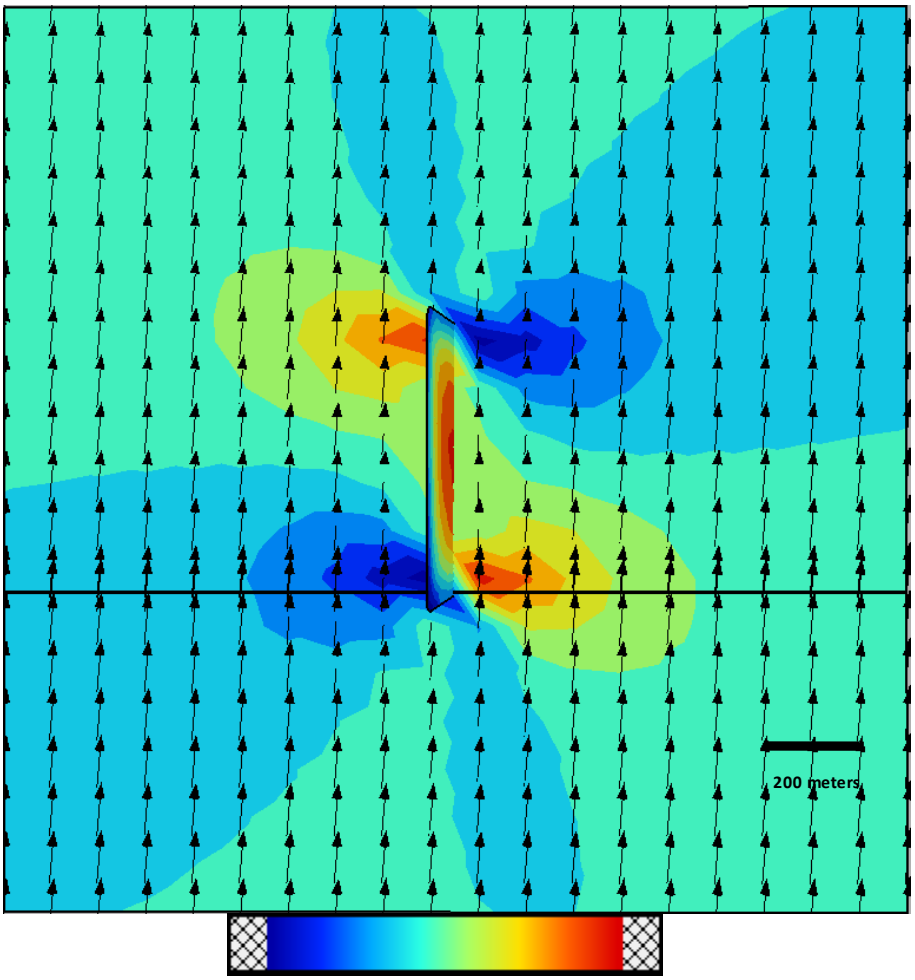

25.0 30.5 MPa

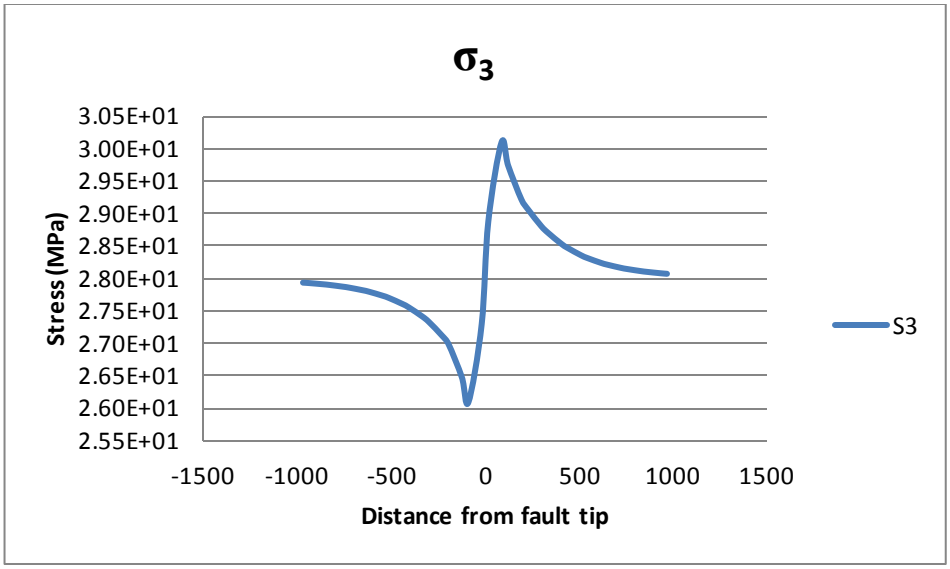

Fault 600 meters, Shale 5˚ at 2.5 km

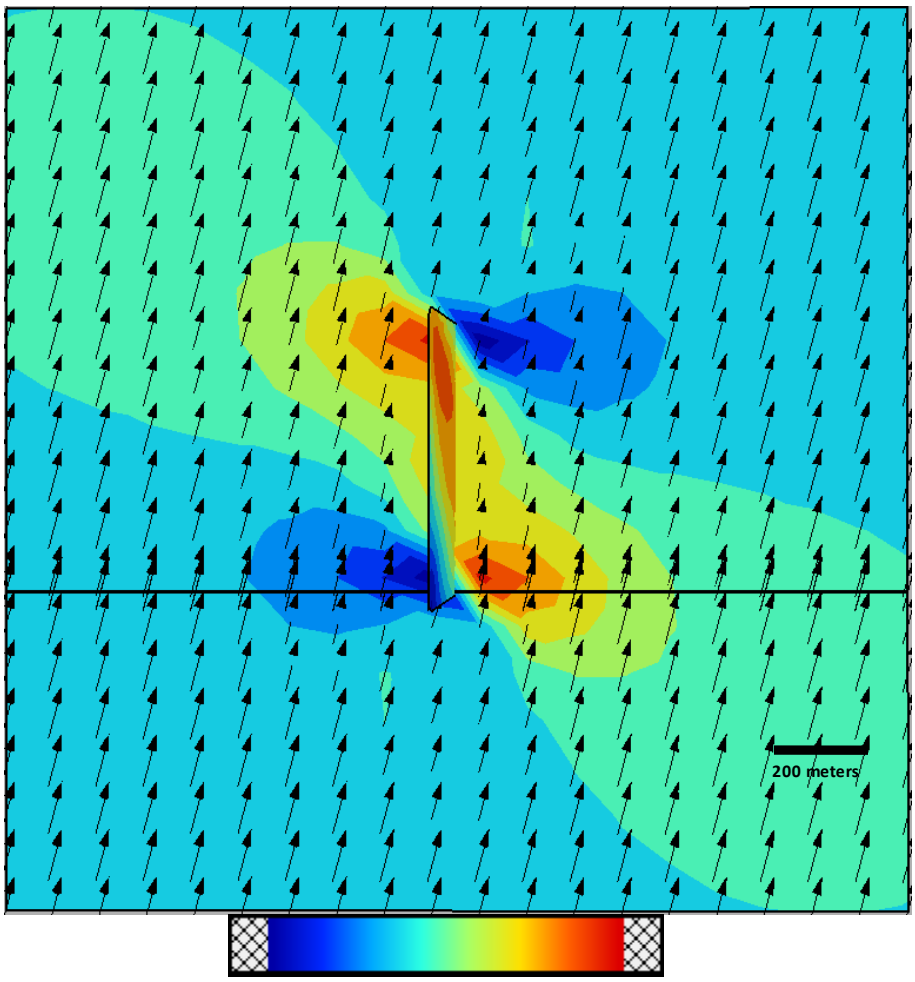

21.0 34.5 MPa

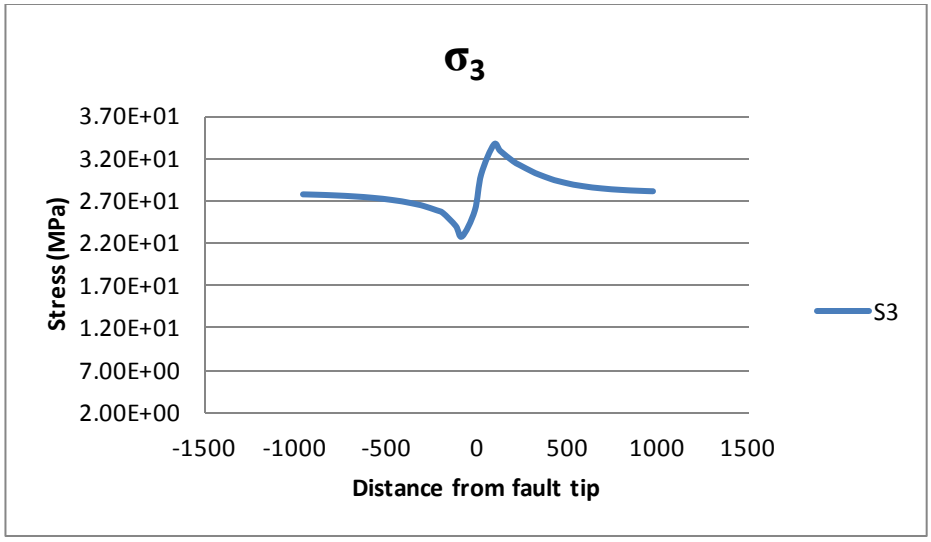

Fault 600 meters, Shale 15˚ at 2.5 km

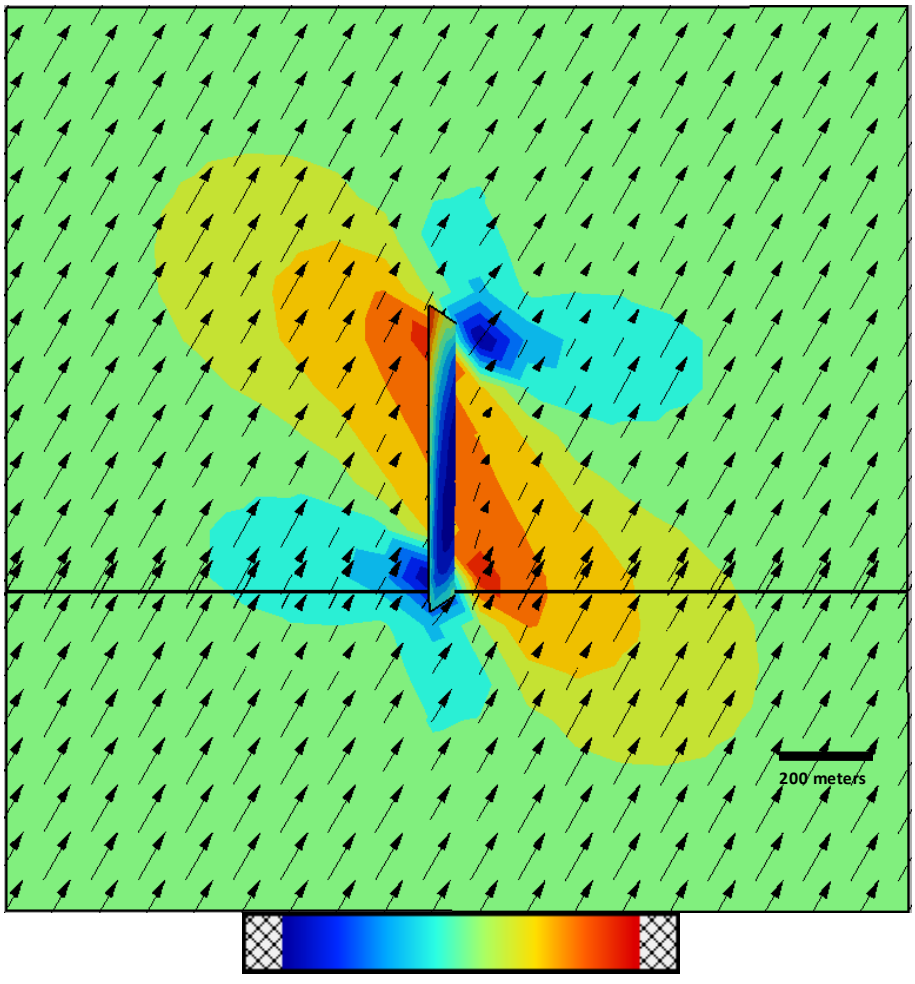

16 35.0 MPa

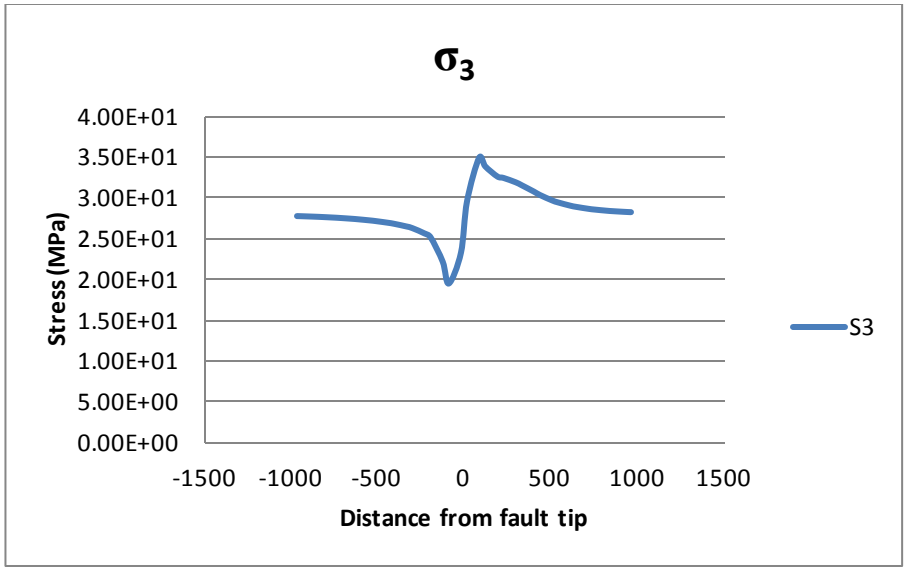

Fault 600 meters, Shale 30˚ at 2.5 km

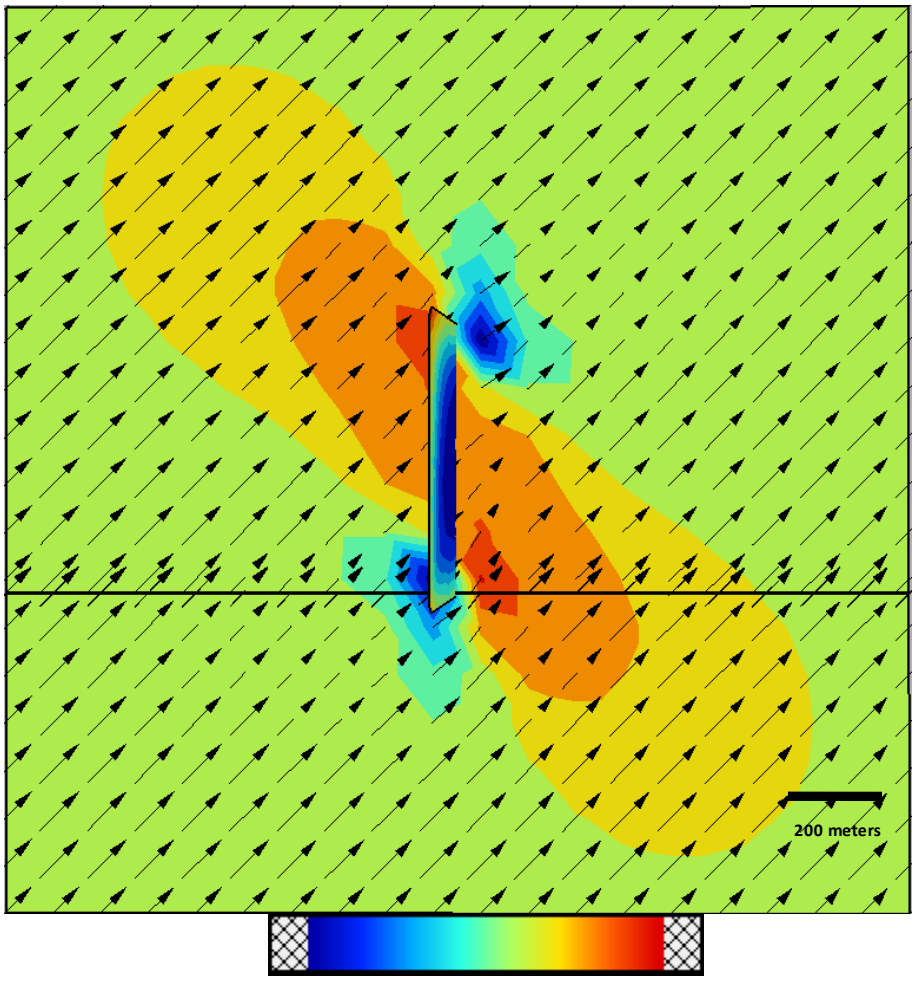

15.0 37.7 MPa

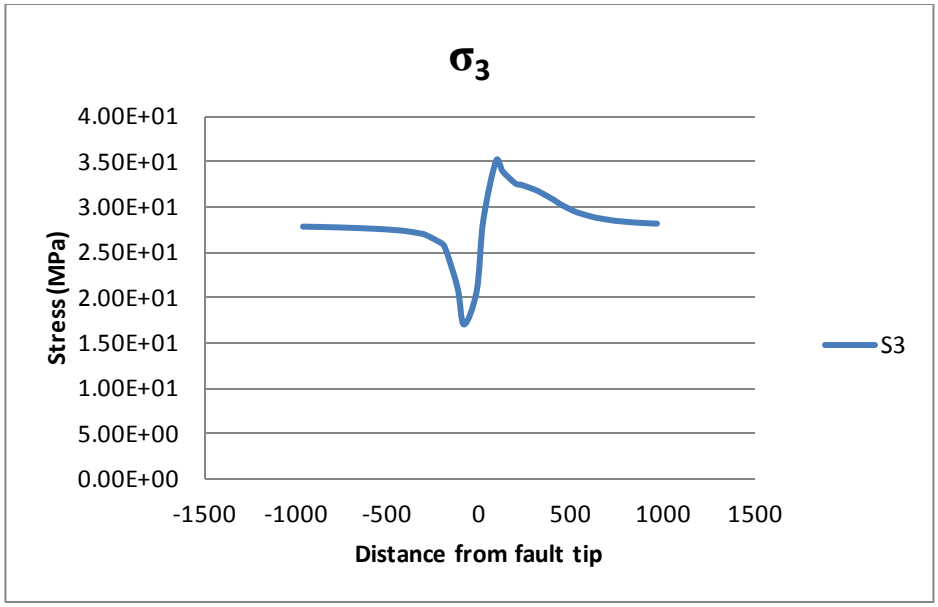

Fault 600 meters, Shale 45˚ at 2.5 km

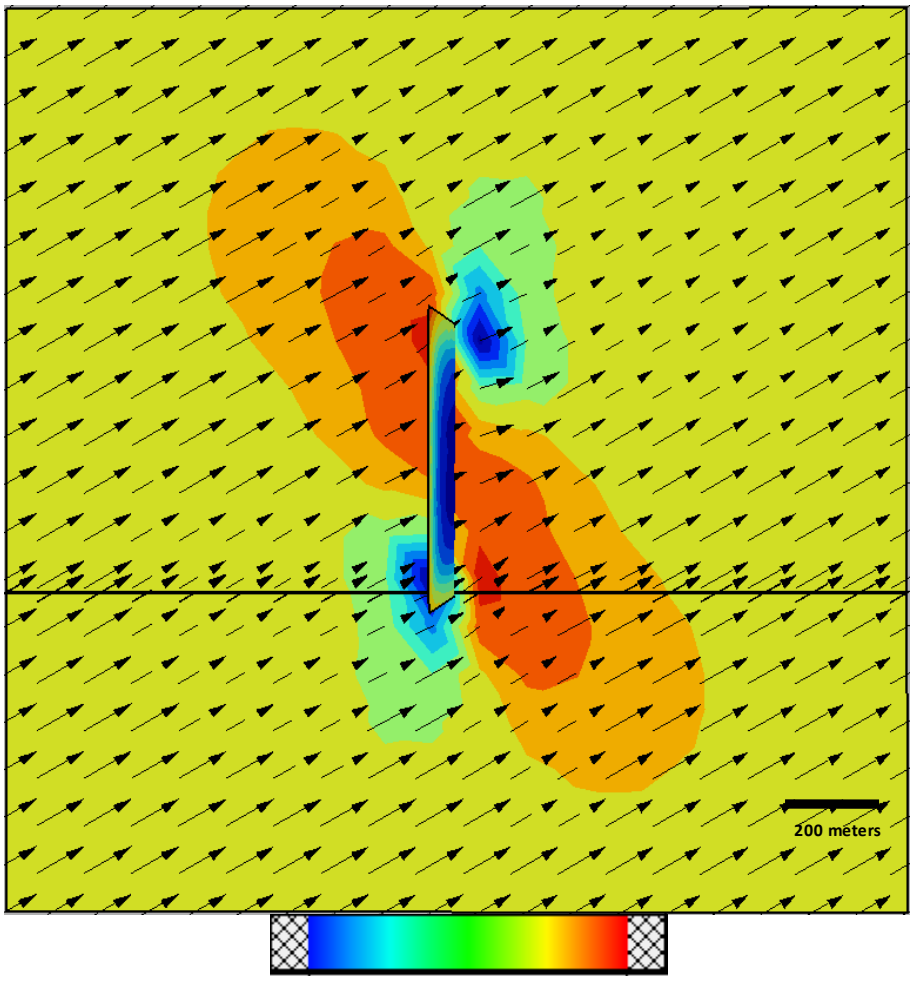

15.0 35.0 Mpa

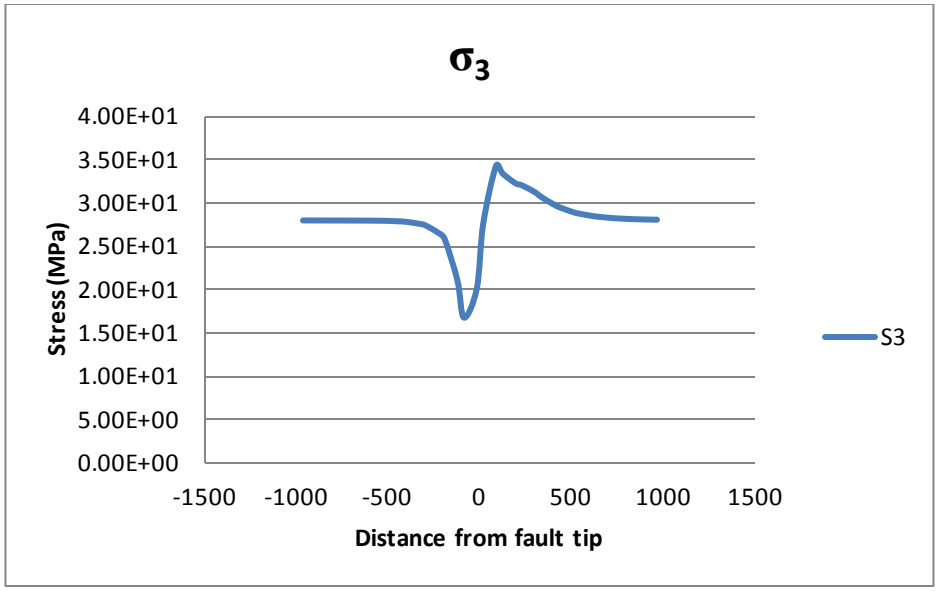

Fault 600 meters, Shale 60˚ at 2.5 km

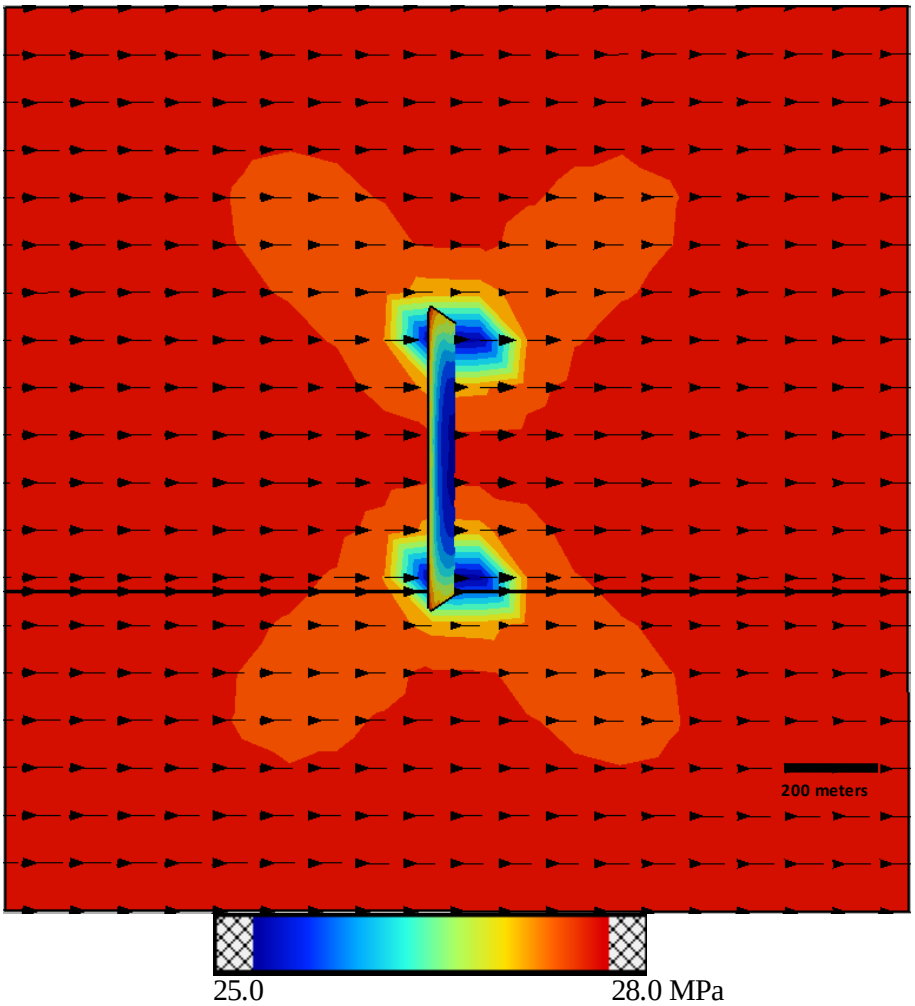

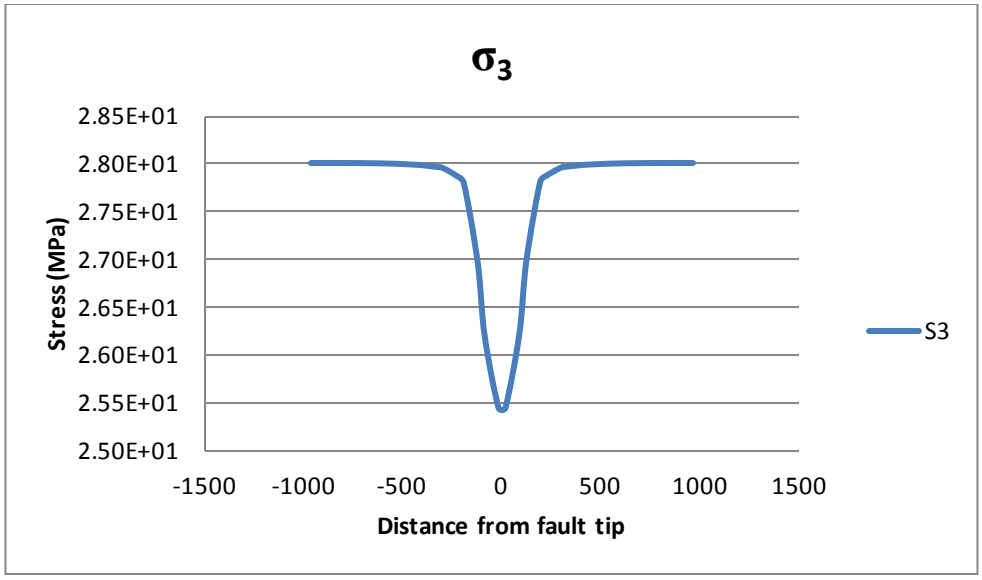

Fault 600 meters, Shale 90˚ at 2.5 km

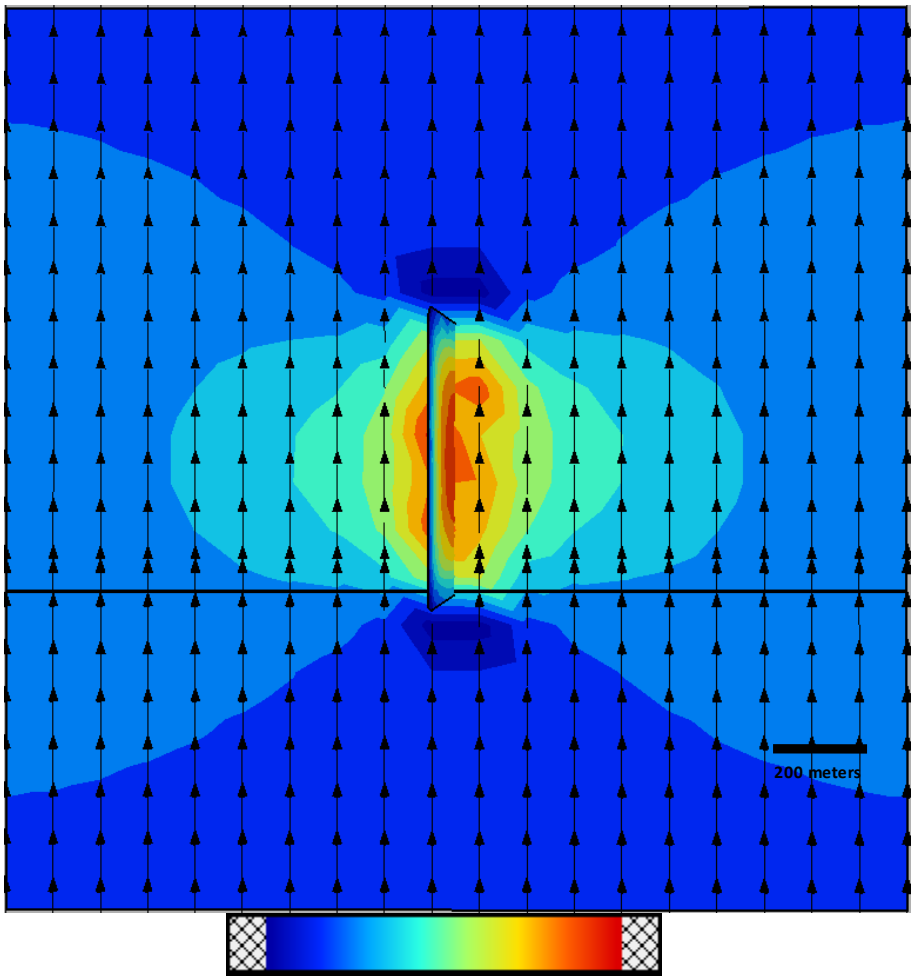

28.0 28.0 MPa

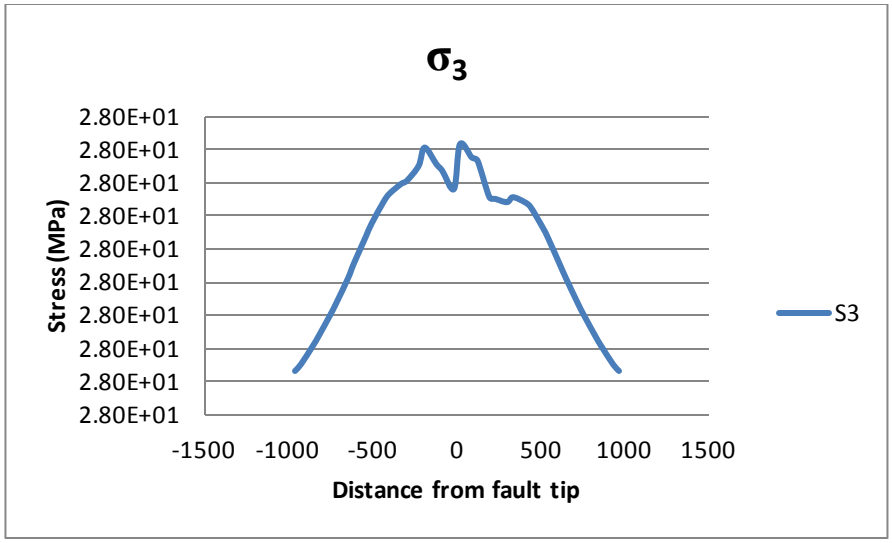

Fault 600 meters, Coal 0˚ at 2.5 km

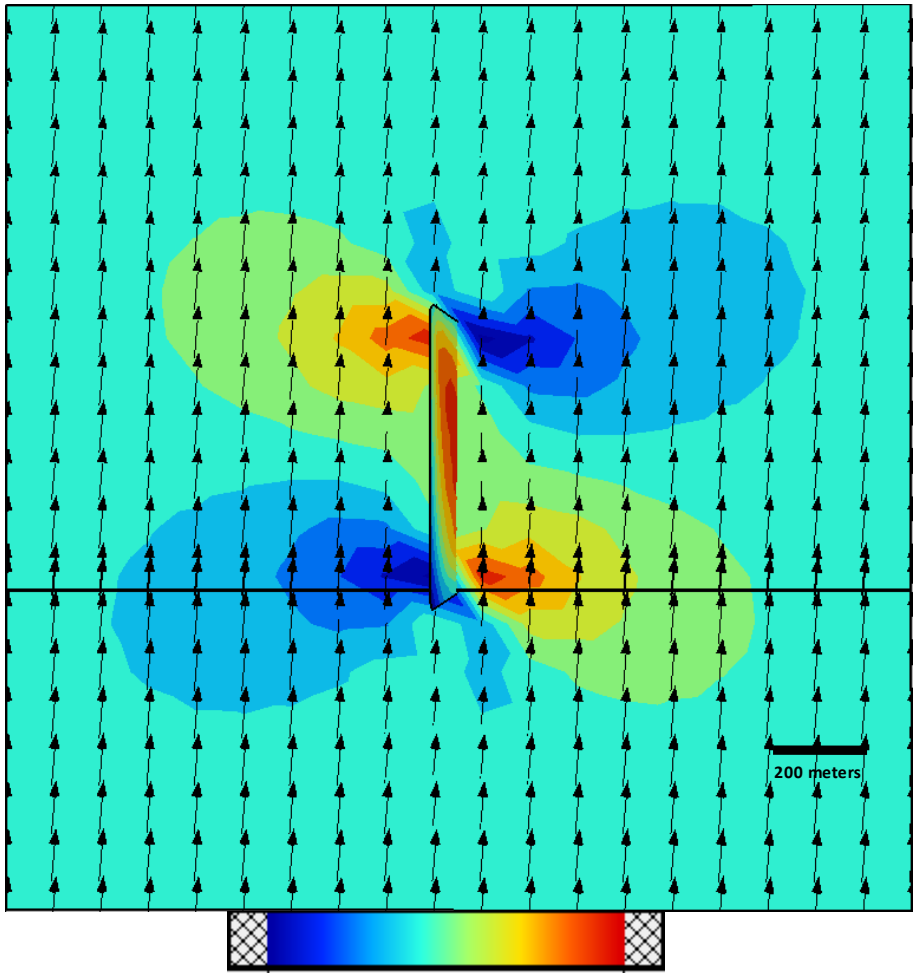

25.5 30.5 Mpa

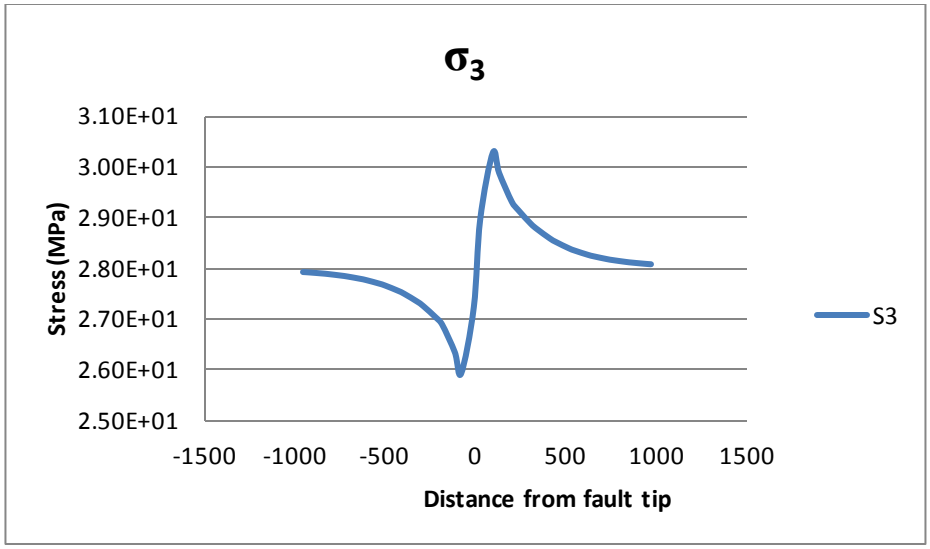

Fault 600 meters, Coal 5˚ at 2.5 km

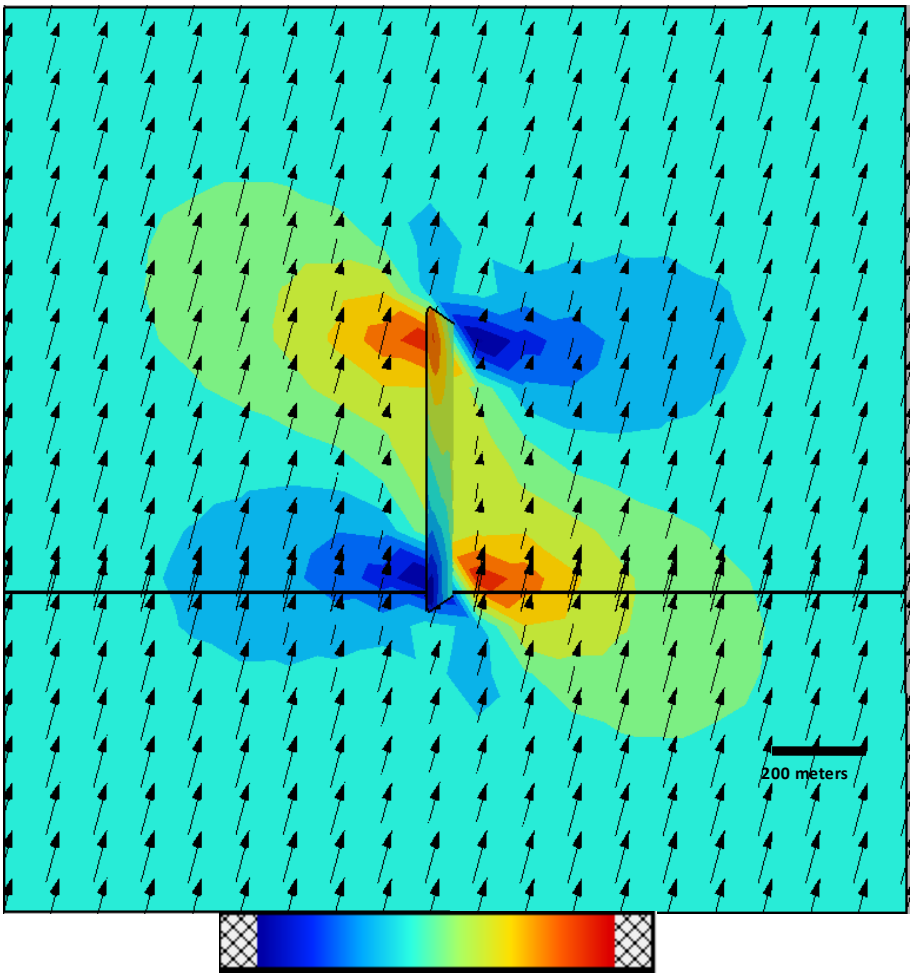

20.0 36.0 MPa

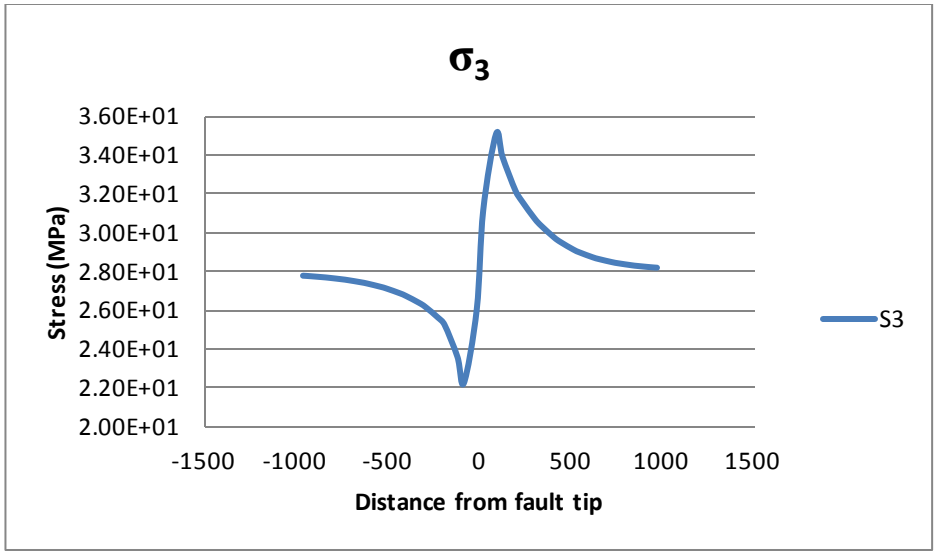

Fault 600 meters, Coal 15˚ at 2.5 km

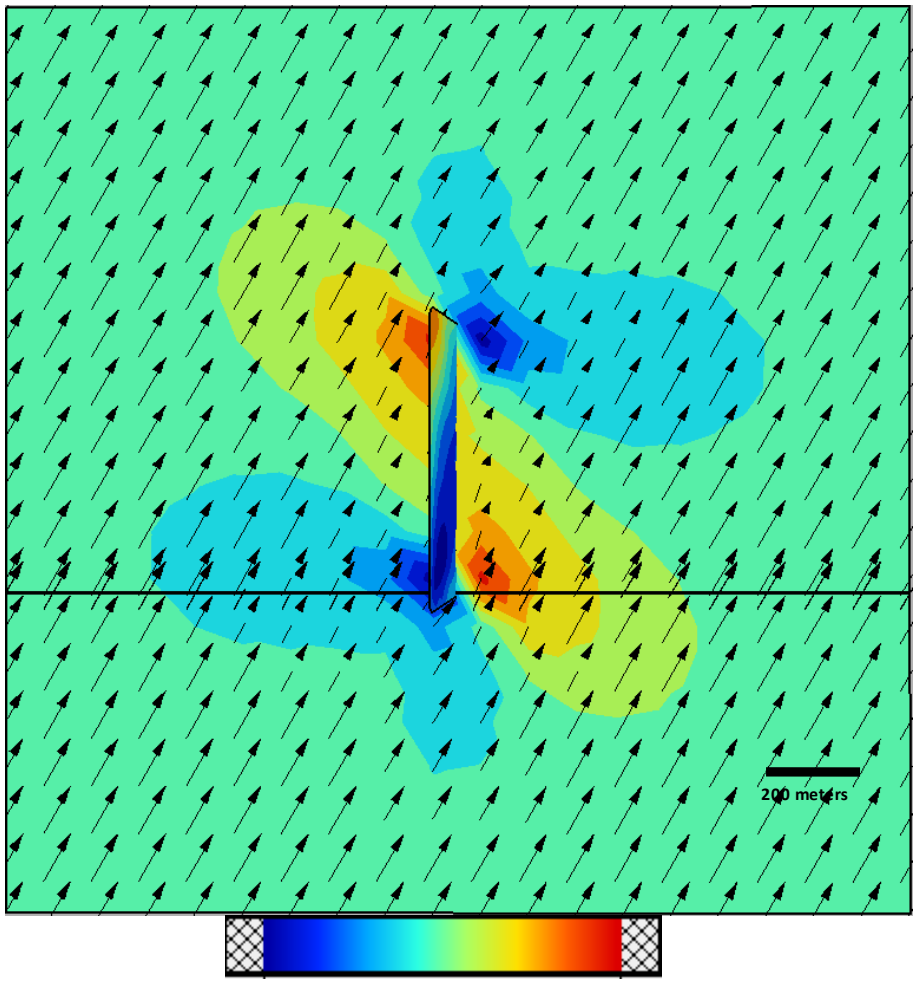

15.0 42.0 MPa

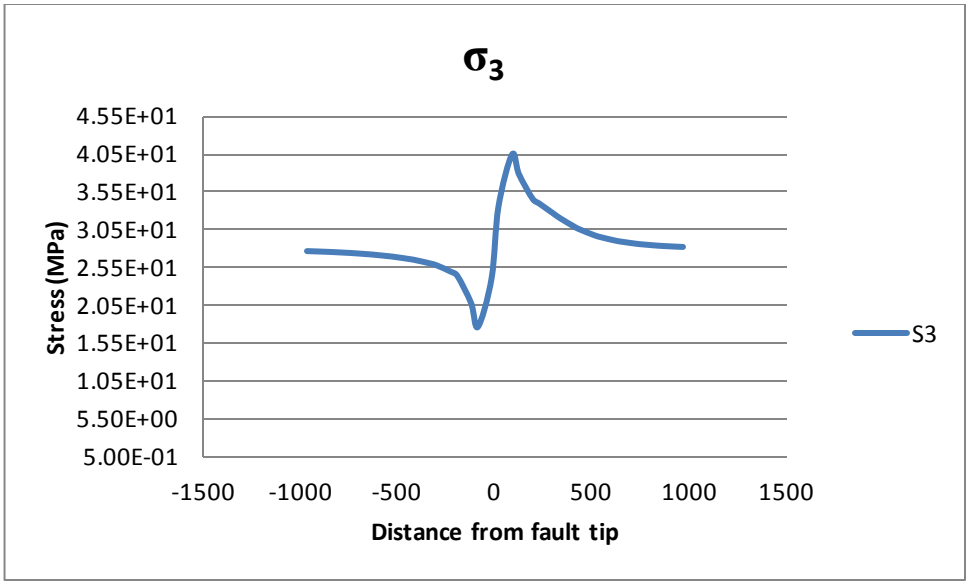

Fault 600 meters, Coal 30˚ at 2.5 km

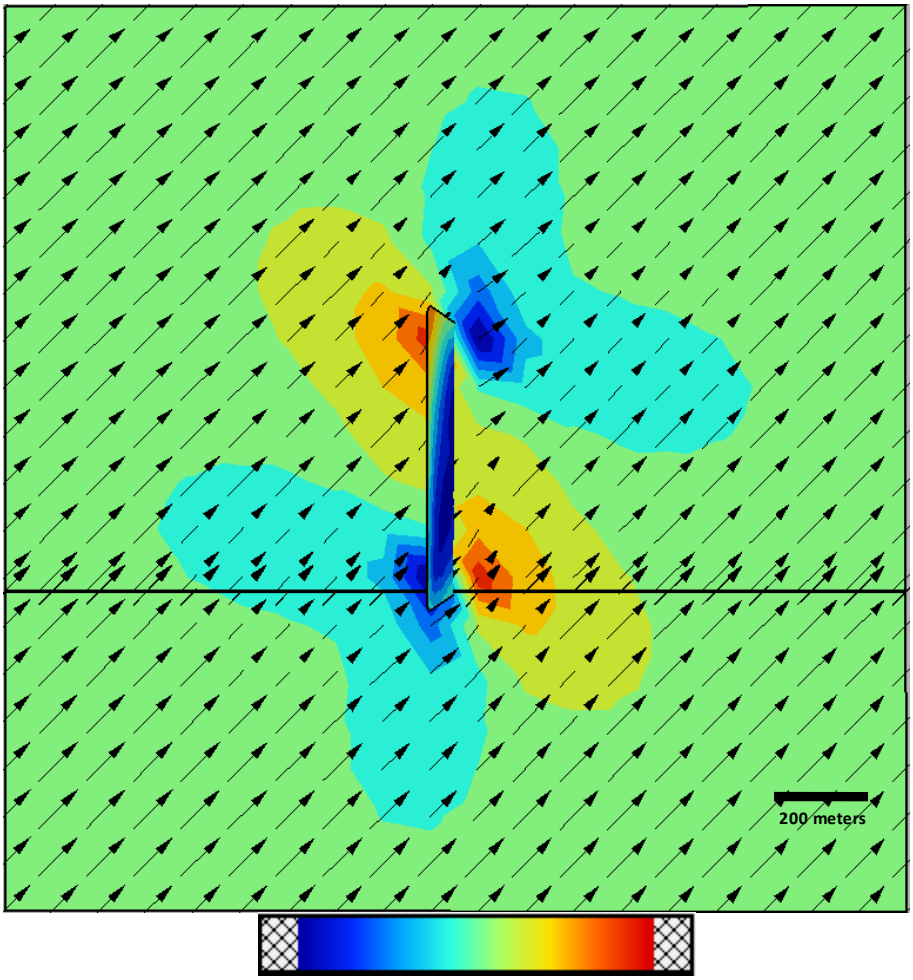

10.0 42.0 MPa

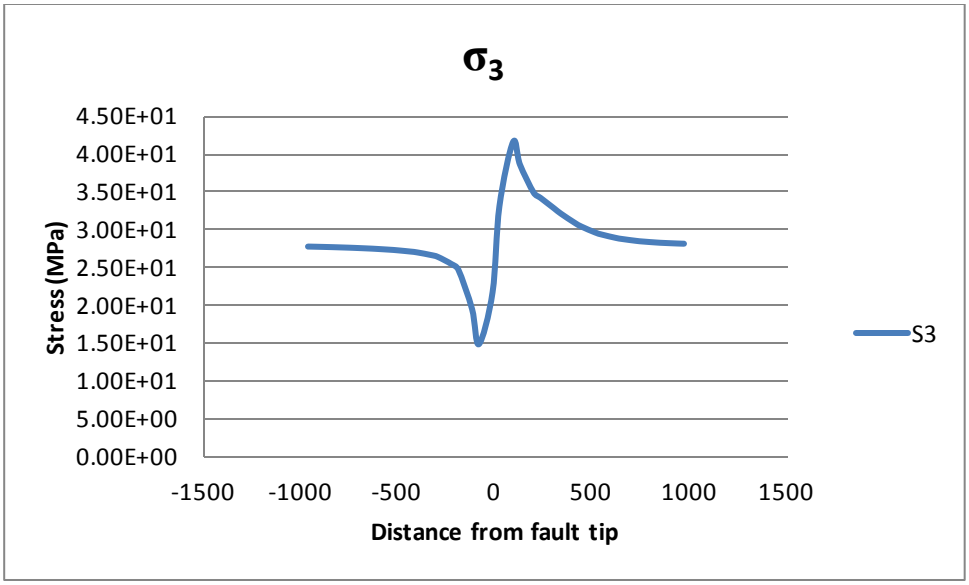

Fault 600 meters, Coal 45˚ at 2.5 km

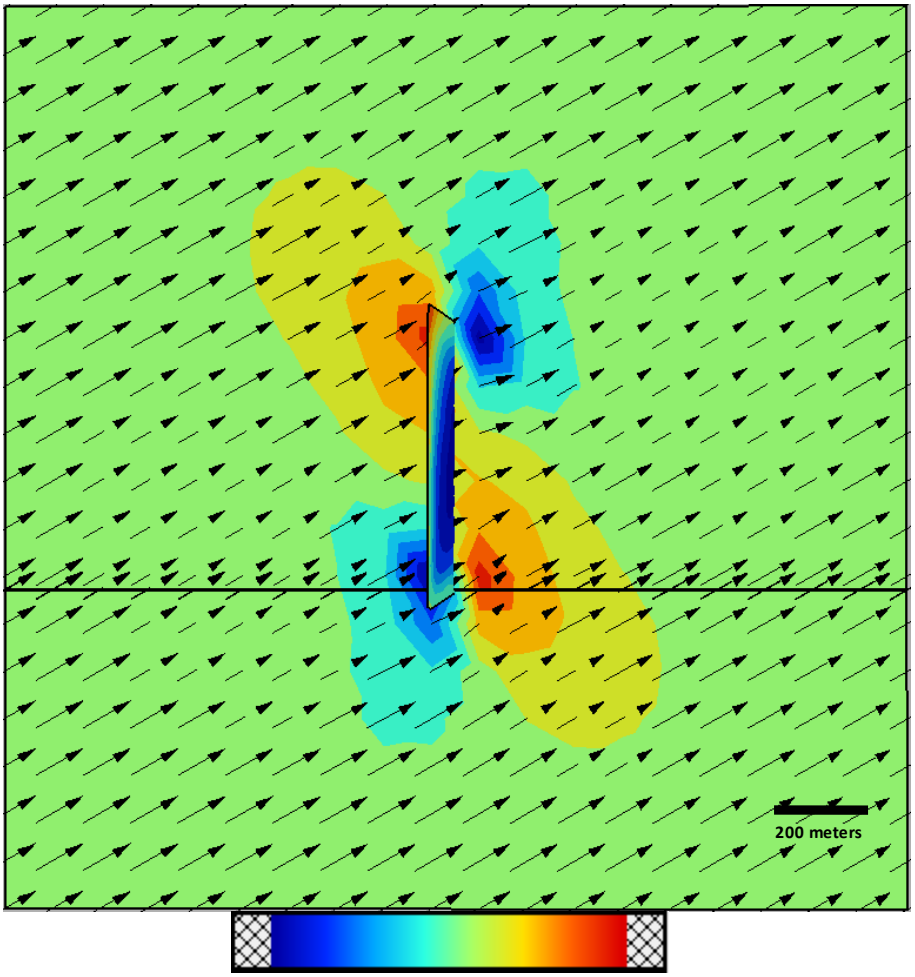

10.0 42.0 MPa

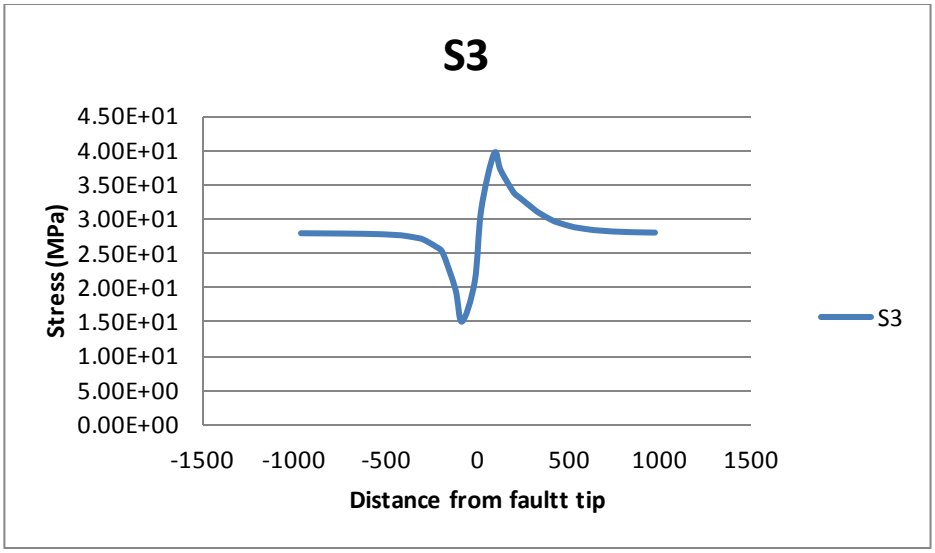

Fault 600 meters, Coal 60˚ at 2.5 km

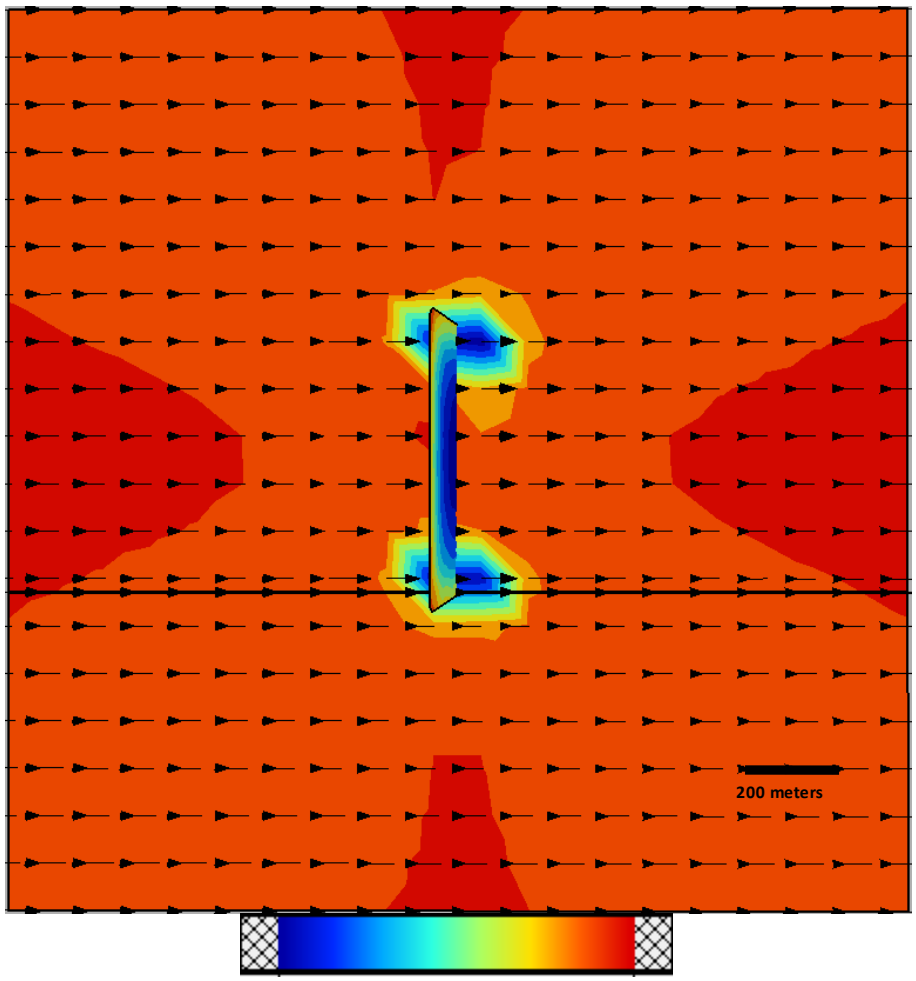

26.0 28.0 MPa

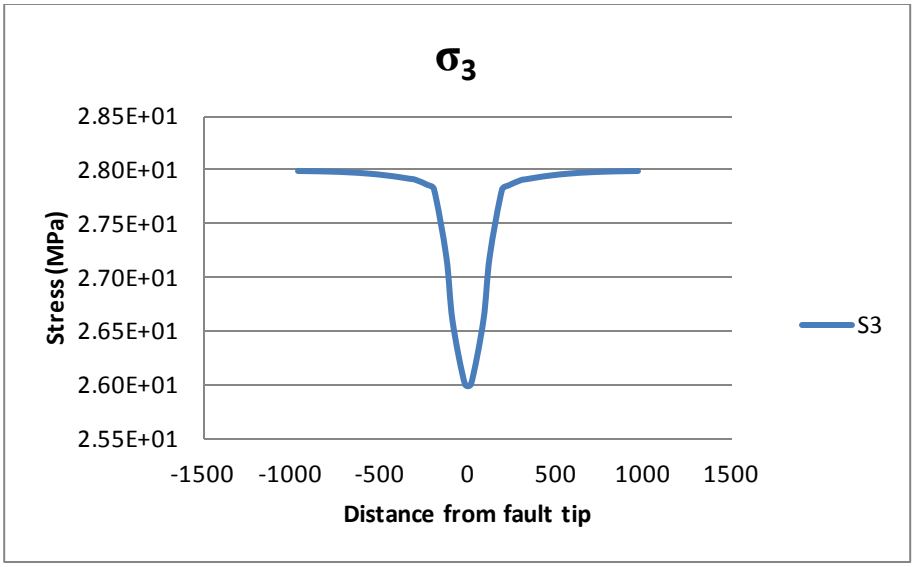

Fault 600 meters, Coal 90˚ at 2.5 km

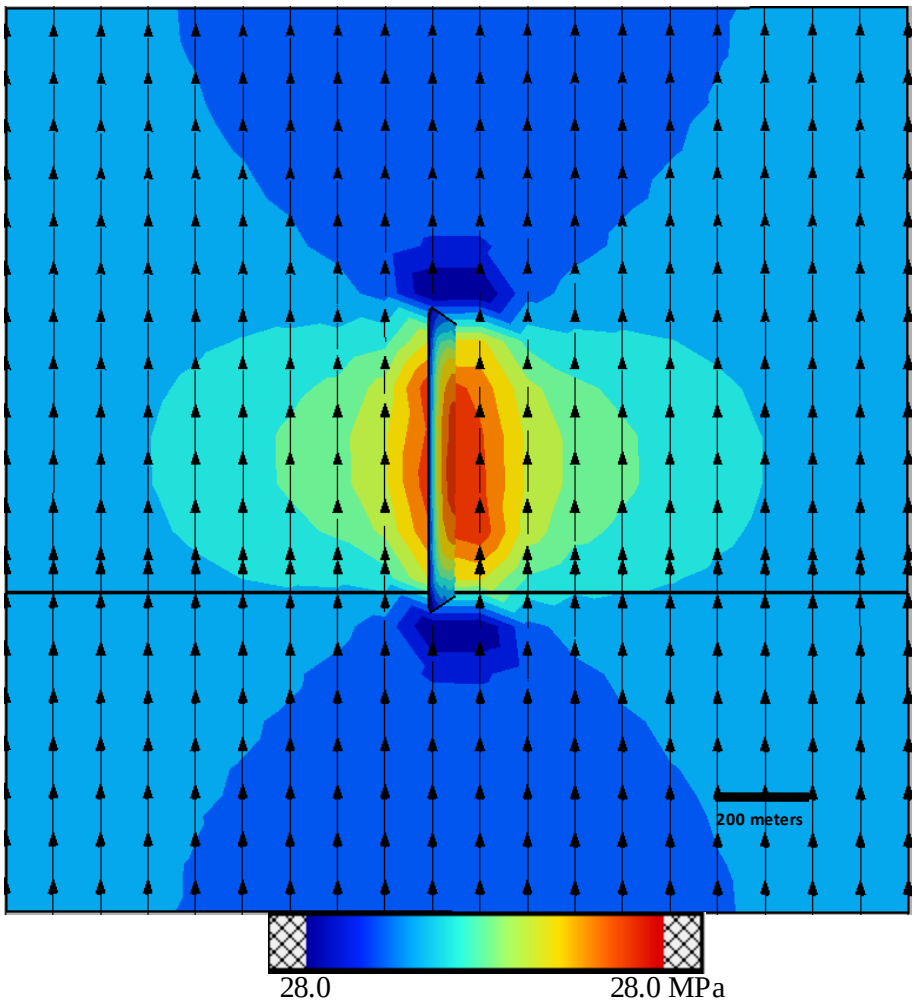

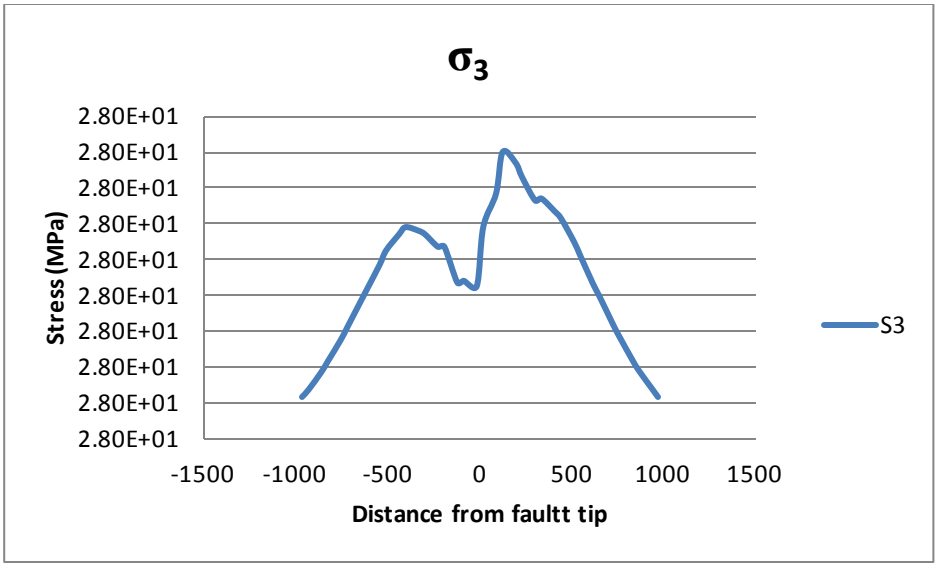

Fault 600 meters, Sandstone 0˚ at 2.5 km

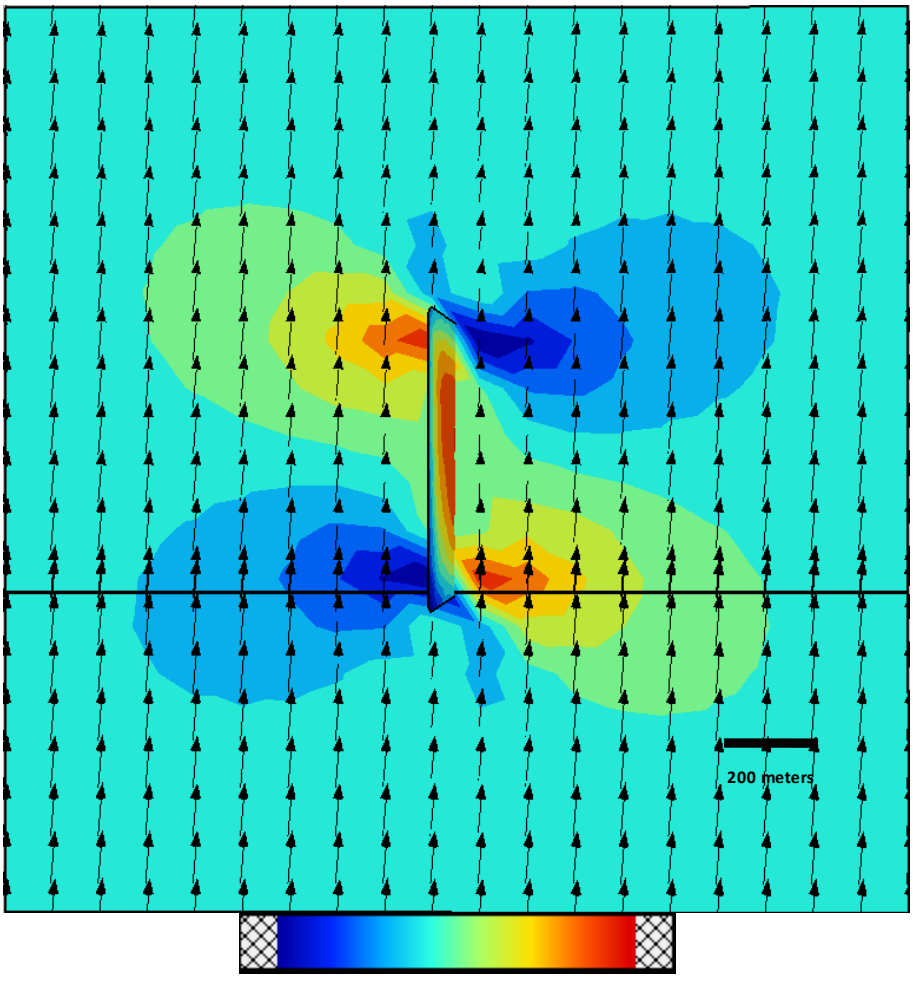

25.0 30.5 MPa

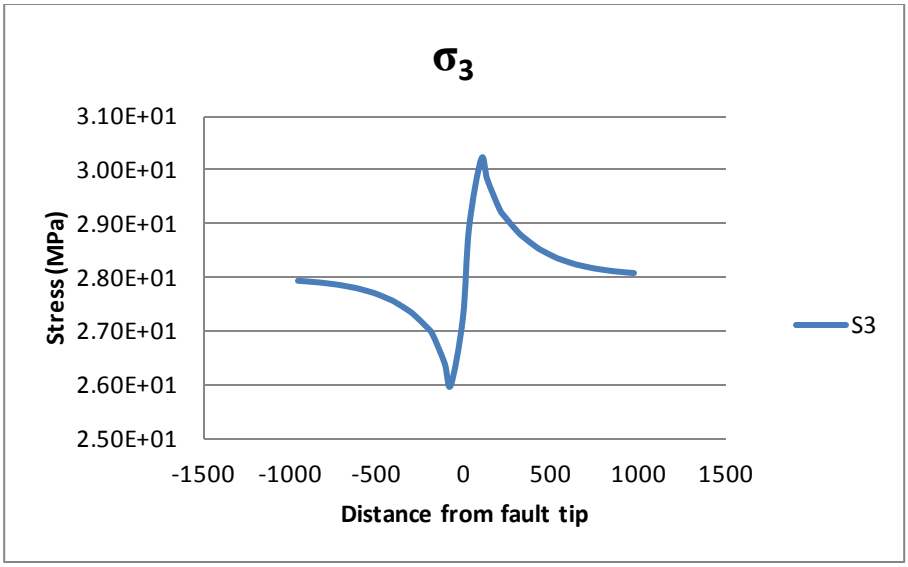

Fault 600 meters, Sandstone 5˚ at 2.5 km

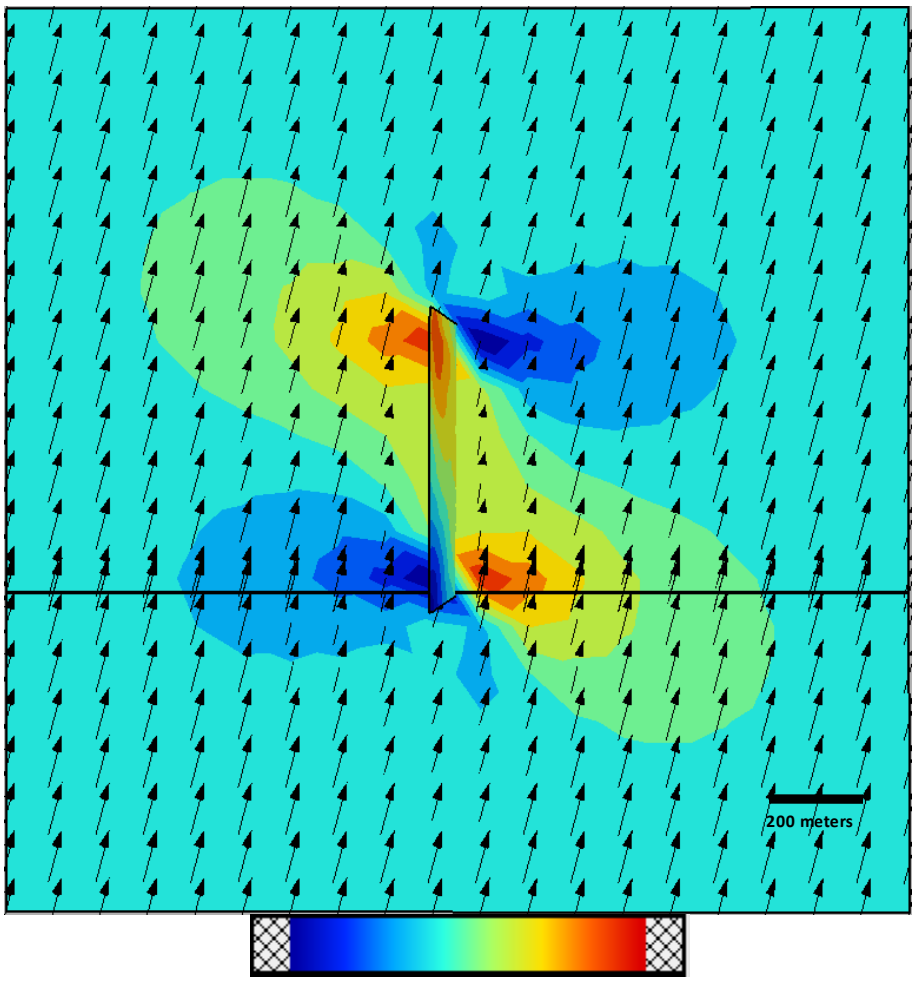

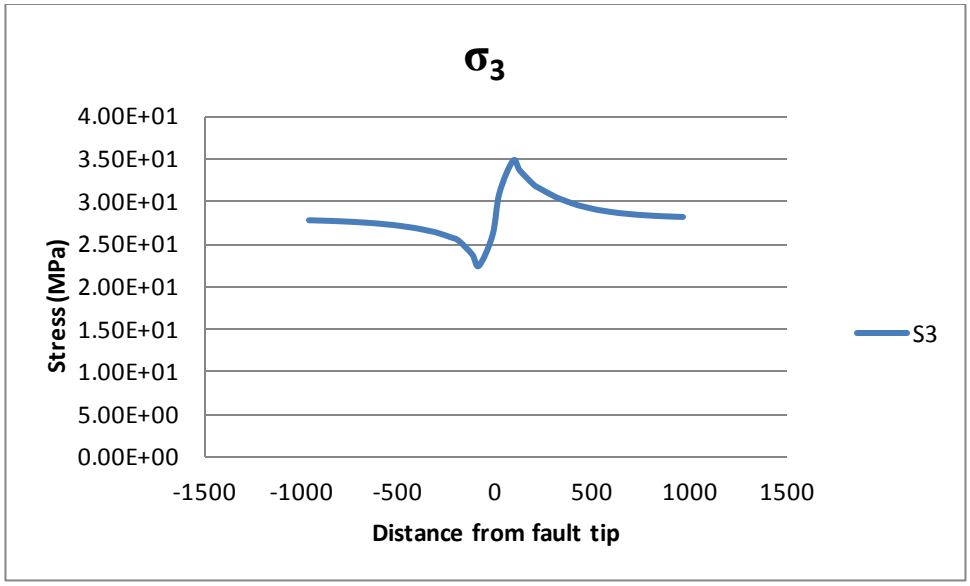

Fault 600 meters, Sandstone 15˚ at 2.5 km

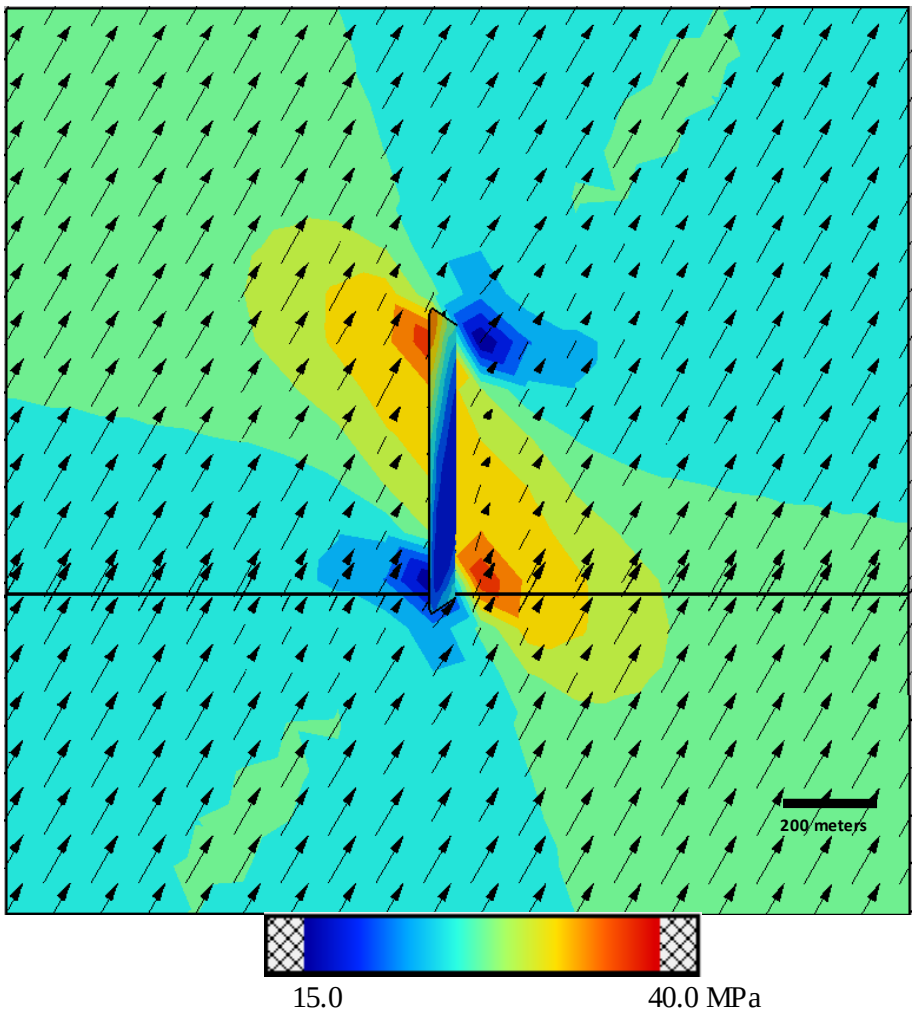

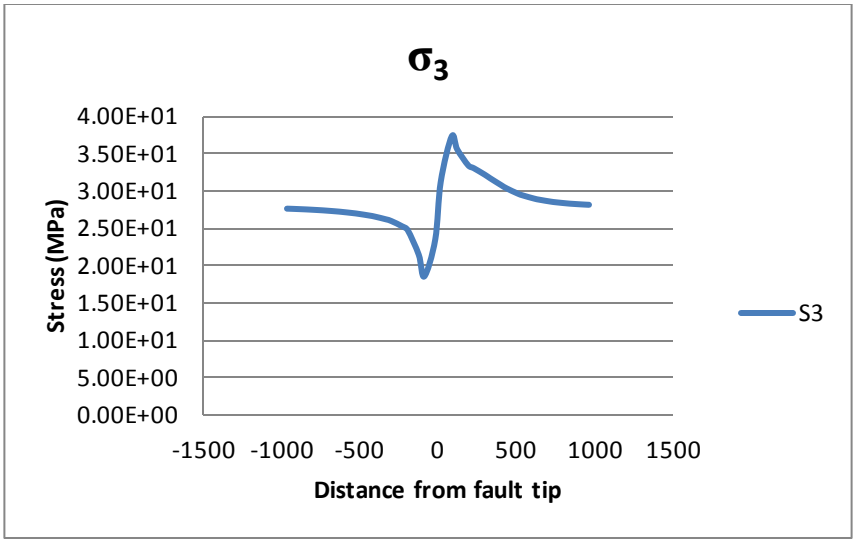

Fault 600 meters, Sandstone 30˚ at 2.5 km

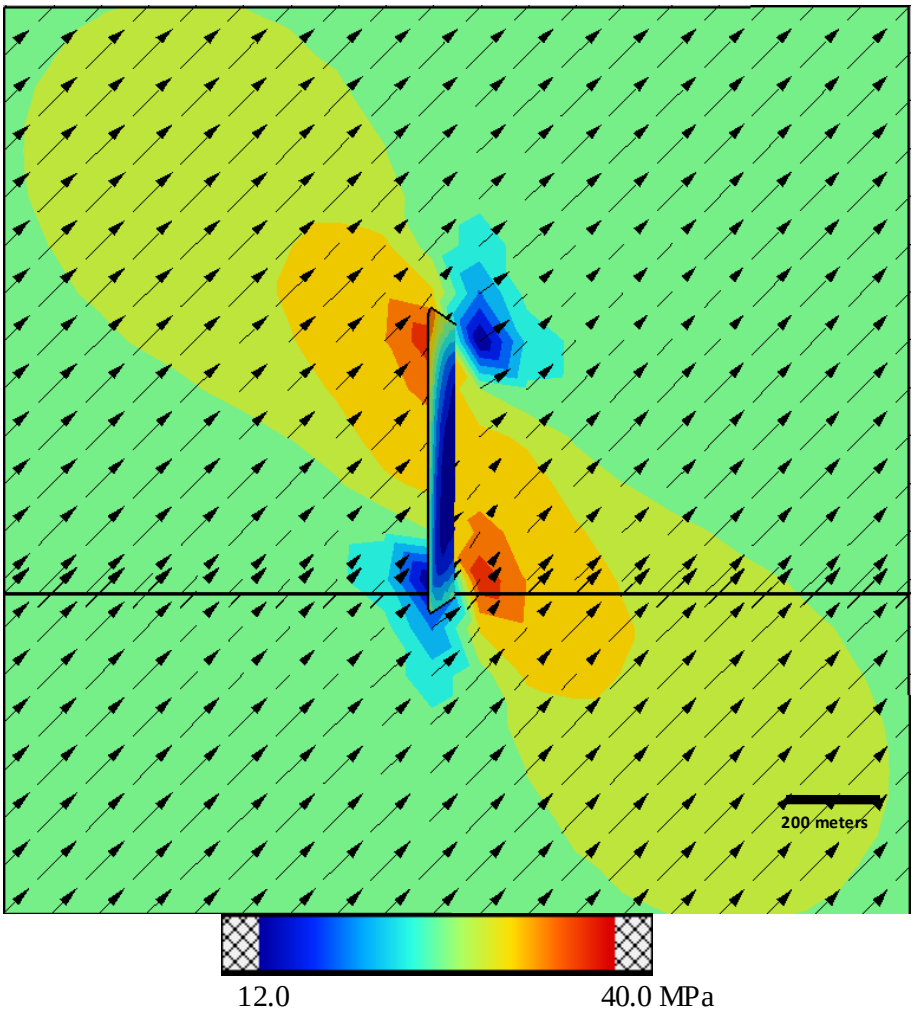

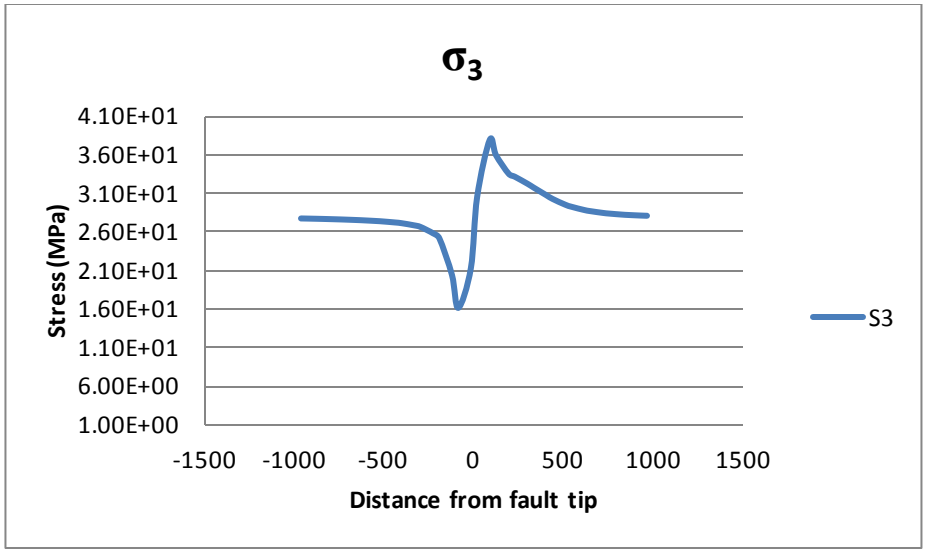

Fault 600 meters, Sandstone 45˚ at 2.5 km

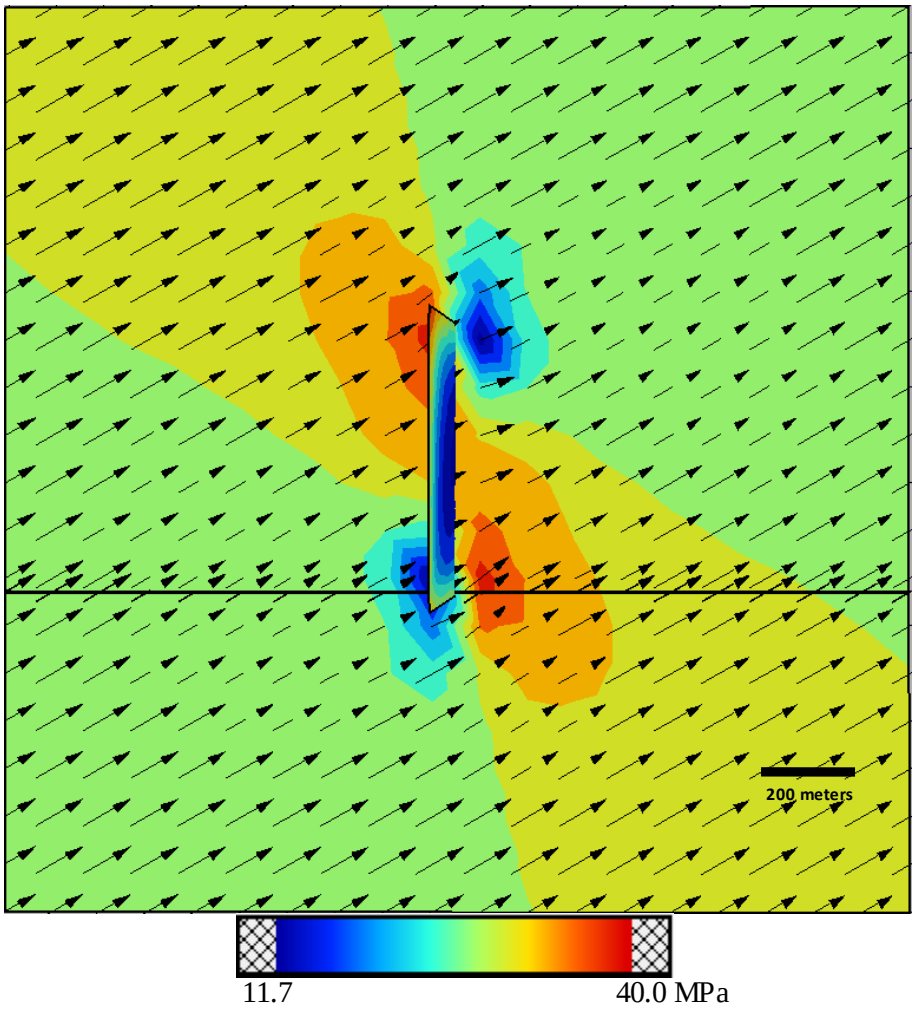

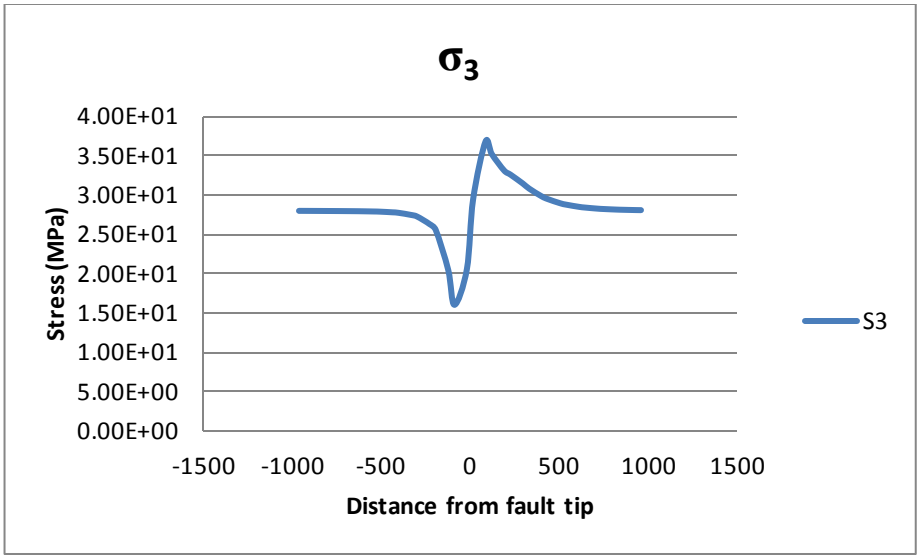

Fault 600 meters, Sandstone 60˚ at 2.5 km

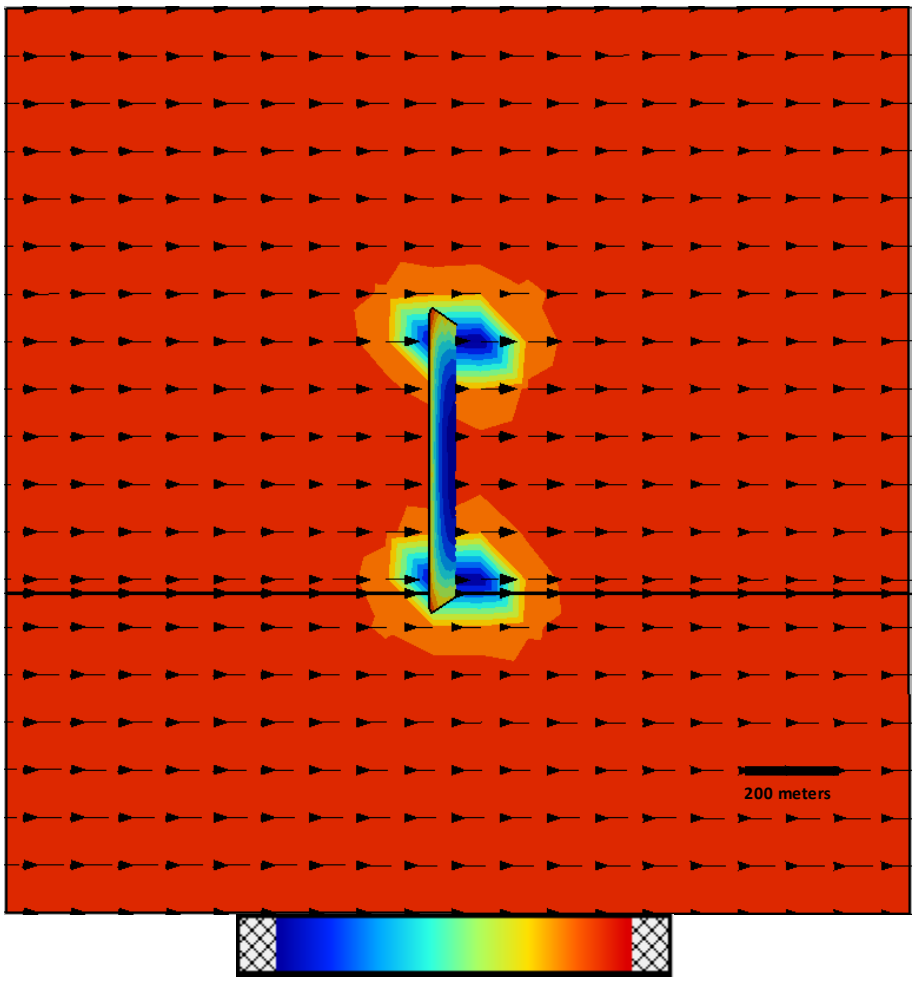

25.0 28.0 MPa

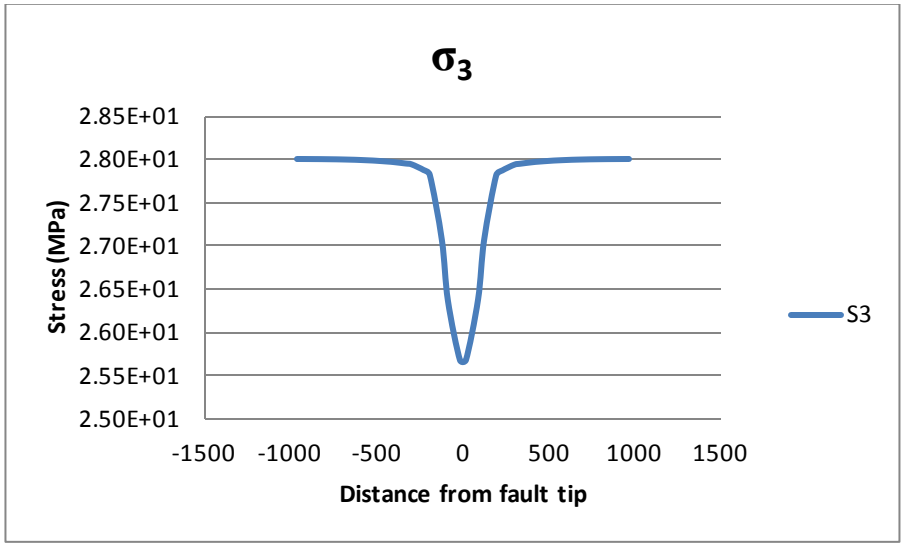

Fault 600 meters, Sandstone 90˚ at 2.5 km

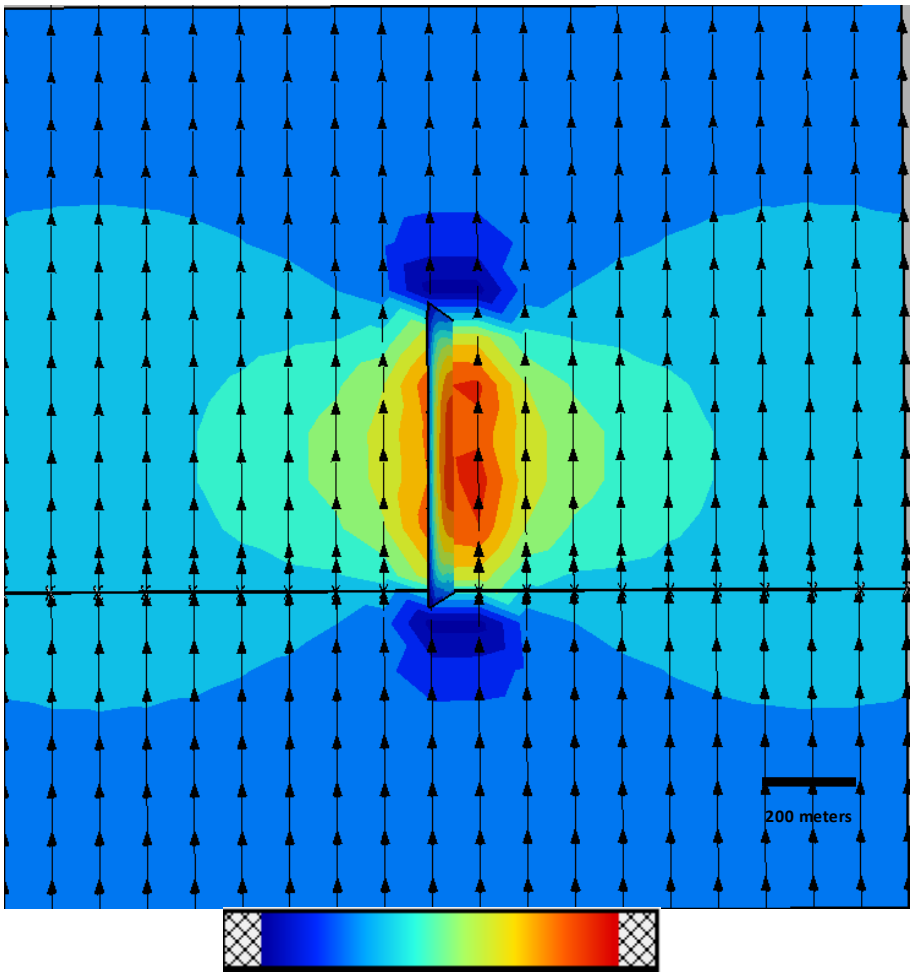

28 28 MPa

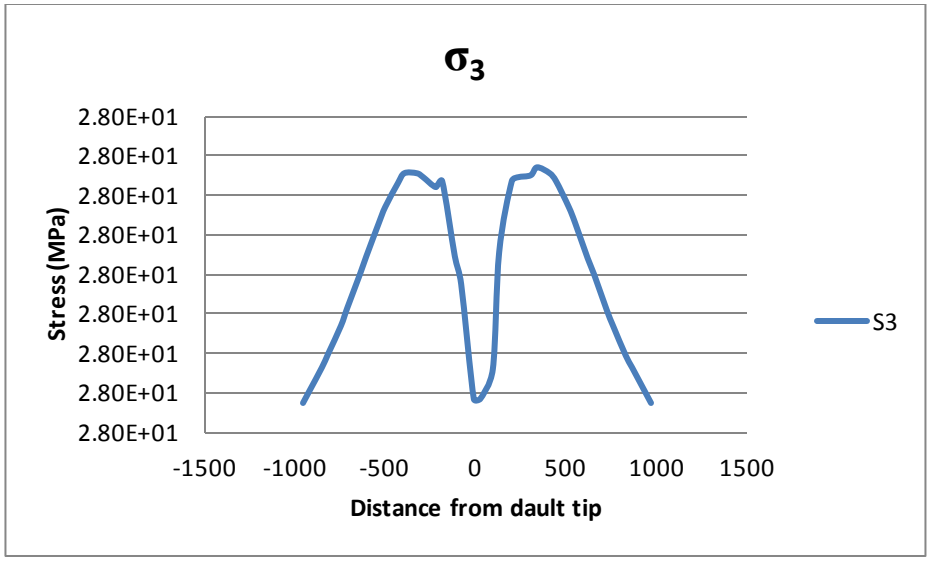

Fault 600 meters, Sandstone 0˚ at 2.6 km

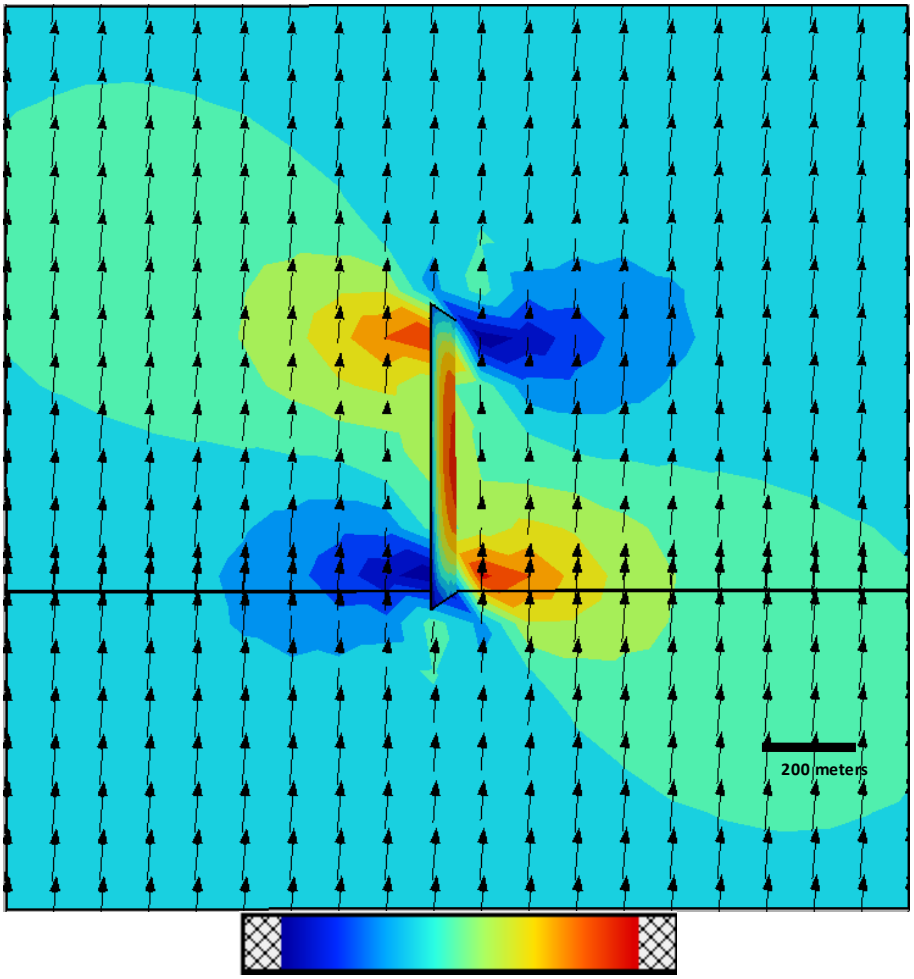

25.0 31.0 MPa

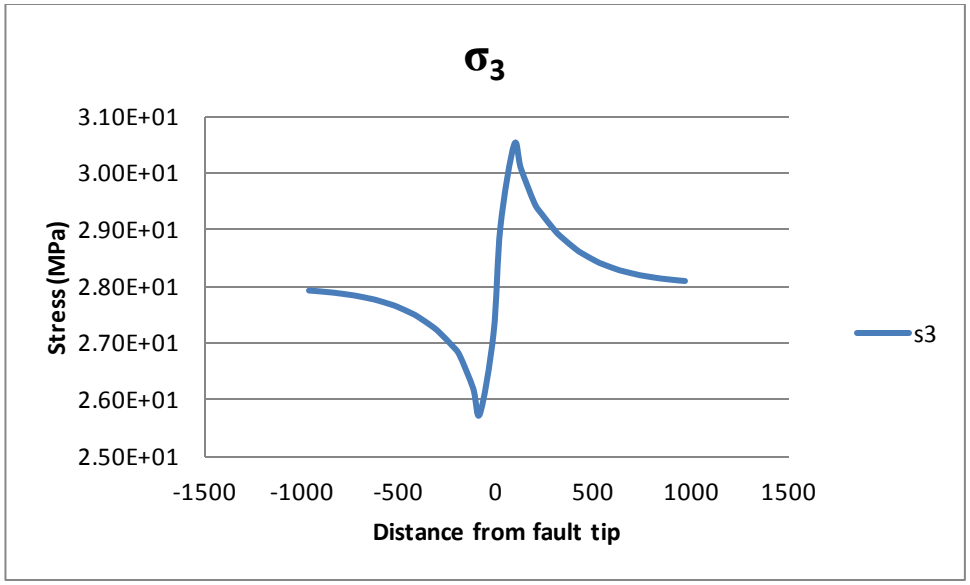

Fault 600 meters, Sandstone 5˚ at 2.6 km

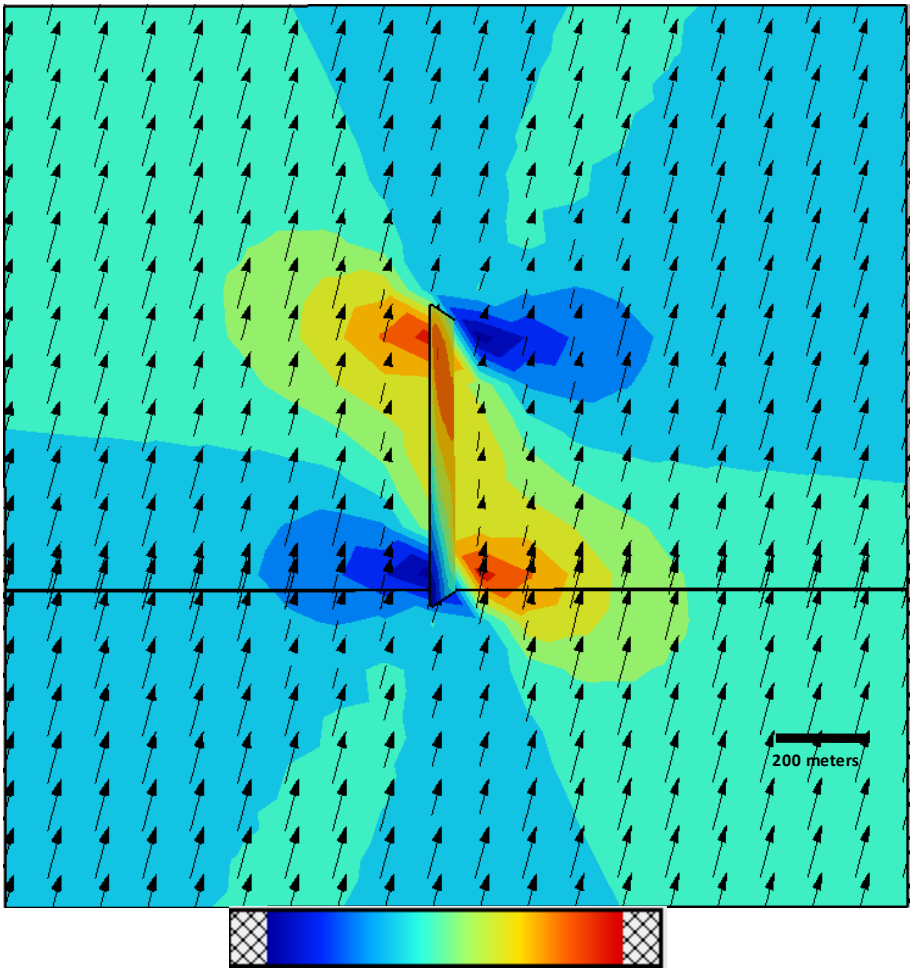

21.0 35.0 MPa

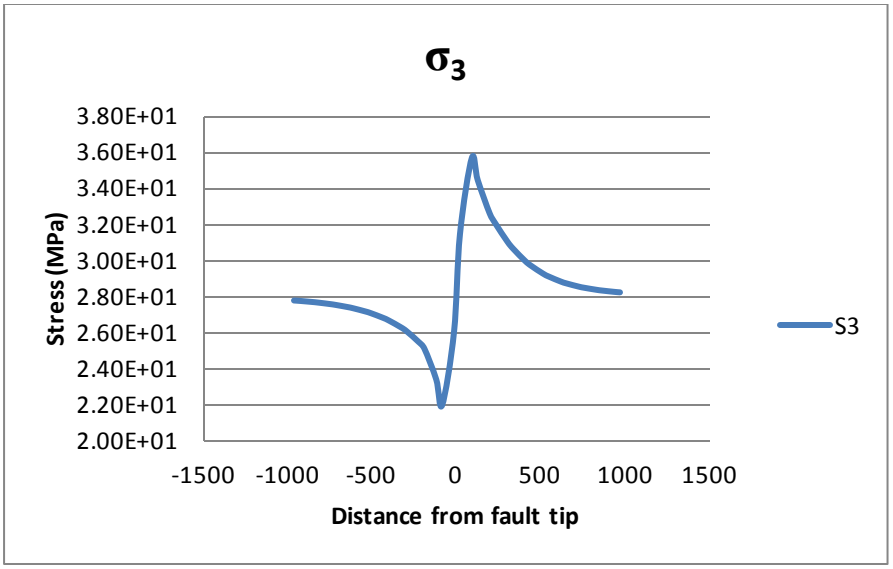

Fault 600 meters, Sandstone 15˚ at 2.6 km

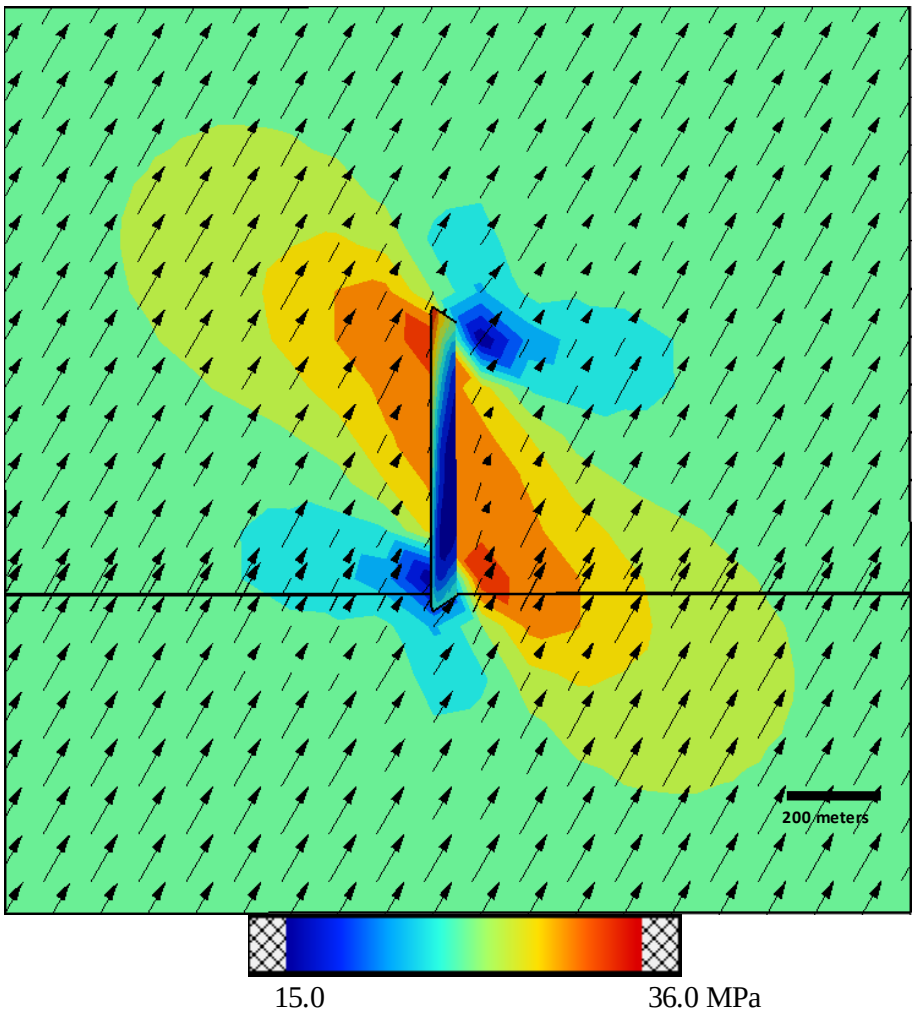

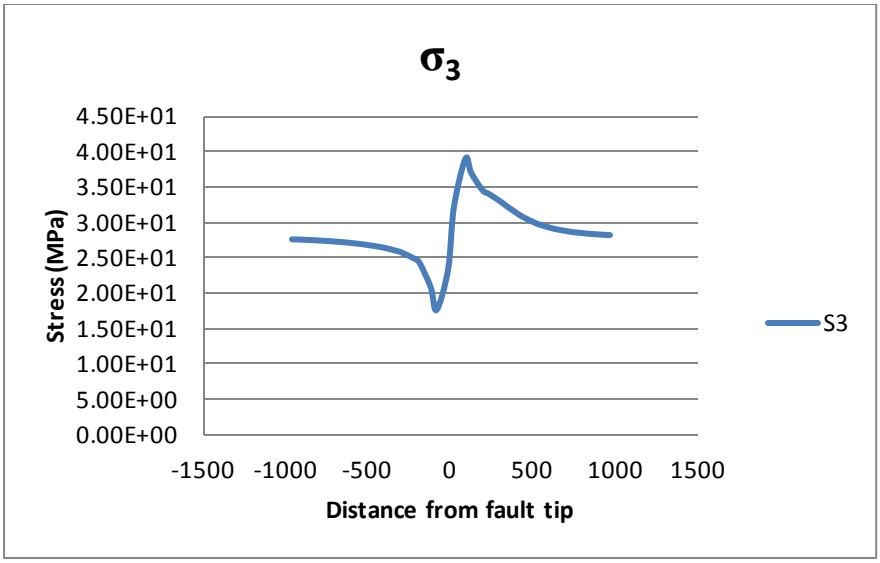

Fault 600 meters, Sandstone 30˚ at 2.6 km

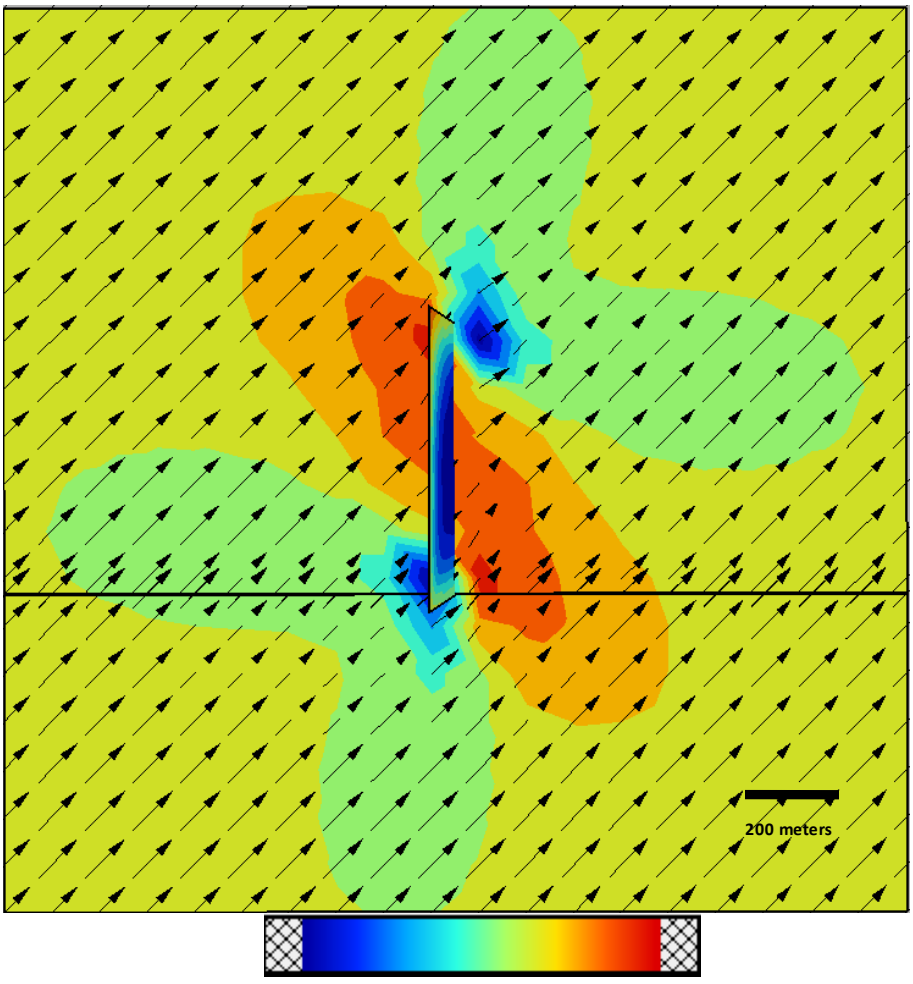

15.0 36.0 MPa

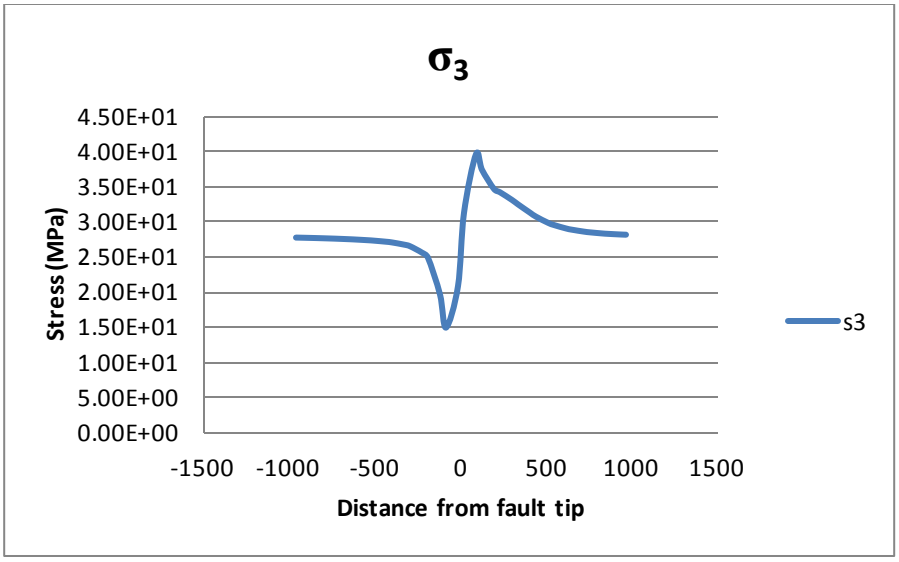

Fault 600 meters, Sandstone 45˚ at 2.6 km

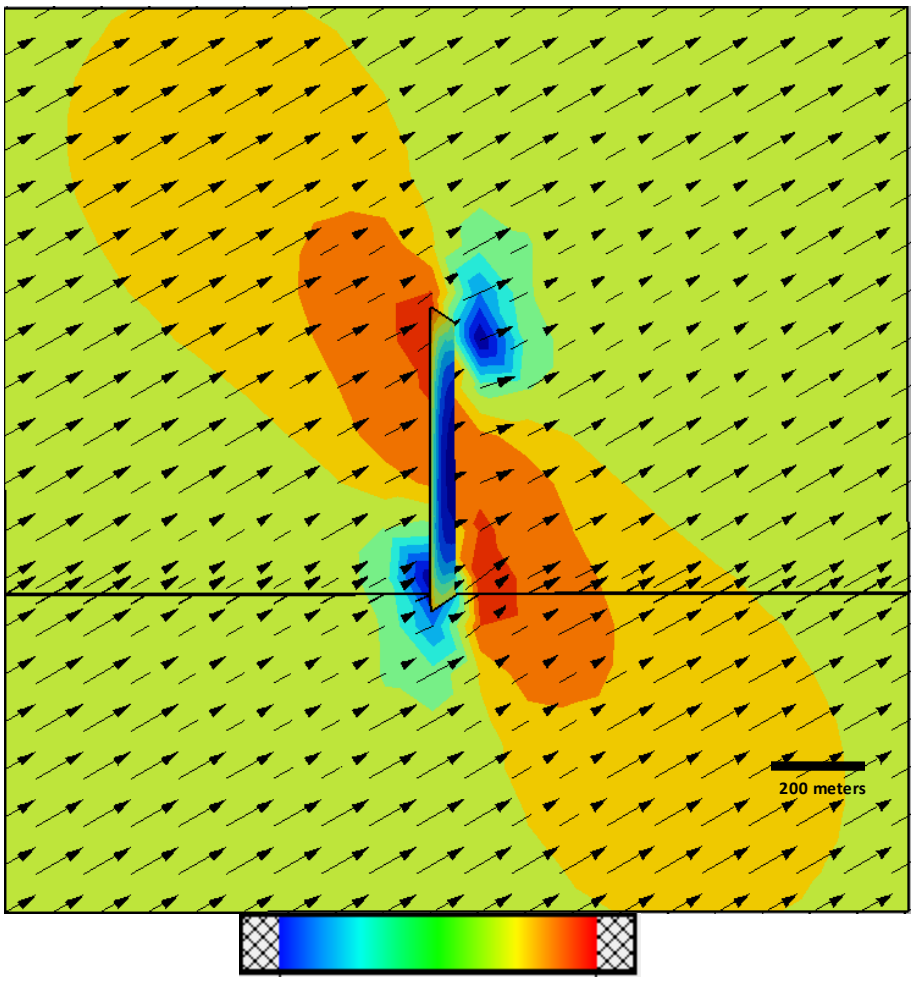

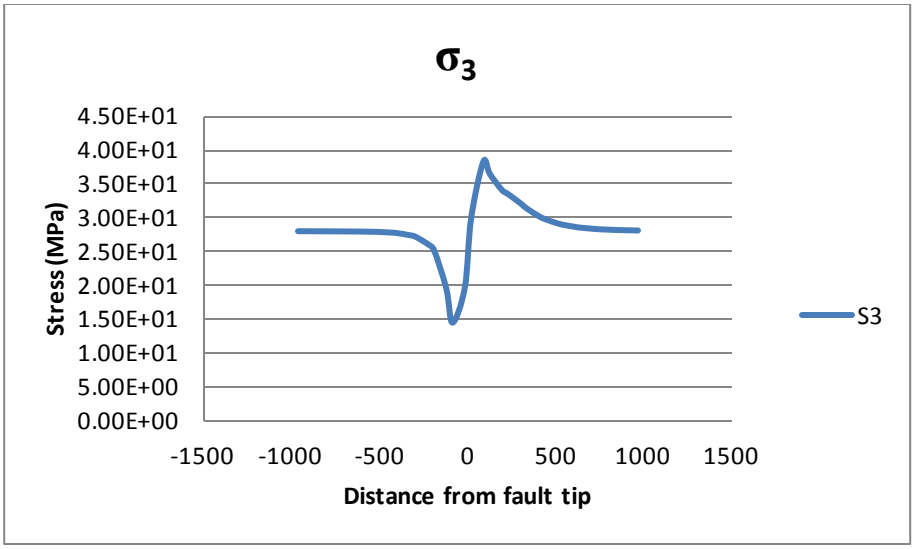

Fault 600 meters, Sandstone 60˚ at 2.6 km

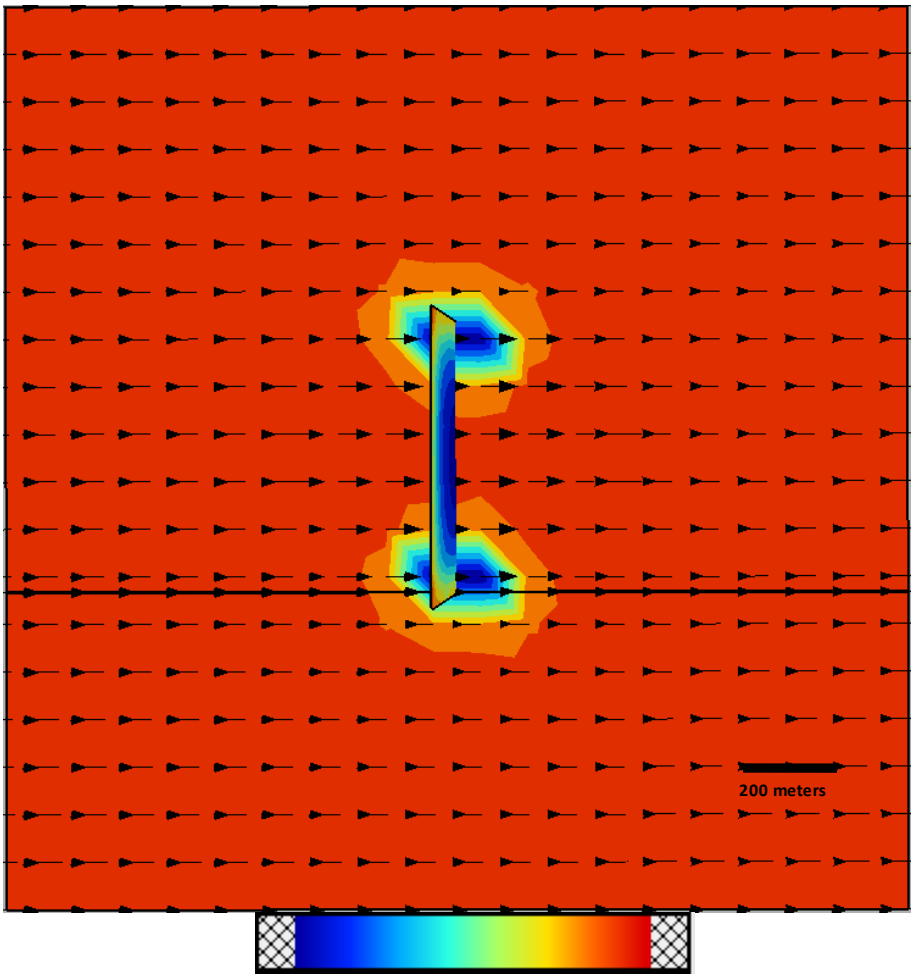

25.0 28.0 MPa

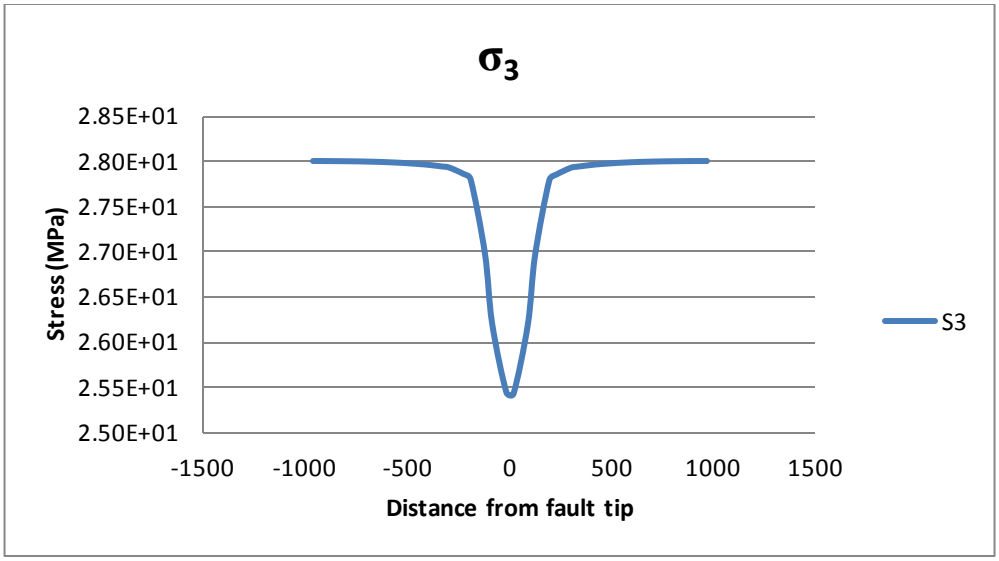

Fault 600 meters, Sandstone 90˚ at 2.6 km

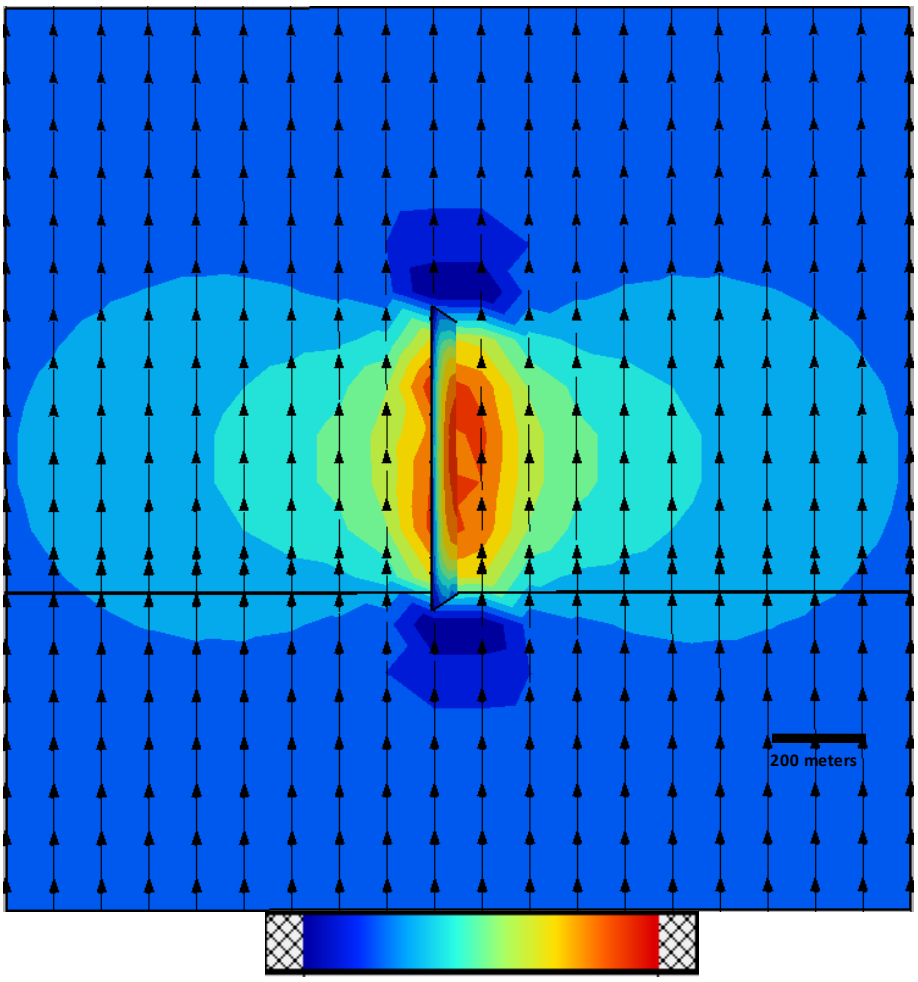

28.0 28.0 MPa

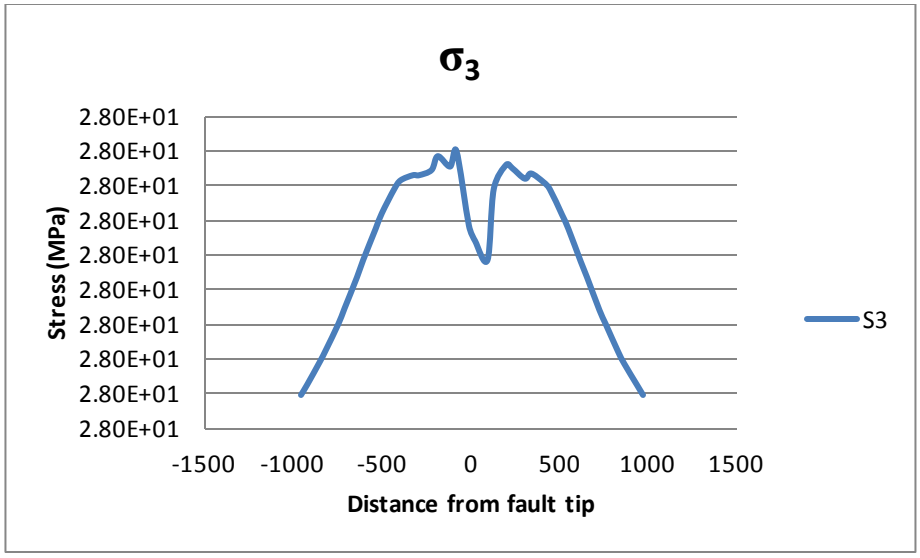

Fault 600 meters, Coal 0˚ at 2.6 km

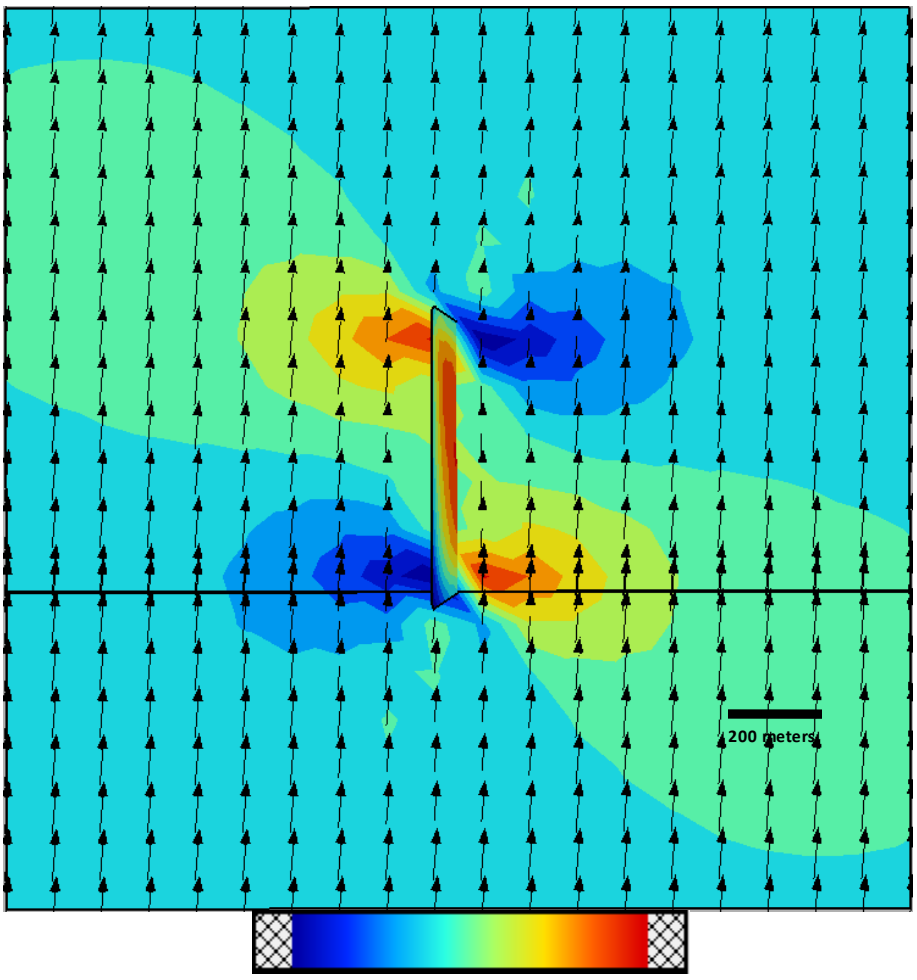

25.0 31.0 MPa

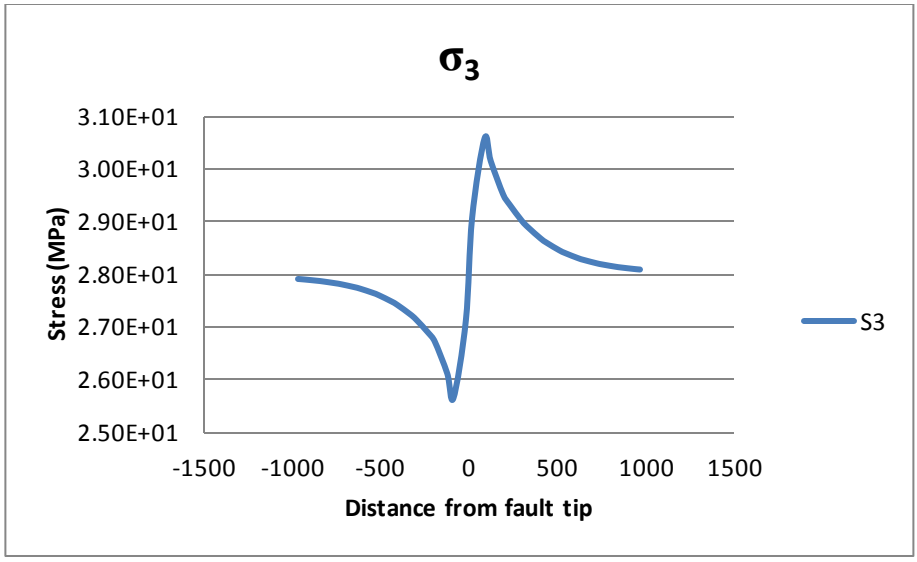

Fault 600 meters, Coal 5˚ at 2.6 km

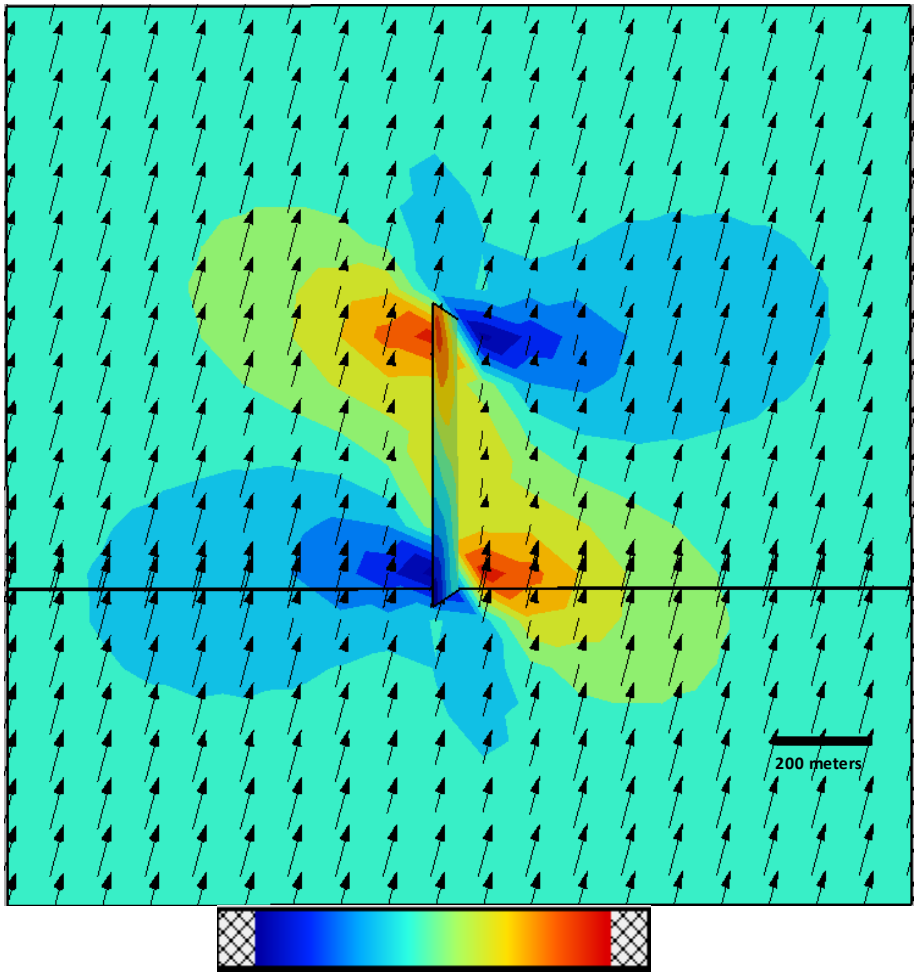

20.0 37.0 MPa

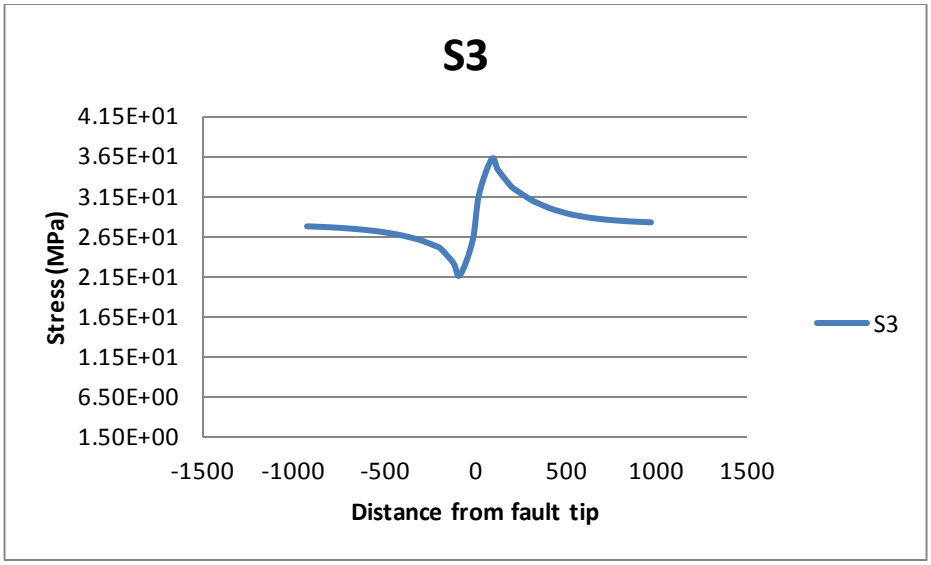

Fault 600 meters, Coal 15˚ at 2.6 km

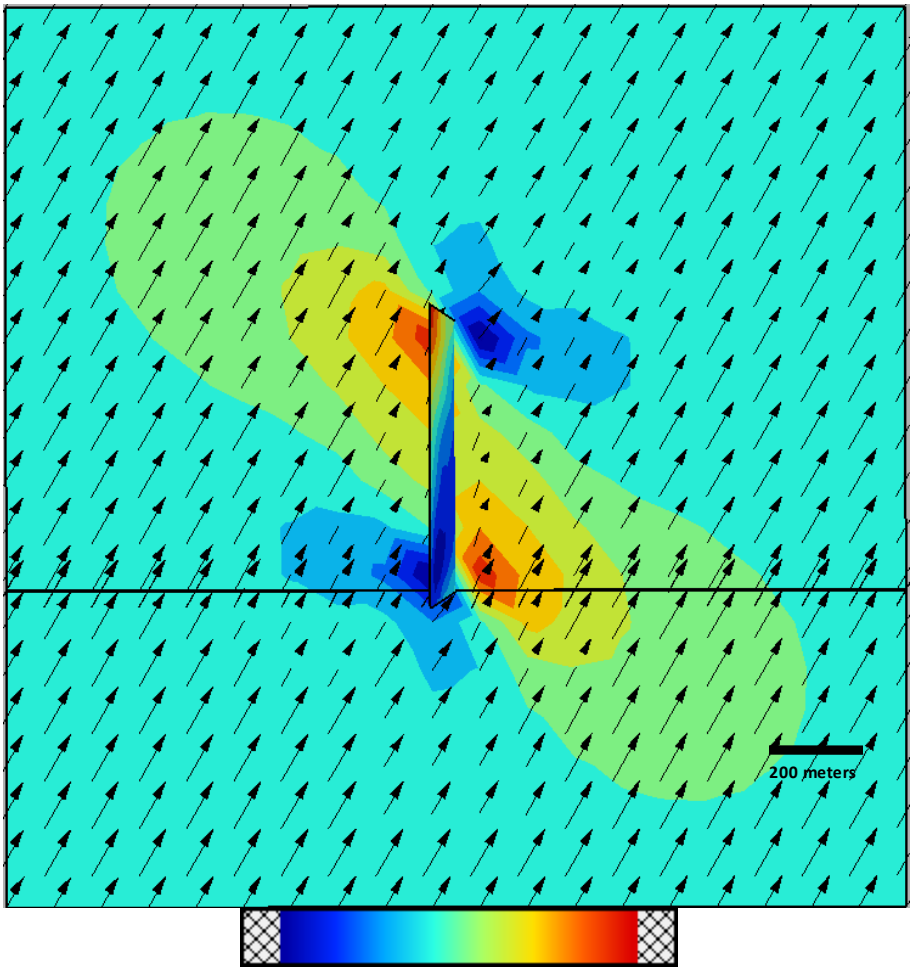

14.0 45.0 MPa

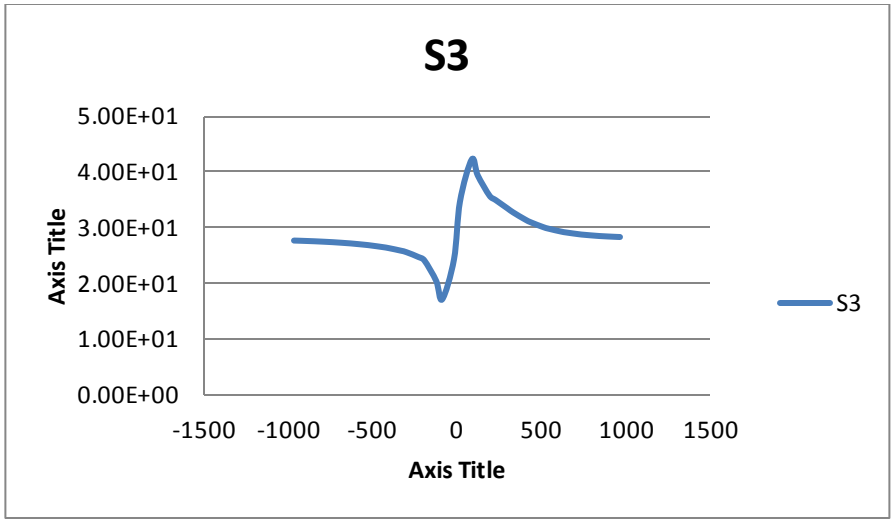

Fault 600 meters, Coal 30˚ at 2.6 km

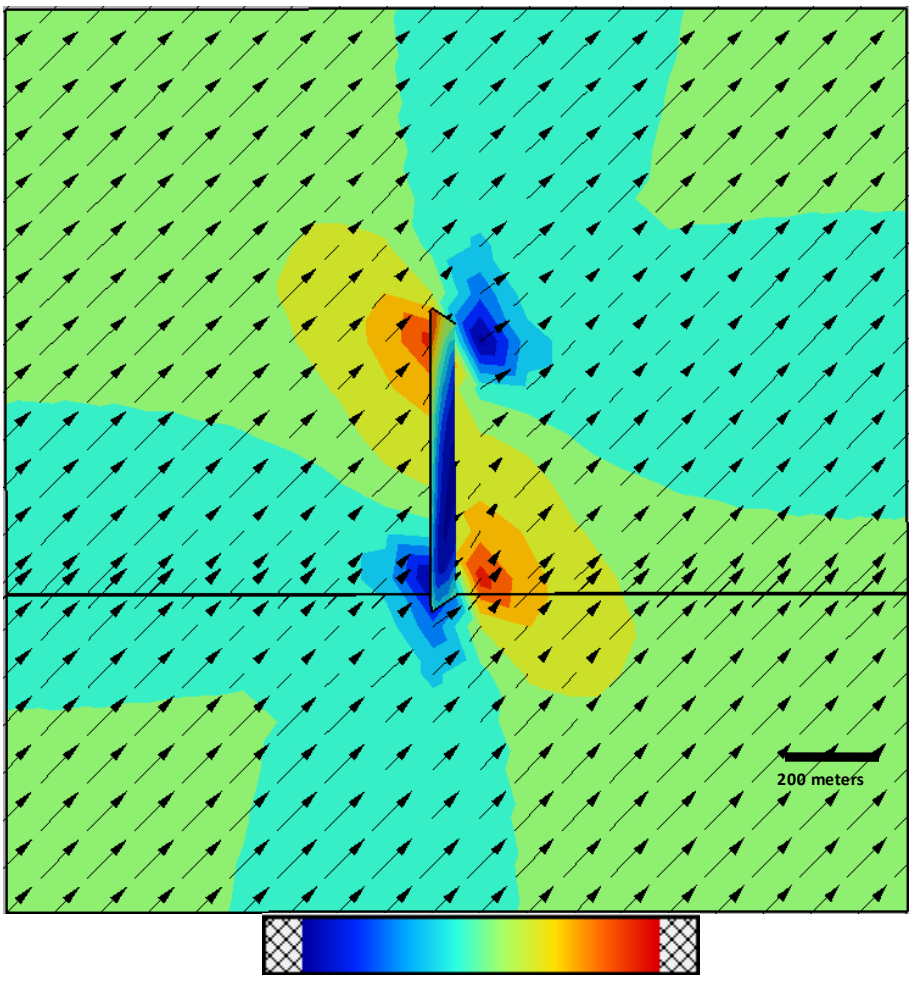

8.0 45.0 MPa

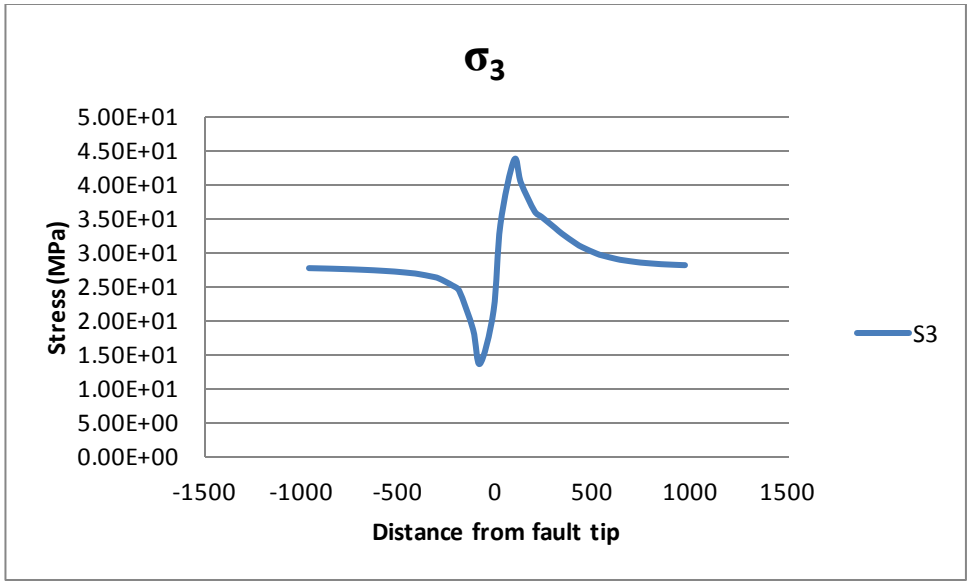

Fault 600 meters, Coal 45˚ at 2.6 km

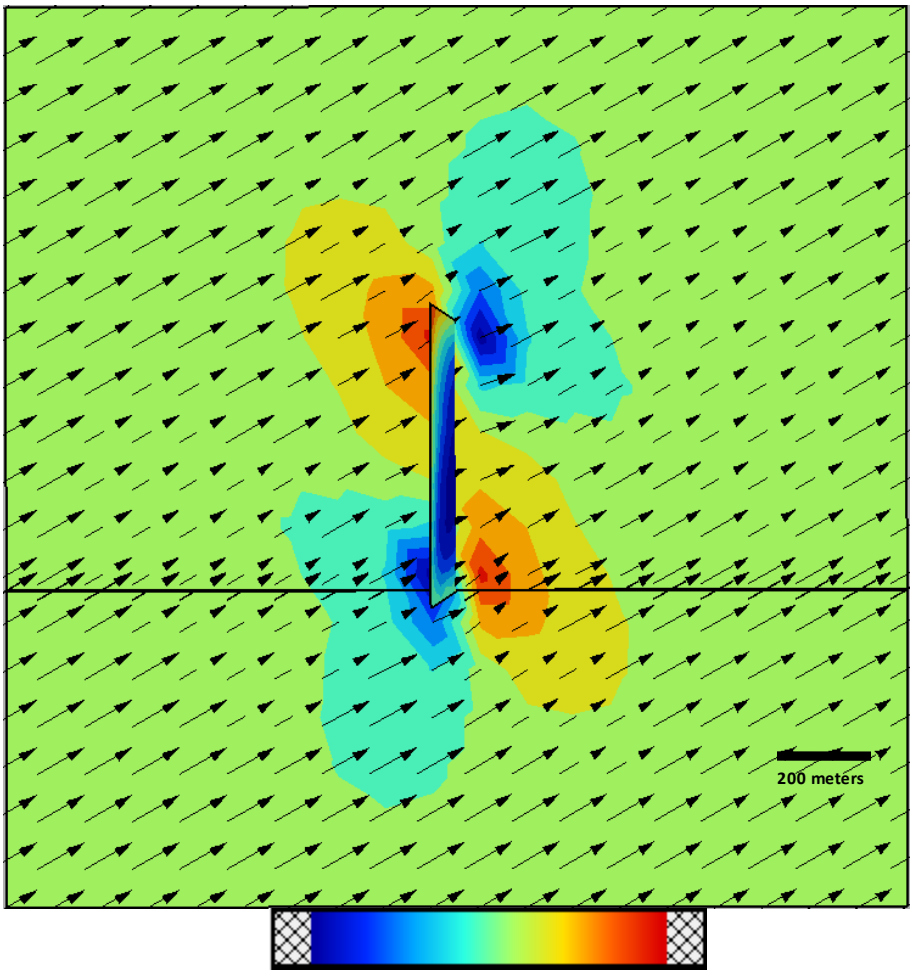

10.0 45.0 MPa

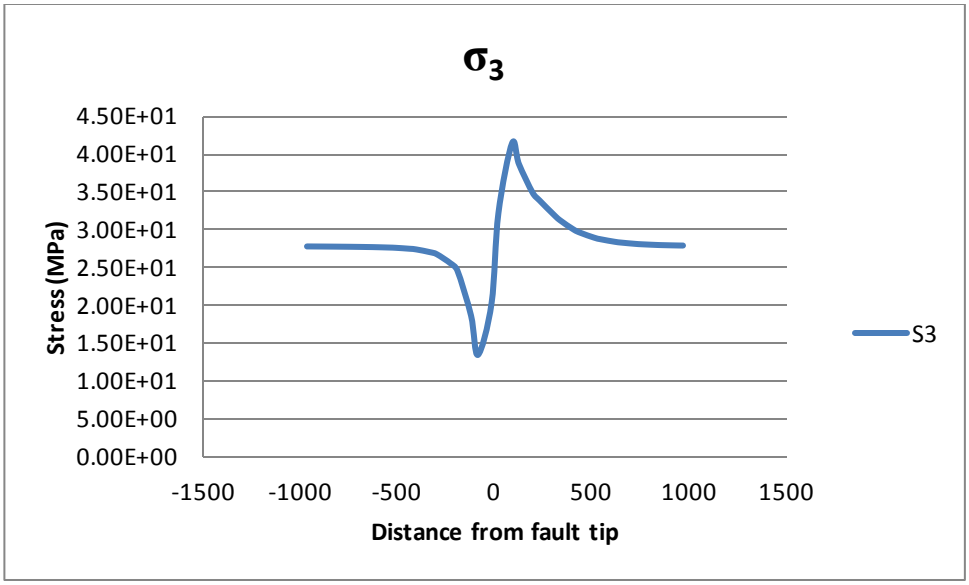

Fault 600 meters, Coal 60˚ at 2.6 km

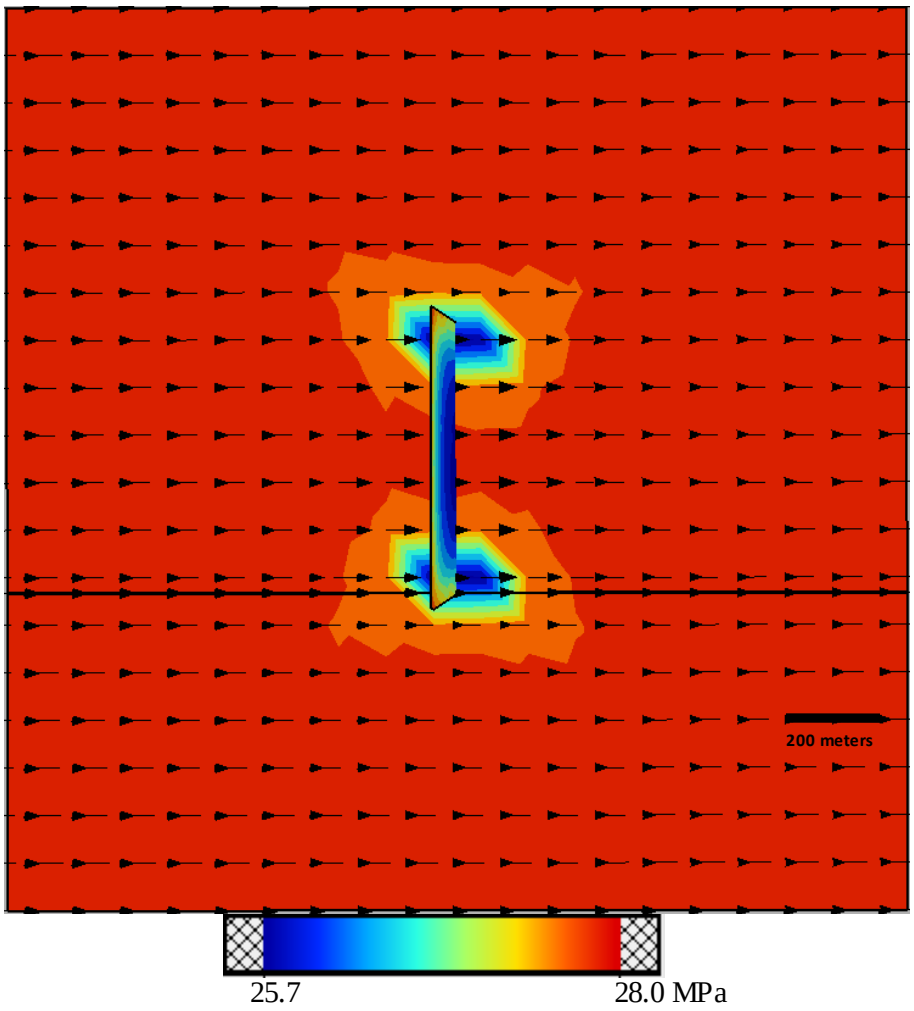

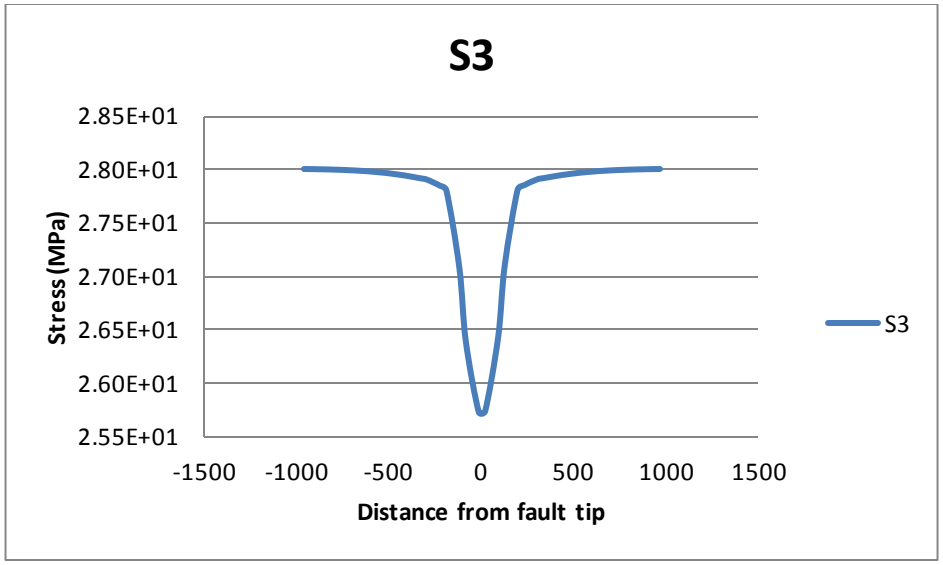

Fault 600 meters, Coal 90˚ at 2.6 km

Appendix B

Lithology

Following figures explain change in Stress magnitude as a result of variation in lithology.

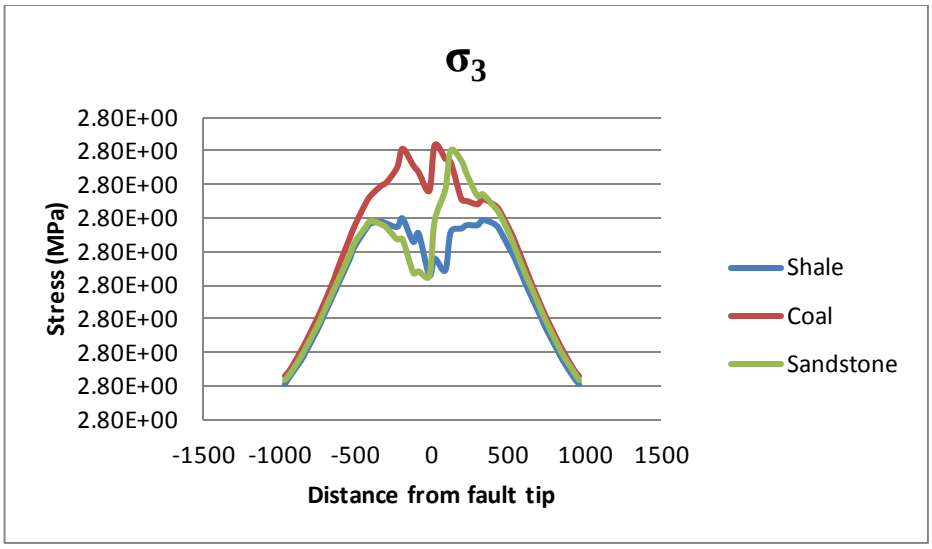

Fault size 600 meters σ_H azimuth 0˚ at 2.5 km

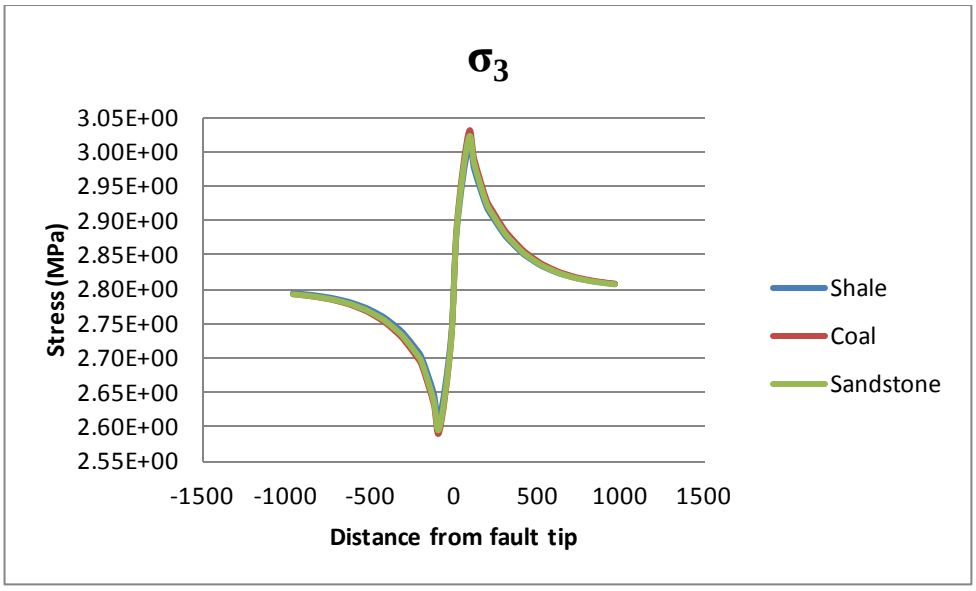

Fault size 600 meters σ_H azimuth 5˚ at 2.5 km

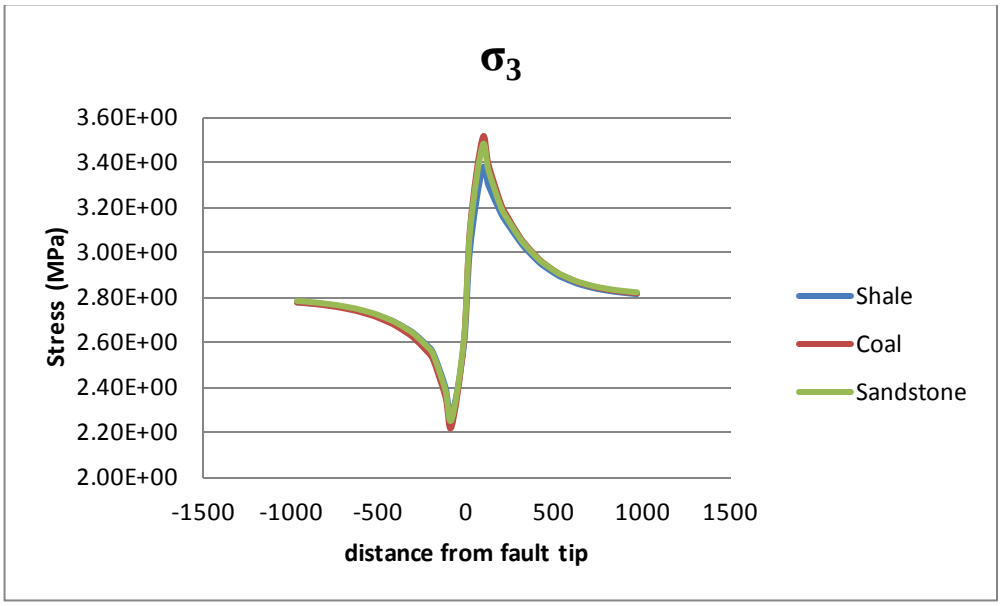

Fault size 600 meters σ_H azimuth 15˚ at 2.5 km

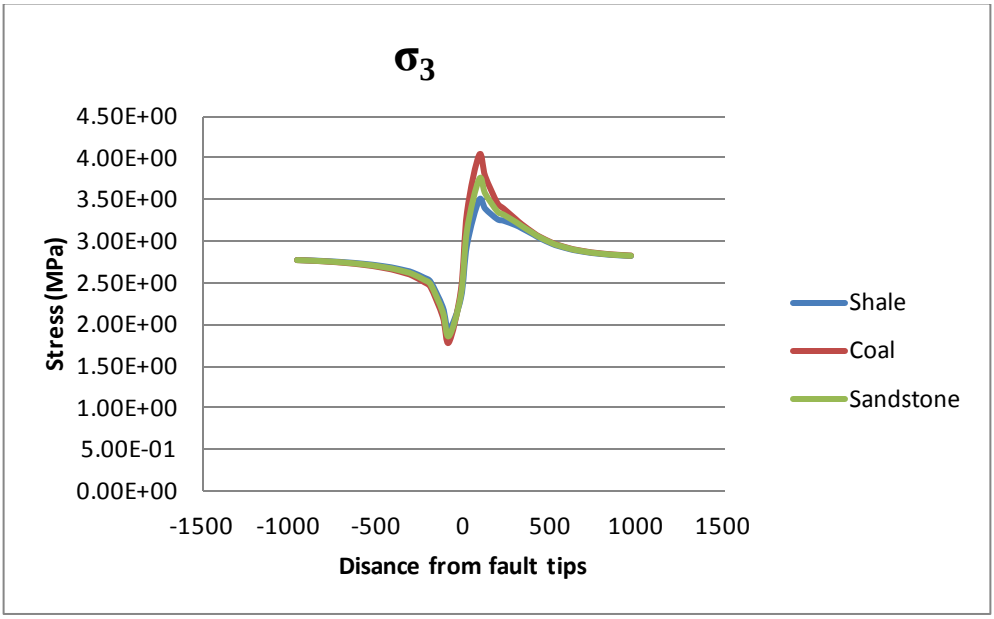

Fault size 600 meters σ_H azimuth 30˚ at 2.5 km

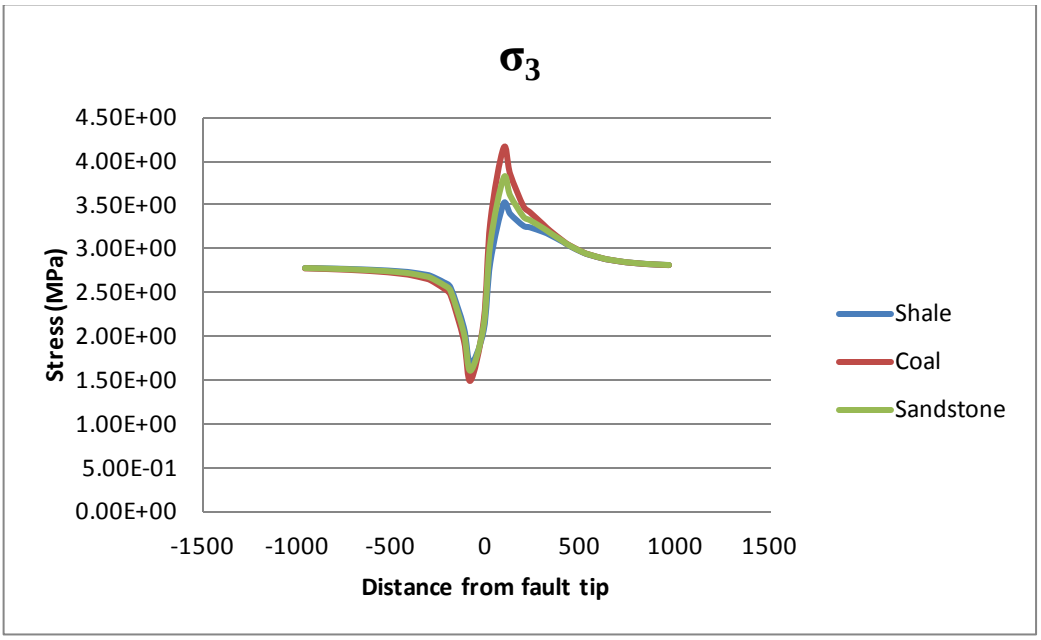

Fault size 600 meters σ_H azimuth 45˚ at 2.5 km

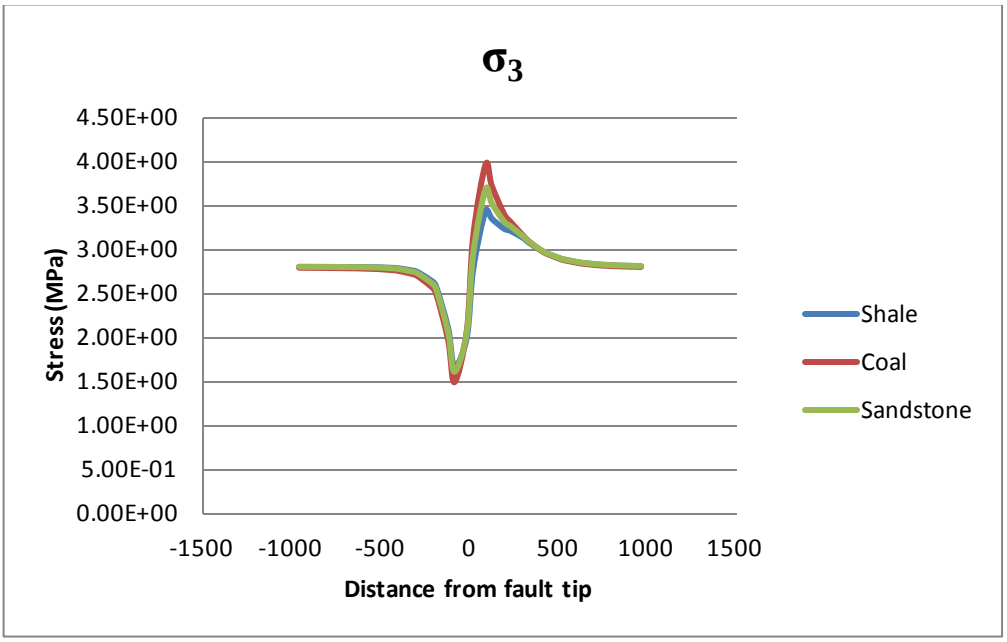

Fault size 600 meters σ_H azimuth 60˚ at 2.5 km

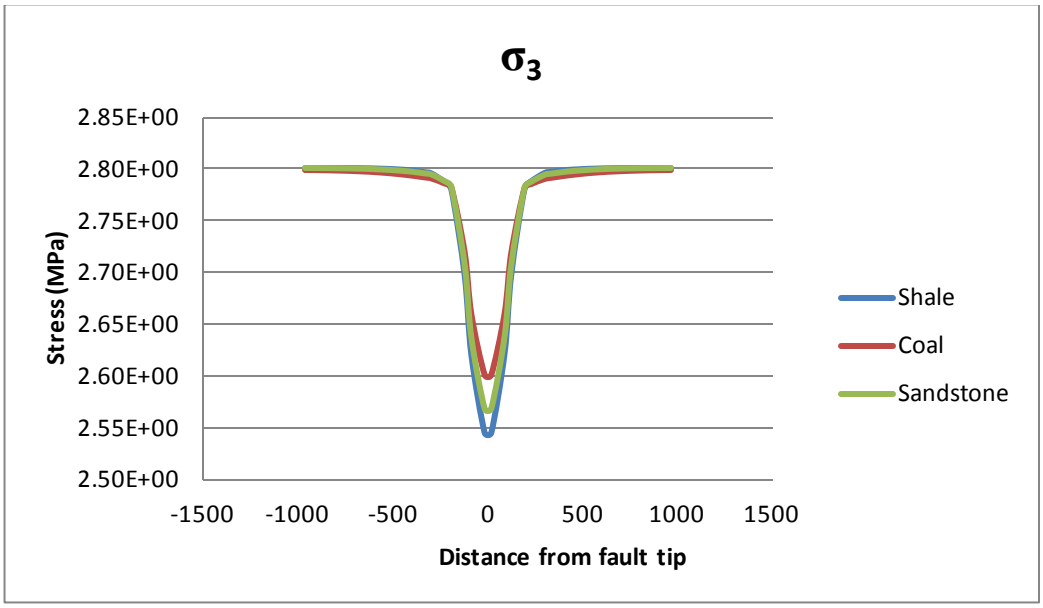

Fault size 600 meters σ_H azimuth 90˚ at 2.5 km

σ_H azimuth

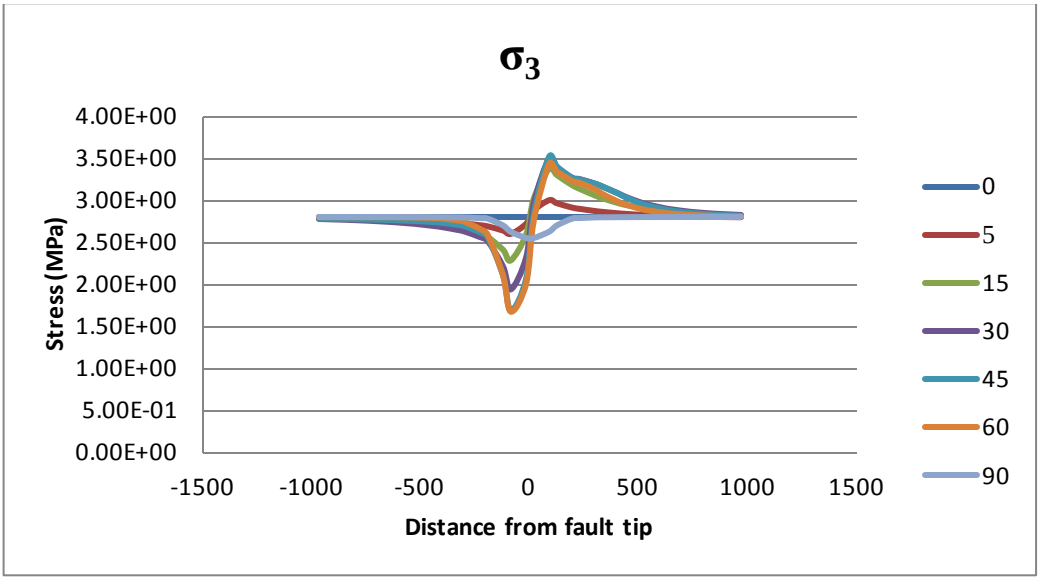

σ_H azimuth combined, fault size 600 meters Shale at 2.5 km depth

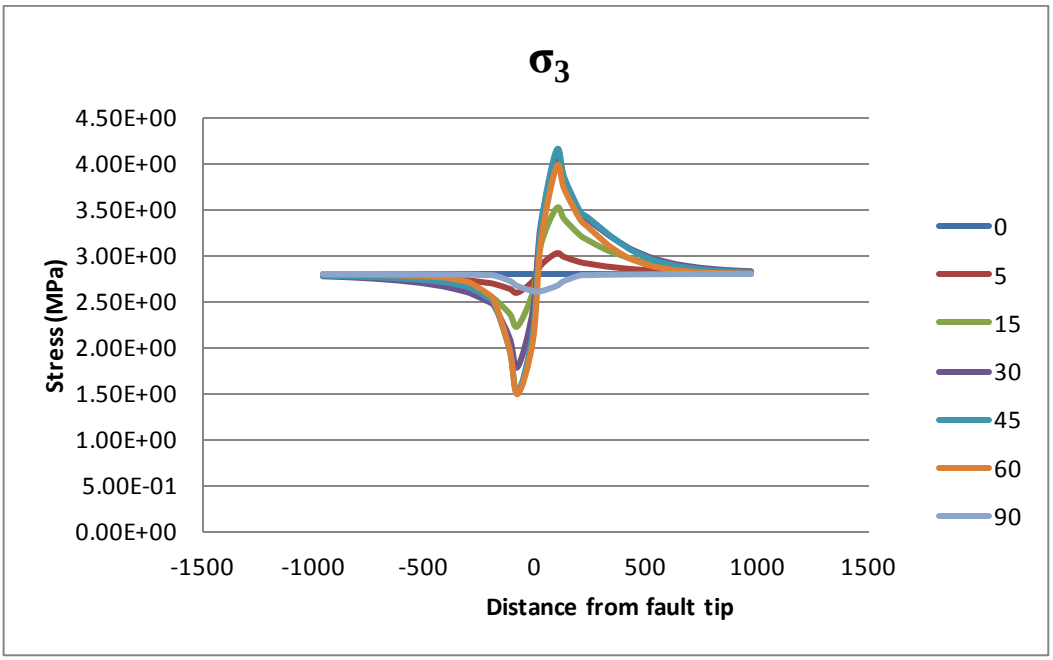

σ_H azimuth combined, fault size 600 meters Coal at 2.5 km depth

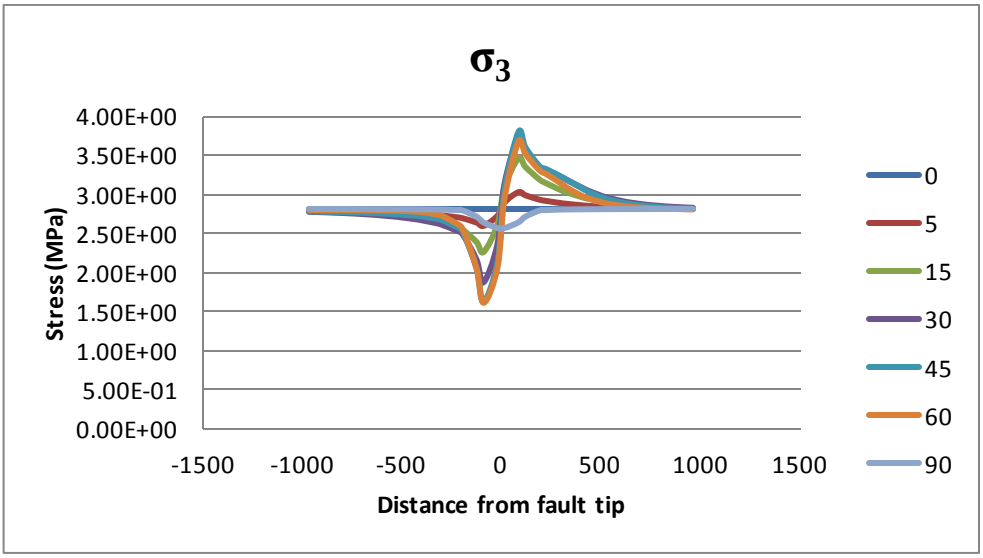

σ_H azimuth combined, fault size 600 meters Sandstone at 2.5 km depth